EFFECTS OF CLIMATE AND GEOCHEMISTRY ON SECONDARY MINERAL DISTRIBUTION AND SOIL ORGANIC CARBON POOLS IN TROPICAL VOLCANIC REGIONS

LYU HAN

2021

ACKNOWLEDGEMENT

First, I would like to express my gratitude to my supervisor, Dr. Shinya Funakawa, Professor of Terrestrial Ecosystems Management and Soil Science, Kyoto University, for his kind guidance, helpful supervision, and continuous encouragement to my Ph.D. study. His patience, motivation, and immense knowledge impressed me and continuously support my research.

I would like to show my thankfulness to my direct advisor, Dr. Tetsuhiro Watanabe, Associate Professor of Kyoto University, for his understanding of my research and valuable suggestions throughout these five years. Whenever I ran into trouble, I could have a discussion and get instant advice from him. He steered me in the right direction of the research and conscientiously encouraged me throughout the Ph.D. study. I also appreciate Dr. Hitoshi Shinjo, Associate Professor of Kyoto University, for his kind attention to my development and helpful advice for improving my research.

Besides my advisors, I would like to thank Dr. Method Kilasara, Associate Professor of Sokoine University of Agriculture, for his kind help and keen supervision during the study trips in Tanzania. I would also like to thank Dr. Arief Hartono, Associate Professor of IPB University, for his valuable support in Indonesia. Without them, the field trip could not be completed.

I sincerely appreciate Dr. Shigeru Araki, Emeritus Professor of Kyoto University, Dr. Tomohiro Nishigaki, Researcher of Japan International Research Center for Agricultural Sciences, and Dr. Makoto Shibata, Assistant Professor of Kyoto University, for their scientific guidance and kind encouragement during the study.

I would like to acknowledge the lab seniors: Dr. Jinsen Zheng, Dr. Kayo Matsui, Dr. Kozue Sawada, Dr. Setiari Marwant, Dr. Athuman J. Mahinda, Dr. Christopher MacCarthy, Ms. Yuri Ichinose, Ms. Yuko Ogawa, and Mr. Shinichi Watanabe. Their suggestions always help me. I also show my thanks to my colleague and friend, Mr. Wahyu Iskandar, Ms. Qian Ma, and Ms. Monika Kumari; we were fighting together for doctoral studies. And all of the colleagues in the Lab of Soil Science and Terrestrial Ecosystems Management, I am so appreciative of being a lab member. Thanks to you all for your kindness and help.

Finally, I must express my very profound gratitude to my parents and my wife for

providing me with unfailing support and continuous encouragement throughout my years of study. This accomplishment would not have been possible without them.

This research was financially supported by Grants from JSPS KAKENHI.

LYU HAN

CONTENTS

LIST OF TABLES

LIST OF FIGURES

CHAPTER 1

INTRODUCTION

1.1 General background

Soil secondary minerals are fundamental and vital components of soil, controlling its chemical and physical properties. Due to their charge characteristics, large surface area, association with organic materials, and potential for the supply of essential elements for vegetation, the distribution of soil secondary minerals is essential for the understanding of the cycles of elements in the ecosystem and is needed for proper environmental and agricultural managements (Schulze, 2018). As an example, the nanocrystalline Al and Fe have strong abilities to adsorb and stabilize phosphate (Parfitt, 2009); and the association of nanocrystalline Al and Fe with organic materials results in organo-mineral complexes, which preserves organic matter and affects other element dynamics in the soil via their surface and charge characteristics (Bruun et al., 2010; Harsh, 2011).

Climatic and geological conditions regulate the formation and weathering of soil minerals, which controls soil secondary mineral distribution. Climatic factors are generally referred to as the temperature and precipitation conditions. Low temperature would retard the crystallization of soil minerals, results in the abundance of nanocrystalline minerals (Churchman and Lowe, 2012). Retarded decomposition of organic input along with the abundant nanocrystalline minerals in low-temperature regions promotes the formation of organo-mineral complexes and preserves the nanocrystalline Al and Fe (Chorover et al., 2004; Takahashi and Dahlgren, 2016). Soil solution composition, which is influenced by both parent material (geology) and precipitation (climate), is important for the neoformation and transformation of secondary minerals (Karathanasis, 2018). The high precipitation may also help the formation of nanocrystalline Al and Fe by reducing the Si activities in the soil solution. For secondary crystalline minerals, the formation of smectite and kaolin minerals is favored in Andisoils with an alternation of moist and dry conditions (Van Ranst et al., 2008). The gibbsite is stable in the soil with intensive leaching (high moisture) and low Si

activities. However, studies in tropical volcanic regions that focus on crystalline and nanocrystalline minerals, especially in regions with moderate pH, are limited.

Soil organic carbon (SOC) regulates the chemical, physical, and biotic properties of the soil, as well as soil minerals. Meanwhile, SOC is a significant carbon pool in the terrestrial ecosystem and stores more carbon than the atmosphere (Jobbagy and Jackson, 2000; Schlesinger, 1995). Rising temperatures promote the decomposition of SOC, which increases the rate of CO_2 released as a greenhouse gas, creating a positive feedback loop for climate change (Davidson and Janssens, 2006).Furthermore, the loss of SOC causes a decrease in soil fertility and has a significant impact on the soil ecosystem, which uses organic carbon as an energy source (Lal, 2004a). Therefore, understanding SOC dynamics and clarifying the factors that control SOC storage under climate change is an urgent priority for mitigating global climate problems.

Temperature has an impact on SOC storage on a broad spatial scale. In mountainous regions, SOC is abundant in high elevation sites with low mean annual temperature (MAT). The change in mean residence time (MRT) of SOC with temperature gradients indicates that the stability of SOC is negatively correlated with MAT (Garten Jr, 2011; Garten Jr and Hanson, 2006). However, the components and stability of SOC are not always controlled by variations in temperature (Djukic et al., 2010; Tian et al., 2016). Net primary production (NPP), which changes with climate, directly regulates carbon input, thus affecting SOC content over a timescale of years. Geochemical properties may be the principal controllers of SOC storage on a decadal or longer timescale, and MAT and mean annual precipitation (MAP) would be secondary predictors, especially in soils with high SOC (Doetterl et al., 2015). The soil organic carbon is mainly associated with the clay and silt via both physical and chemical protection. Notably, the nanocrystalline Al and Fe minerals have a strong ability to accumulate SOC through organo-mineral interactions (Asano and Wagai, 2014; Sollins et al., 2009; Takahashi and Dahlgren, 2016). Factors influencing SOC storage and distribution have been studied, while the controlling factors interact with each other and influence SOC simultaneously (Doetterl et al., 2015). Also, SOC is not homogenous but consists of various functional pools that have different MRTs and are controlled by specific stabilization mechanisms

(von Lützow et al., 2007). Hence dividing SOC into different pools and determining the effects of climatic and geochemical properties on the size, proportion, and stability of each SOC pool is required to understand the SOC stabilization mechanism and to make models that predict the change of SOC stocks under future climate conditions.

In volcanic regions of Tanzania and Indoneisa, the soils are formed on relative recent tephra deposits (relatively similar parent materials in each region). The soils at the sampling sites are mainly formed on tephra deposits under well-drained conditions (Crow and Barber, 2005; Fontijn et al., 2012; Little and Lee, 2006; Little and Lee, 2010). In these regions, the variation in elevation leads to a continuous change in temperature and precipitation. According to the world map of Köppen-Geiger climate classification (Peel et al., 2007), the climate changes with the latitude and elevation. For example, in Tanzania, Mt. Kilimanjaro and Mt. Meru are in the tropical savanna to oceanic climate, and the climate in Mt. Kieyo is humid subtropical; in Indonesia, both Java and Sumatra sites are in tropical rainforest climate. Because of the diversity of climatic conditions, various distributions of soil secondary minerals were expected to be found in each region. Meanwhile, the volcanic regions of Tanzania and Indonesia, where has diverse climates, similar parent materials, rich in nanocrystalline minerals, and dense cover of largely-undisturbed vegetation, are the ideal regions for studying the controlling factors for soil secondary minerals distribution and SOC dynamics.

1.2 Study objectives

The objectives of this study were to present the impacts of climate and geochemistry on two of the predominant components of soil: soil secondary minerals and organic matters, and to evaluate their effects on soil properties in tropical volcanic regions. Studies that focused on the soils along the elevation gradient in volcanic regions of Tanzania and Indonesia were conducted to achieve these objectives. First, I clarified the factors that control the distribution of secondary nanocrystalline and crystalline minerals in the soils of volcanic regions, Tanzania. Then, the effect of climatic, biotic, and geochemical properties on SOC storage and stability were evaluated for both topsoil and subsoil in Tanzania and Indonesia. Moreover, the effects of soil minerals and

organic matter on soil charge characteristics were studied.

The thesis comprises the following chapters: In Chapter 2, the effects of climate and geology on the formation and distribution of soil secondary minerals in volcanic regions of Tanzania, are discussed. In Chapter 3, SOC storage and stability are evaluated by sizes and mean residence times of SOC pools, and the controlling effects of climate and nanocrystalline minerals on SOC pools in topsoil of volcanic regions in Tanzania and Indonesia, are discussed. In Chapter 4, factors that control the SOC pools in subsoil (same sites as Chapter 3) are clarified, and the differences of controlling factors, SOC pools' sizes and stabilities between topsoil and subsoil, are discussed. Chapter 5 states the control of climate on soil charge characteristics through SOC and soil mineral distributions. In Chapter 6, general discussion and conclusion of previous chapters are summarized.

CHAPTER 2

EFFECTS OF CLIMATE ON DISTRIBUTION OF SOIL SECONDARY NANOCRYSTALLINE AND CRYSTALLINE MINERALS

2.1 General

The distribution of secondary minerals under the specific combinations of temperature and precipitation increases our understanding of the secondary mineral formation and further helps to understand the elemental cycling in the soil. Environmental conditions in the volcanic regions are unique, and the volcanic materials are sensitive to the change in temperature and precipitation. Relatively low temperature retards the crystallization process, which preserves the Al, Fe, and Si as nanocrystalline secondary minerals (Churchman and Lowe, 2012). Lower temperature at higher elevation sites retards the decomposition of organic matter, which also maintains the poorly crystalline conditions of secondary minerals in Hawaii (Chorover et al., 2004). At high elevations (>900 m asl), high rainfall, low evapotranspiration, and temperatures result in greater leaching and favor the precipitation of nanocrystalline materials in Taiwan (Tsai et al., 2010). Smectite, Al-interlayered minerals, and kaolinite were dominant in the clay mineralogical assemblage in well drained Andisols in central Java, Indonesia, while the 2:1 clay minerals and kaolinite could be unstable under perudic and intensive leaching conditions (Van Ranst et al., 2008). The gibbsite abundance in soils is the result of intense weathering, and the presence of halloysite is probably coupled to the contemporary soil moisture regime at the La Selva, Costa Rica (Kleber et al., 2007a). Still, research studies in semi-humid tropical volcanic areas regarding the effects of temperature and precipitation on the distribution of nanocrystalline and crystalline minerals are scarce.

Tanzania, in eastern Africa, has volcanic regions in the northern and southern highland and a unique range of climate conditions. Thus, the volcanic regions of Tanzania are ideal study sites to investigate the effects of climate on the distribution of soil secondary minerals developed from pyroclastic (fragmental) volcanic deposits, namely tephra (Lowe, 2011). The climatic conditions

are different from those associated with previous studies in volcanic regions, such as in eastern and southeastern Asia that have intensive precipitation (Van Ranst et al., 2008); in western USA with temperate and moist conditions (Rasmussen et al., 2007); and in southern Europe that is in a typical Mediterranean climate. In the northern and southern highlands of Tanzania, including Mt. Kilimanjaro, Mt. Meru, and Mt. Kieyo, the soils are formed on relative recent tephra deposits. The soils at the sampling sites, (see below) are mainly formed on tephra deposits under well drained conditions (Fontijn et al., 2012; Little and Lee, 2006; Little and Lee, 2010; Wilkinson et al., 1986). In these mountains, the variation in elevation leads to a continuous change in temperature and precipitation in a relatively limited area. According to the world map of Köppen-Geiger climate classification (Peel et al., 2007), Mt. Kilimanjaro and Mt. Meru are in the tropical savanna to oceanic climate (Aw to Cwb and Cfb), and the climate in Mt. Kieyo is humid subtropical (Cwa). Because of the diversity of climatic conditions, various distributions of soil secondary minerals were expected to be found on different tephra deposits in each region.

The parent materials in Mt. Kilimanjaro (phonolite), Mt. Meru (phono-tephrite), and Mt. Kieyo (phonolite–trachyte–trachy-andesite) (volcanic compositional classifications are based on (Le Maitre et al., 2005)) are all alkaline or sub-alkaline tephra deposits, but the difference in chemical composition of the parent materials are not clear. The total elemental contents can be applied to estimate the parent materials and hence to classify the soils into informal groups (Watanabe et al., 2017). Al, Fe, and Si are essential elements for the formation of soil secondary minerals. Because of the relative immobility of Al, Fe, and Si in the soil in normal conditions (e.g., compared with K, Na, and Ca), the total Al, Fe, and Si tend to reflect the original composition of the parent materials. The K, Na, Ca, and Mg are included in primary minerals and reflect the parent materials, but they are mobile and, therefore, also reflect the weathering degree.

Soil solution composition is important for the neoformation and transformation of secondary minerals. Soil secondary minerals, such as the nanocrystalline minerals (e.g., allophane and ferrihydrite), smectite, kaolinite, and gibbsite, are formed though the neoformation process, based on solution composition such as $H_4SiO_4^0$ and pH (Karathanasis, 2018). Transformations, such as

the mica transformation to vermiculite, are also affected (Watanabe et al., 2006). Climate affects soil solution composition, for example, drier conditions cause high $H_4SiO_4^0$ activity and intense precipitation causes low pH. However, studies in moderately dry regions with moderate pH, as in the Tanzanian volcanic regions, are still limited.

The objective of this chapter was to 1) investigate the soil properties in tropical (Tanzanian) volcanic regions; 2) and to estimate the effects of climate on the distribution of secondary nanocrystalline and crystalline minerals in the soils of tropical (Tanzanian) volcanic regions. Thirty sites were chosen to investigate the distribution of soil secondary minerals. Temperature and precipitation varied at the elevations and locations of the sites. All the sites were divided into groups according to their location and chemical composition of the parent tephra deposits. The stabilities of the primary and secondary minerals were determined. I assumed that the distribution of secondary minerals would be affected by the climate, temperature, and precipitation at the sites. The formation of nanocrystalline minerals, which may have a strong ability in SOC stabilization, would be promoted at humid and cool sites with high Al or Fe contents in the soil solution.

2.2 Materials and Methods

2.2.1 Sampling Sites and Soil Samples

Sites of this study were in the volcanic regions of Tanzania in the northern and southern highlands. The northern sites were around Mt. Kilimanjaro and Mt. Meru, and the southern sites were around Mt. Kieyo. Thirty sites were selected across the volcanic regions of Tanzania (Table 2.1 and Fig. 2.1).

In detail, 21 sites were in the northern regions including the southeast humid region of Mt. Kilimanjaro (11 sites; KL-SE), the northwest dry region of Mt. Kilimanjaro (five sites; KL-NW), and the moderately humid region of Mt. Meru (five sites; MR). Nine sites were in southern regions, including the central region (within 10 km of the crater) of Mt. Kieyo (four sites; S-KY-C) and the remote (10–50 km from the crater) region of Mt. Kieyo (five sites; S-KY-R). All sampling sites are within a radius of 50 km from the crater of each mountain. The elevations of the sampling sites ranged from 540 m to 2800 m asl. The annual mean temperatures at all sites ranged from 13 to 25°C, and the annual mean precipitation at the sites ranged from 720 to 2350 mm (representative of 1970–2000) (Fick and Hijmans, 2017). The drainage of the soils at all sites is good. Soil temperature regimes ranged from isohyperthermic to isomesic, and the moisture regimes ranged from ustic to udic. The soils were classified as Andisols, Alfisols, and Vertisol according to Soil Taxonomy (Soil Survey Staff, 2014).

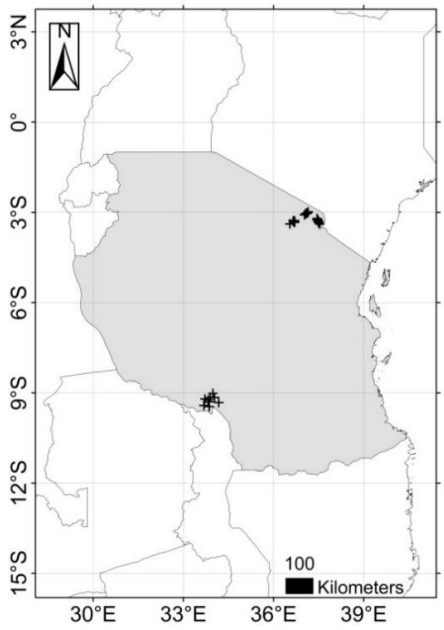

Fig. 2.1 Locations of soils (black crosses) sampled in three regions (boxes) of Mt. Kilimanjaro, Mt. Meru, and Mt. Kieyo in Tanzania (grey shading)

Table 2.1 Information of study sites in Mt. Kilimanjaro, Mt. Meru and Mt. Kieyo

Region	Sites	Parent materials	Elevation	MAT [a]	MAP [a]	EP [a]	STR [b, c]	SMR [b, c]	Soil classification [c]
	No.		m	°C	mm				
Mt. Meru (MR)	5	Phono-tephritic tephra	1360–2240	14.7–19.6	920–1420	37–724	Isothermic (3), Isomesic (1), Isohyperthermic (1)	Ustic (3), Udic (2)	Haplustands (2), Hapludands (2), Haplusterts (1)
Northwest of Mt. Kilimanjaro (KL-NW)	5	Phonolitic tephra	1400–2440	13.2–19.2	750–1180	−119–510	Isomesic (3), Isothemic (2)	Ustic (3), Udic (2)	Haplustalfs (3), Hapludalfs (1), Hapludands (1)
Southeast of Mt. Kilimanjaro (KL-SE)	11	Phonolitic tephra	910–2800	13.2–22.5	720–1640	−372–778	Isothemic (6), Isomesic (4), Isohyperthermic (1)	Udic (9), Ustic (2)	Hapludands (9), Haplustalfs (2)
Remote region of Mt. Kieyo (S-KY-R)	5	Basaltic to tephritic; trachytic to andesitic tephra	540–2410	14.1–24.8	1480–2350	746–1248	Isothermic (3), Isohyperthermic (2)	Udic (4), Ustic (1)	Hapludands (2), Hapludalfs (2), Haplustox (1)
Central region of Mt. Kieyo (S-KY-C)	4	Basaltic to tephritic; trachytic to andesitic tephra	1090–2730	12.6–21.5	1940–2090	1089–1296	Isothemic (4)	Udic (4)	Fulvudands (2), Hapludands (1), Hapludalfs (1)

[a] MAT, mean annual temperature; MAP, mean annual precipitation; EP, excess precipitation.

[b] STR, soil temperature regime; SMR, soil moisture regime.

[c] Soil classifications are according to the Keys to Soil Taxonomy (Soil Survey Staff, 2014).

Information on parent material at the sites was obtained from geological maps of Tanzania (Tanzania Geological Survey, 1959) and the previous studies (Fontijn et al., 2012; Little and Lee, 2006; Little and Lee, 2010; Wilkinson et al., 1986). In the northern highland, volcanic materials were widely distributed. Most of them were typical alkaline volcanic materials: basaltic, phonolitic, and phono-tephritic. There was a difference in parent materials between Mt. Kilimanjaro (phonolitic) and Mt. Meru (phono-tephritic) (Little and Lee, 2006; Little and Lee, 2010). In the southern highland, volcanic materials from Mt. Kieyo were rather complex: basaltic–basanitic–tephritic and phonolitic–trachytic–trachy-andesitic (Fontijn et al., 2012).

In Mt. Kilimanjaro, the oldest phases of volcanic activity began at ~2.5 Ma. The summit crater in Kibo, one of the three volcanic cones, showed the last volcanic activity of Mt. Kilimanjaro (0.15–0.2 Ma) and influenced the northwestern and southeastern slopes of Kilimanjaro (Nonnotte et al., 2008). The volcanic activity in the Meru area occurred in two main episodes, the earlier around 2.0–1.5 Ma and the later around 0.3–0.06 Ma. Minor activities lasted until the present century (1910 AD) at Mt. Meru (Wilkinson et al., 1986). Volcanic activity at Mt. Kieyo started in the mid-Pleistocene, and the oldest volcanic deposit was dated at 0.42 ± 0.03 Ma (Simkin and Siebert, 1994). All the soils (A and B horizons) at sampling sites are formed on the recent tephra deposits.

The local vegetation varied depending on the elevations and local climates. According to the map of the potential natural vegetation of eastern Africa (The Vegetationmap4africa team, 2017), and field observations at the northern sites, the density of vegetation cover in the humid regions was much higher than in dry regions. With an increase in elevation, the precipitation generally increases and the temperature decreases, and the vegetation changed from wooded grassland to rain forest. The relative high precipitation and low evaporation provide enough water resource for the growing of woody plant at the high elevation sites.

For the climate, Mt. Kilimanjaro has a typical equatorial climate. There are two rainy seasons, the long season beginning in March and the short season beginning in November. The driest quarter is from June to September. Climate information, including annual mean temperature and

precipitation, and monthly mean temperature and precipitation at each sampling site were obtained from the WorldClim database (Fick and Hijmans, 2017). The map of climate conditions was prepared by using ArcGIS software (ESRI). The potential evapotranspiration at all sites was estimated (Thornthwaite, 1948) from the monthly temperatures. Excess precipitation (EP), an index for the soil moisture, was calculated by precipitation minus potential evapotranspiration.

Soil profiles were prepared and examined at each site. Soil samples from the top to the bottom horizon were collected at all the sites. Soils from the B horizon were used for the main analyses; most of the samples were collected at a depth of 30–50 cm to reduce the influence of organisms, human activities, and recent volcanic activities. All the samples were air-dried and sieved through a 2 mm mesh before the analyses.

2.2.2 Total Elemental Composition

Total elemental contents were determined by dissolving the whole soil sample in aqua regia and HF in a sealed Teflon container (Hossner, 1996). The dissolution solution was diluted and filtered through a membrane filter of a 0.45 μm pore size (Millipore). The elements (Si, Al, Fe, Ca, Mg, K, and Na) in solution were analyzed by Inductively Coupled Plasma-Atomic Emission Spectrometry (ICP–AES) (ICPE-9000, Shimadzu). The total reserve in bases (TRB) as a weathering index was calculated as the sum of the total Ca, Mg, K, and Na contents (Takeda et al., 2004; Watanabe et al., 2017).

2.2.3 Physicochemical Properties

Soil pH was measured with a glass electrode (Benchtop pH meter F-70 Series, Horiba) at a soil/liquid (H_2O or 1 M KCl) ratio of 1:5 (g/mL). The total C and total N contents of the samples were determined by the dry-combustion method using an NC analyzer (Elementar Analysensysteme, Vario MAX). The CEC of the soil samples was determined by ammonium acetate Method using a solution extracted by 1 M NH_4OAc at pH 7 (Soil Survey Laboratory Staff, 1996).

For the soil particle size analysis, the organic matter of the soil samples was removed by H_2O_2, the pH was adjusted to 9 to 10, and the sample was ultrasonicated. The coarse (0.2–2 mm) and fine (0.02–0.2 mm) sand contents were determined using the sieving method, the silt (2–20 mm) and clay (<2 mm) contents of the sample were determined using the pipette method (Gee and Or, 2018). The clay fraction was then collected under Stokes' law for mineralogical analysis.

2.2.4 Mineralogy

The Al_o, Fe_o, and Si_o, which are included in nanocrystalline minerals and organo-Al complex, were extracted by shaking with ammonium oxalate (0.2 M, pH 3.0); Fe (Fe_d), which represents free iron oxides, extracted by citrate (0.75 M) and hydrosulfite sodium (1 g in 50 mL). Al (Al_p), which represents organo-Al complexes, was extracted by Na-pyrophosphate (0.1 M, pH 10.0) (Blakemore, 1987). The extracts with ammonium oxalate and dithionite-citrate were diluted and filtered through the membrane filter of a 0.45 μm pore size. The extracts with Na-pyrophosphate were filtered through the membrane filter of a 0.025 μm pore size (Millipore) and then diluted. The contents of all the extracts were measured by ICP-AES. The ratio of free Fe oxides (Fe_d) to total Fe (Fe_t) was used as a weathering index along with TRB.

The collected clay fraction was treated as follows: K saturated and dried at 25°C, K saturated and dried at 350°C, K saturated and dried at 550°C, Mg saturated and dried at 25°C, and Mg saturated and dried at 25°C then solvated in glycerol. Totally, 5 treatments were in the X-ray diffractometer analyses. (Harris and Norman White, 2015). The formamide test was applied to distinguish halloysite from kaolinite. The clay fraction is sprayed with formamide, and X-rayed after 30 mins to 1 hour of spraying (Churchman et al., 1984). The mineral composition of the saturated clay fraction was determined using an X-ray diffractometer (XRD) (Miniflex 600, Rigaku) with Cu Kα radiation under the voltage of 40 kV and a current of 15 mA. Peaks in the X-ray diffractionograms were classified into dominant (height is more than twice than other peaks), clear, not clear (height is higher than three times but lower than five times of background noise), and not detected.

The amounts of gibbsite and kaolinite in the clay fraction sample were quantified by differential thermal analysis (DTA) using a TA-60WS thermal analyzer (DTG60, Shimadzu). Iron oxides were removed from clays before DTA by sodium dithionite-citrate solution (pH 7.3) in 80°C water bath to avoid interferences to Al hydroxide (gibbsite). The DTA was performed at a heating rate of 20°C min^{-1} in a N_2 atmosphere.

2.2.5 Thermodynamic Stability of Minerals

The thermodynamic stabilities of the secondary minerals of all 30 samples were analyzed. Soil water extracts of all samples were collected by leaving standing with a soil to water ratio of 1:2 and using a soil sample weight of 80 g. The samples were shaken once a day for 1 week at 25°C and 101 kPa. The sample was then filtered and the solution that passed through a membrane filter of 0.025 μm pore size was collected.

The pH and F^- concentrations were determined using glass electrodes (Benchtop pH meter F-70 Series, Horiba). The aluminum species in the solution were measured before and after passing through a column filled with cation exchange resin (pH 4.2) (Amberlite, IR-120B(H)). The amount of Al retained by the resin was assumed to be inorganic Al (Driscoll, 1984). Aluminum, Fe, and Si concentrations in the solution were measured by ICP-AES. The inorganic C content was measured using a total organic C analyzer (TOC-V CSH, Shimadzu). The cations (Ca^{2+}, Mg^{2+}, K^+, Na^+, and NH_4^+) and the anions (Cl^-, NO_3^-, and SO_4^{2-}) concentrations were measured by a high-performance liquid chromatograph (HPLC-HIC-6A equipped with a CDD-6A detector, Shim-pack IC-C3 for cations, and Shim-pack ICC-A1 for anions, Shimadzu). The ion activities were calculated using Visual MINTEQ 3.1 (Jon Petter Gustafsson, KTH, Sweden). Solubility diagrams that show the solubility of minerals and stability diagrams that show the relative stability of minerals (Van Breemen and Brinkman, 1976) were used to evaluate the stabilities of the minerals in the samples. The thermodynamic equilibrium constants for the stability diagrams of gibbsite, kaolinite, smectite, quartz, and amorphous SiO_2 were taken from Karathanasis (Karathanasis, 2018) and muscovite were taken from Lindsay (Lindsay, 1979).

2.2.6 Statistical Analysis

A principal component analysis was conducted based on the standardized total elemental contents to investigate the parent materials and weathering intensity. The normality of the data for the physiochemical and mineralogical properties, climatic conditions, and elevation was tested. The Pearson product-moment correlation coefficient was used to assess the correlation between physiochemical properties, mineralogical properties, climatic conditions, and elevation. Because most of the total elemental contents were not normally distributed even after being converted to logarithms or square roots, a Spearman rank correlation was applied to them. One-way ANOVA and multiple comparisons were applied to find the difference in the physicochemical and mineralogical properties between groups. Equal variances were assumed based on Duncan method, and the significance level was 0.05. All analyses were completed using IBM SPSS Statistics version 20.0 software.

2.3 Results

2.3.1 Climate at Sampling Sites

The climates of each region are shown in Table 2.1. The values of annual mean temperature negatively correlated with elevation for all the sites ($r = -0.99$, $P < 0.01$). The value of EP is negatively correlated to the elevation for the sites in the northern regions (MR, KL-NW and KL-SE) ($r = -0.60$, $P < 0.01$). In the southern regions, there was no significant correlation between elevation and mean annual precipitation (MAP) because the precipitation is strongly influenced by Lake Malawi. In the regions, MR, KL-NW, and KL-SE, in the northern highland, MAP was relatively lower (720–1640 mm) than in the regions in the southern highland (1480–2350 mm). The MAP in KL-SE was higher than KL-NW because the wind direction during the rainy season in the northern highland is from the southeast (the Indian Ocean) to northwest.

2.3.2 Parent Materials

The total elemental contents and correlations between the contents for all samples are shown in Tables 2.2 and 2.3, respectively. The Si content was negatively correlated with Al and Fe contents, and Al content was positively correlated with Fe content. The Si content was positively correlated with K and Na. The Al content was negatively correlated with Ca, K, and Na. The Fe content was positively correlated with Mg and negatively with K and Na. These correlations indicated that Si, Al, and Fe were associated with base elements reflecting primary minerals (e.g., Si and K in mica, Fe and Mg in mafic minerals) and that the weathering degree was relatively low.

Table 2.2 Total elemental contents of soil samples in different sampling regions

Region	Sites no.	Al	Fe	Ca	K	Mg	Na	Si
					g kg^{-1}			
MR	5	58 ± 4	64 ± 6	46 ± 11	15 ± 7	17 ± 4	12 ± 7	190 ± 28
KL-NW	5	130 ± 10	99 ± 19	6.9 ± 5.8	6.6 ± 2.1	4.0 ± 1.0	3.2 ± 1.5	160 ± 13
KL-SE	11	130 ± 22	110 ± 37	3.4 ± 1.4	3.3 ± 0.9	4.9 ± 1.8	1.5 ± 0.9	100 ± 32
S-KY-R	5	130 ± 19	63 ± 25	1.7 ± 1.0	8.8 ± 5.0	1.3 ± 0.3	14 ± 10	150 ± 17
S-KY-C	4	110 ± 5	29 ±8	5.2 ± 1.6	27 ± 6	1.7 ± 0.4	36 ± 5	190 ± 47

Mean ± standard deviation.

Table 2.3 Correlation matrix (Spearman) for total elemental contents of soils (30 sites)

	Al	Fe	Ca	K	Mg	Na
Fe	0.42**					
Ca	−0.60**	0.02				
K	−0.56**	−0.75**	0.39**			
Mg	−0.27	0.59**	0.71**	−0.21		
Na	−0.45**	−0.77**	0.20	0.84**	−0.37*	
Si	−0.60**	−0.63**	0.22	0.71**	−0.17	0.53**

** Correlation is significant at the 0.01 level (2−tailed).

* Correlation is significant at the 0.05 level (2−tailed).

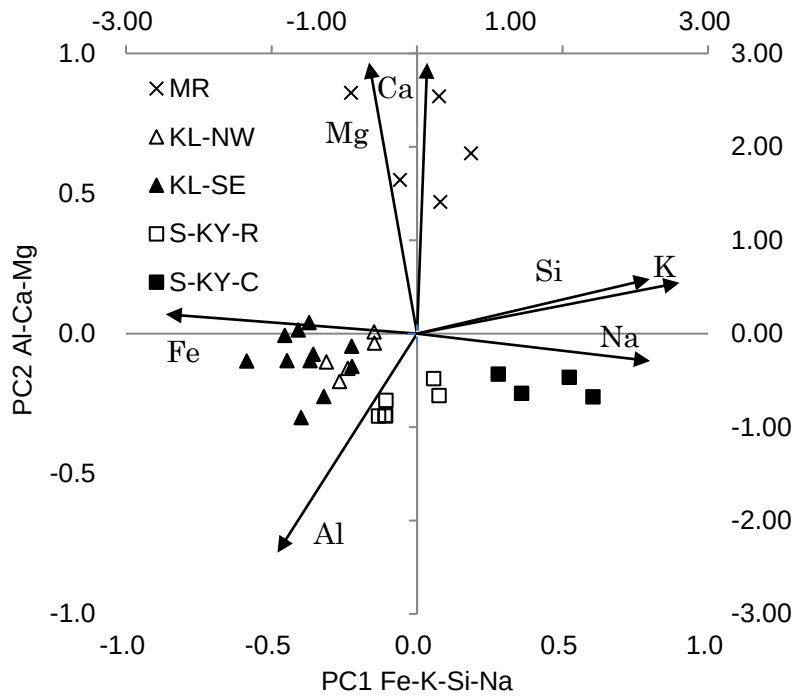

Fig. 2.2 Scores for the principal component analysis for the five sampling regions (MR: Mt. Meru, KL-NW: northwest side of Mt. Kilimanjaro, KL-SE: southeast side of Mt. Kilimanjaro, S-KY-R: remote region of Mt. Kieyo, and S-KY-C: central region of Mt. Kieyo)

The principal component analysis on the result of total elemental analysis was applied to reduce the dimensions and to investigate the parent materials of the soil samples. The first and second principal components represented 81% of the total variance (Table 2.4). According to the component matrix, the first component was the "Fe-Si-K-Na" factor (PC1), which would reflect the type of volcanic deposits (mafic or felsic) of the samples. The second component was the "Al-Mg-Ca" factor (PC2). Coefficients were high for Al, Mg, and Ca and represented 33% of the variance. Both the two components can represent weathering degree of the samples because base cations deplete with weathering (i.e., a direction from quadrants 1 to 3 in Fig. 2.2). The samples from the same region (MR, KL, S-KY-R, and S-KY-C) were found in a similar location in Fig. 2.2 based on the principal component scores. As described above (Table 2.1), at all sites the parent materials are tephra deposits (i.e. fragmental materials). Combining the result of total elemental analysis, the result indicated that the samples in each region have similar parent materials and degrees of weathering.

Table 2.4 Rotated component matrix of the principal component analysis for the total elemental contents of soils (30 sites)

	Rotated Component [a]	
	PC1	PC2
Al	−0.48	−0.78
Fe	−0.86	0.07
Ca	0.04	0.97
K	0.90	0.18
Mg	−0.17	0.97
Si	0.80	0.20
Na	0.80	−0.10
Variance	48%	33%

[a] Rotation converged in 3 iterations.

In the northern regions, KL-NW and KL-SE had low scores for PC1 and rather low scores for PC2. They had high Fe contents (99 ± 19 and 110 ± 37 g kg^{-1}, respectively) and low base elements (Table 2.2). MR had high score for PC2, which indicated high contents of Mg and Ca (17 ± 4 and 46 ± 11 g kg^{-1}, respectively). In the southern regions, the total Fe and Mg contents, which are high in mafic parent materials, of the soils in S-KY-C (29 ± 8 and 1.7 ± 0.4, respectively) and S-KY-R (63 ± 25 and 1.3 ± 0.3, respectively) were relatively low. Compared with S-KY-R, S-KY-C was rich in Si with high K and Na contents, which are high in felsic parent materials. The S-KY-C had a high score for PC1, indicating high Si, K, and Na contents. The S-KY-R had lower scores for both PC1 and PC2. In addition, in these five groups, MR and S-KY-C had high contents of base elements (Table 2.2 and Fig. 2.2).

2.3.3 Soil Physicochemical Properties

The physicochemical properties of the samples in each group are summarized in Table 2.5. The pH (H_2O) was near neutral in all the samples. Sand contents in MR (42 ± 17%) and S-KY-C (57 ± 25%) were higher than those in KL-SE, KL-NW and S-KY-R; whereas, the clay contents had an opposite trend. The pH (KCl) for all the sites correlated with EP ($r = -0.52$, $P < 0.01$) (Table 2.6). The total C correlated with elevation and mean annual temperature (MAT) ($r = -0.60$, $P < 0.01$, and $r = -0.53$, $P < 0.01$, respectively). The sand contents of all sites negatively correlated

with EP ($r = -0.44$, $P < 0.05$).

Table 2.5 Physicochemical properties of the soils in each site

Site	pH(H_2O)	pH(KCl)	CEC [a]	Total C	Soil texture		
			$cmol_c\ kg^{-1}$	$g\ kg^{-1}$	Clay (%)	Silt (%)	Sand (%)
MR	7.2 ± 0.5 a	5.9 ± 0.3 a	36 ± 7 ab	24 ± 19	20 ± 16 c	38 ± 3 ab	42 ± 17 a
KL-NW	6.9 ± 0.4 ab	5.4 ± 0.5 b	42 ± 14 a	29 ± 30	49 ± 20 ab	44 ± 20 a	7.6 ± 1.4 b
KL-SE	6.0 ± 0.7 c	5.0 ± 0.3 bc	24 ± 17 ab	43 ± 42	34 ± 15 bc	43 ± 11 a	23 ± 13 b
S-KY-R	6.4 ± 0.4 bc	4.6 ± 0.2 c	16 ± 12 b	20 ± 16	59 ± 21 a	22 ± 9 b	19 ± 16 b
S-KY-C	6.7 ± 0.5 abc	5.0 ± 0.2 bc	23 ± 4 ab	22 ± 15	15 ± 13 c	28 ± 15 ab	57 ± 25 a

[a] CEC, cation exchange capacity.

Mean ± standard deviation. Means followed by different letters indicate the data were statistically different at $P < 0.05$ among soil groups.

Table 2.6 Pearson's correlation coefficients between climatic data and soil properties

	pH (H_2O)	pH (KCl)	Total C	Sand	Fe_o [a]	Al_o	Si_o	$Al_o + 1/2Fe_o$	Fe_o/Fe_d	Fe_d/Fe_t	Kaolinite
Elevation			0.60^{**}		0.48^{**}	0.61^{**}	0.52^{**}	0.61^{**}	0.51^{**}		-0.58^{**}
MAT[b]			-0.53^{**}		-0.42^{*}	-0.52^{**}	-0.46^{*}	-0.53^{**}	-0.48^{**}		0.56^{**}
EP[b]		-0.52^{**}		0.44^{*}		0.39^{*}		0.37^{*}		0.64^{**}	

** Correlation is significant at the 0.01 level (2-tailed); * Correlation is significant at the 0.05 level (2-tailed).

[a] MAT, mean annual temperature; EP, excess precipitation; Fe_o, Al_o and Si_o, oxalate-extractable Fe, Al and Si, respectively; Fe_d, dithionite-citrate-extractable Fe; Fe_t, total Fe.

2.3.4 Distribution of Soil Minerals

The TRB values in MR (460 ± 91 $cmol_c\ kg^{-1}$) were highest in these five samples followed by those for S-KY-C (270 ± 39 $cmol_c\ kg^{-1}$), which means high contents of primary minerals in the soils in these regions (Table 2.7 and Fig. 3.3a). TRB values of all the sites were relatively high (Table 2.7) probably because of the influence of recent volcanic activities. The weathering indices (TRB and Fe_d/Fe_t) of KL-SE and KL-NW were similar in the same range of elevation (Fig. 3.3a and 3.3b, Table 2.7). On the other hand, the Fe_d/Fe_t of S-KY-R was higher than that in the northern groups (Fig. 3.3b, Table 2.7), indicating more Fe is in the free Fe oxides rather than in the primary minerals. The values of TRB in MR were higher than in S-KY-C, and the values of Fe_d/Fe_t and Fe_o/Fe_d (Fe activity ratio) were lower than those in S-KY-C (Table 2.7).

Table 2.7 Mineral properties of the soils for each group

Region	Fe_o [a]	Al_o [a]	Si_o [a]	Fe_d [a]	Al_o + 1/2 Fe_o	Fe_o/Fe_d	Fe_d/Fe_t [a]	TRB [a]
			g kg^{-1}					$cmol_c$ kg^{-1}
MR	7.2 ± 2.4 b	17 ± 14 b	11 ± 15 ab	14 ± 4 b	20 ± 14 b	0.52 ± 0.13 b	0.21 ± 0.05 c	460 ± 91 a
KL-NW	14 ± 6 ab	16 ± 22 b	5.8 ± 9.5 b	39 ± 11 a	23 ± 24 ab	0.40 ± 0.28 bc	0.40 ± 0.08 b	110 ± 98 c
KL-SE	16 ± 7 a	31 ± 28 ab	7.8 ± 7.4 ab	38 ± 9 a	39 ± 31 ab	0.44 ± 0.23 bc	0.37 ± 0.11 b	72 ± 16 c
S-KY-R	7.3 ± 2.3 b	13 ± 10 b	4.4 ± 7.0 b	40 ± 13 a	16 ± 11 b	0.20 ± 0.11 c	0.67 ± 0.16 a	100 ± 62 c
S-KY-C	13 ± 3 ab	46 ±9 a	19 ± 6 a	17 ± 8 b	52 ± 8 a	0.79 ± 0.16 a	0.57 ± 0.08 a	270 ± 39 b

[a] Fe_o, Al_o and Si_o, oxalate-extractable Fe, Al and Si, respectively; Fe_d, dithionite-citrate-extractable Fe; Fe_t, total Fe; TRB, total reserve in bases.

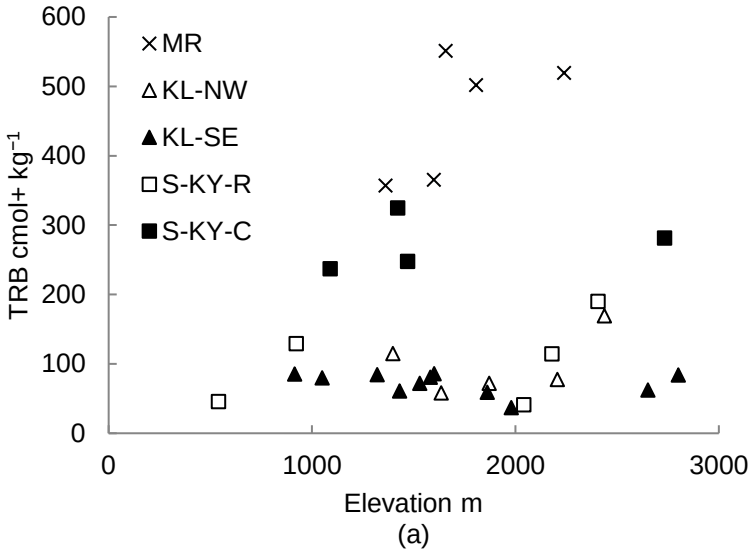

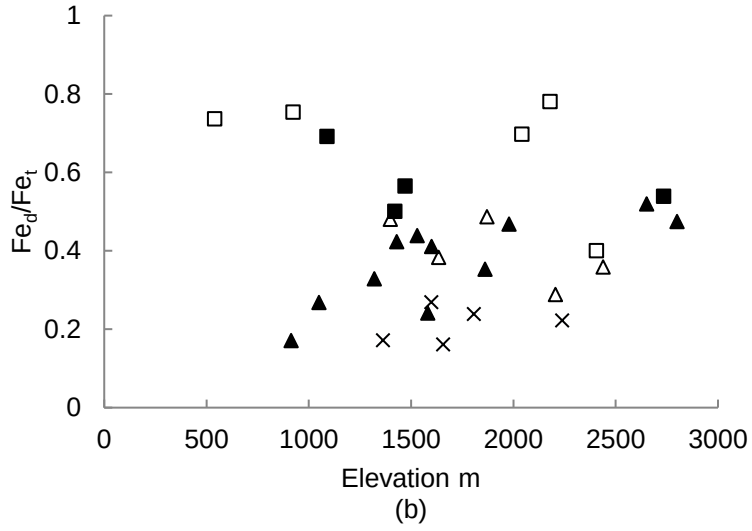

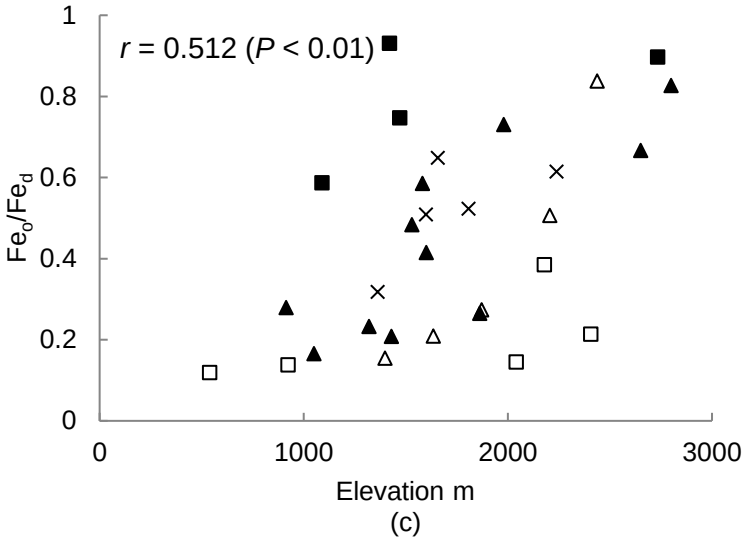

Fig. 2.3 Mineralogical properties (ratio of free Fe oxides to total Fe: Fe_d/Fe_t, total reserve in bases: TRB, and Fe activity ratio: Fe_o/Fe_d) of the samples from different regions at different elevations

The results of selective extraction are shown in Table 2.7 and Fig. 2.4. The values of Al_o + 1/2 Fe_o were high in S-KY-C and the high elevation sites of KL-SE, which had relatively high EP in the northern highland (Fig. 2.4a and 2.4b). The Fe_o was higher in KL-SE than in S-KY-R and MR. The Si_o contents were higher in S-KY-C, which had high total Si content and high TRB, compared to those in KL-NW and S-KY-R (Table 2.7). The Fe_d contents were lower in MR and S-KY-C than in the other three groups. The Fe_o/Fe_d, which shows the activity of free iron oxides, was rather high in all groups, indicating a high proportion of nanocrystalline Fe as ferrihydrite of the Fe oxides. The Fe_o/Fe_d was relatively low in S-KY-R (0.20 ± 0.11), and it was higher in S-KY-C (0.79 ± 0.16) than in MR, KL-SE, and KL-NW (0.52 ± 0.13, 0.44 ± 0.23, and 0.40 ± 0.28, respectively). The KL-SE, having a similar parent material but with a more humid condition compared with KL-NW, had high Al_o + 1/2 Fe_o and Fe_o/Fe_d values.

In high elevation sampling sites (> 1500 m), most of the values of Al_o + 1/2 Fe_o were higher than 20 g kg^{-1}(Fig. 2.4b), which is one of the criteria for the Andic soil property. Significant correlations between Al_o + 1/2 Fe_o and elevation, MAT, and EP were found based on the data from all sites (r = 0.61, P < 0.01; r = −0.53, P < 0.01; r = 0.37, P < 0.05, respectively). The Al_o + 1/2 Fe_o showed different trends in the ranges greater and smaller than 500 mm of EP (Fig. 2.4a). For

greater than 500 mm of EP, Al_o + 1/2 Fe_o were high, but low for areas with less than 500 mm of EP. In the regions with low weathering degree (MR and S-KY-C) and in the relatively dry region (KL-NW), Al_o + 1/2 Fe_o increased with an increase in EP. The value of Fe_o/Fe_d, an indicator of the crystallinity of Fe oxides, was positively correlated with elevation (r = 0.51, P < 0.01) and negatively correlated with MAT (r = −0.48, P < 0.01) (Table 2.6).

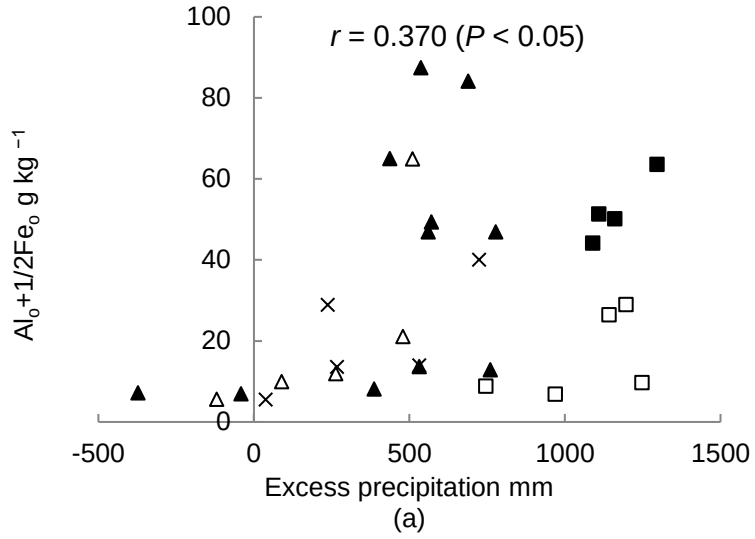

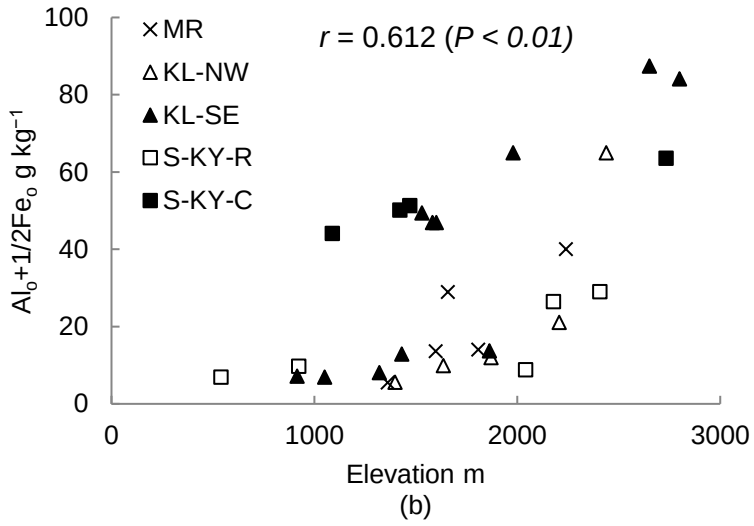

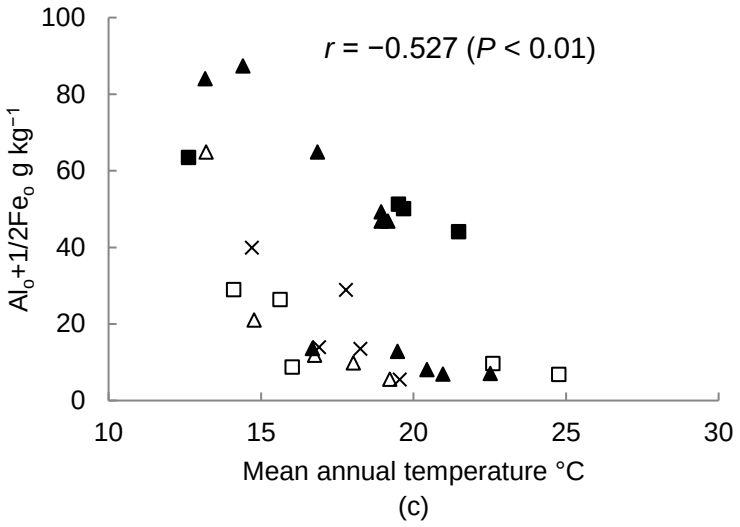

Fig. 2.4 Distributions of nanocrystalline minerals in each region at different elevations under varied climatic conditions

The X-ray diffractionograms showed that more than half of the clay samples had a 0.7-nm peak (Table 2.8). However, a clear peak shift from 0.7-nm to 1.0-nm was not found when the formamide test was applied, indicating the absence of halloysite (Churchman et al., 1984), and instead kaolinite was identified. Most of the clay samples had a 0.7-nm peak in S-KY-R, KL-NW, and the low elevation sites of the other regions. Mica peaks appeared in a few samples at low elevation sites, which might be influenced by windblown mica derived from surrounding materials other than volcanic deposits (e.g., Lowe, 1986). No peak at 1.4-nm was detected for all the samples. The result of the DTA showed that the kaolinite content in S-KY-R (620 ± 170 mg kg^{-1}) was higher than in MR, KL-SE, and S-KY-C, and there was no significant difference between S-KY-R and KL-NW. Gibbsite was found in KL-SE, S-KY-R, and S-KY-C with rather high EP (> 500 mm) (Fig. 2.5). The gibbsite content in KL-SE was higher than in S-KY-R and S-KY-C at similar elevations (Table 2.8).

The kaolinite contents negatively correlated with elevation (r = −0.58, P < 0.01) and positively correlated with temperature (r = 0.56, P < 0.01). The gibbsite contents did not correlate with climatic data (Table 2.6) but correlated with pH (H_2O) (r = −0.62, P < 0.01).

Table 2.8 Mineral properties of the soil for each site

Site	Elevation	Detection by XRD [a]			Detection by DTA [a]	
		1.4 nm	Kaolinite	Mica	Gibbsite	Kaolinite
	m				g kg^{-1} clay	
Mt.Meru (MR)						
MR1	1360	−	(+)	(+)	0.2	330
MR2	2240	−	−	(+)	0.1	2.0
MR3	1660	−	−	−	0.2	220
MR4	1810	−	−	−	19	2.3
MR5	1600	−	(+)	+	0.6	380
Northwest of Mt.Kilimanjaro (KL-NW)						
KL-NW1	2210	−	++	(+)	5.0	310
KL-NW2	2440	−	−	−	0.1	9.3
KL-NW3	1870	−	++	+	0.8	600
KL-NW4	1640	−	++	(+)	0.1	720
KL-NW5	1400	−	++	+	0.1	560
Southeast of Mt.Kilimanjaro (KL-SE)						
KL-SE1	1580	−	−	−	220	17
KL-SE2	910	−	++	+	0.1	580
KL-SE3	2800	−	−	−	0.2	−
KL-SE4	2650	−	−	−	16	−
KL-SE5	1980	−	−	−	310	−
KL-SE6	1860	−	(+)	−	390	270
KL-SE7	1600	−	−	−	220	86
KL-SE8	1530	−	−	−	290	61
KL-SE9	1430	−	+	+	230	420
KL-SE10	1320	−	++	(+)	9.4	730
KL-SE11	1050	−	++	+	8.3	590
South-Remote region of Mt.Kieyo (S-KY-R)						
S-KY-R1	2410	−	(+)	−	0.4	430
S-KY-R2	2180	−	++	−	27	650
S-KY-R3	2040	−	++	−	170	450
S-KY-R4	920	−	++	−	48	780
S-KY-R5	540	−	++	−	21	770
South-Central region of Mt.Kieyo (S-KY-C)						
S-KY-C1	2730	−	−	(+)	−	−
S-KY-C2	1470	−	−	−	2.3	280
S-KY-C3	1420	−	−	−	−	−
S-KY-C4	1090	−	++	−	110	480

[a] XRD, DTA: ++, dominant; +, clear; (+), not clear; –, not detected.

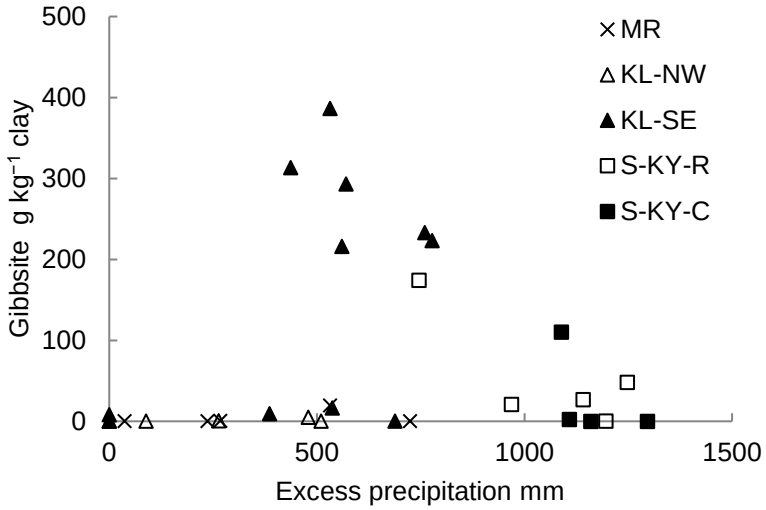

Fig. 2.5 Relationship between excess precipitation and gibbsite contents in the clay fractions of the soil samples from each region.

2.3.4 Stability of Minerals Determined by Composition of Soil Water Extracts

The pH of the soil water extracts of the soil samples from MR, KL-NW, KL-SE, S-KY-R and S-KY-C were near neutral, ranging from 6.5 to 8.0, 6.4 to 7.3, 5.0 to 7.3, 5.8 to 6.9, and 6.3 to 7.4, respectively. The logarithmic $H_4SiO_4^0$ activities of soil samples from MR, KL-NW, KL-SE, S-KY-R, and S-KY-C ranged from −3.7 to −3.3, −4.0 to −3.4, −4.2 to −3.8, −4.4 to −3.6, and −3.8 to −3.7, respectively. The $H_4SiO_4^0$ activities and pH were relatively high in MR, and $H_4SiO_4^0$ activities were relatively low in KL-SE.

Solubility diagrams were applied to assess the solubility of minerals in the samples. Because Al in the soil water extracts could not be detected, S-KY-R5, KL-NW5, KL-SE2, KL-SE6 and KL-SE9 were excluded (Fig. 2.6, 2.7 and 2.8). According to the solubility diagram, smectite was able to exist in MR, S-KY-C, KL-NW, and the high elevation sites of KL-SE. At KL-SE1, KL-SE5, and KL-SE6 (the three plots below the kaolinite dissolution line in Fig. 2.6) were under saturated with kaolinite indicating dissolution of kaolinite. At the sites of S-KY-R3 and S-KY-R4 were plotted below the kaolinite line, indicating kaolinite was present but decreasing. In most of the samples, amorphous Al was under saturated, which meant it decreased except for some sites in MR, S-KY-C, KL-NW, and the high elevation sites of KL-SE.

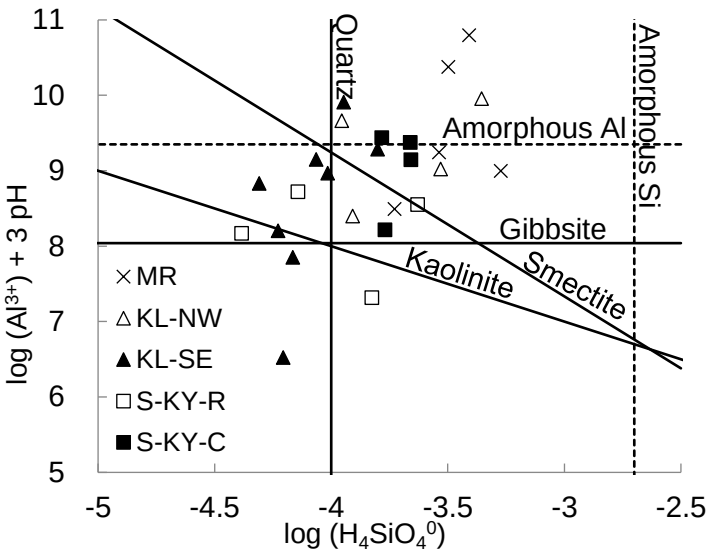

Fig. 2.6 Composition of the soil water extract of samples from different regions plotted on solubility diagrams

Because the five excluded samples lacked the data for Al^{3+} activity, it was better to use stability diagrams without Al^{3+} to show the relative stabilities of minerals in each group. Fig. 2.7 represented the relative stabilities of gibbsite, kaolinite, and smectite. The result showed that most of the samples were in the gibbsite or kaolinite stability fields. Nine samples from KL-SE and three samples from S-KY-R were in the gibbsite stability field. All the samples from S-KY-C and four samples from KL-NW were in the kaolinite stability field. Twenty-six samples were not in the field of smectite stability, and four samples from MR and one sample from KL-NW were on the boundary of the smectite stability and kaolinite stability fields (Fig. 2.7). The samples that contained high amounts (> 20 g kg^{-1} clay) of gibbsite were from KL-SE and S-KY-R and, under high EP conditions (> 500 mm), were in the field of gibbsite with low $H_4SiO_4^0$ activities.

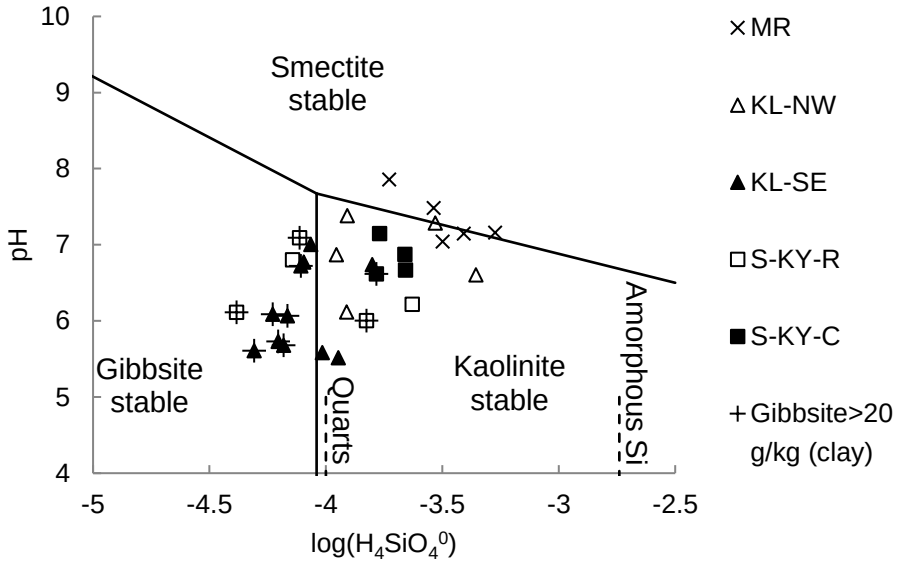

Fig. 2.7 Composition of the soil water extracts of samples from different regions plotted on stability diagrams representing the relative stability of smectite, kaolinite, and gibbsite

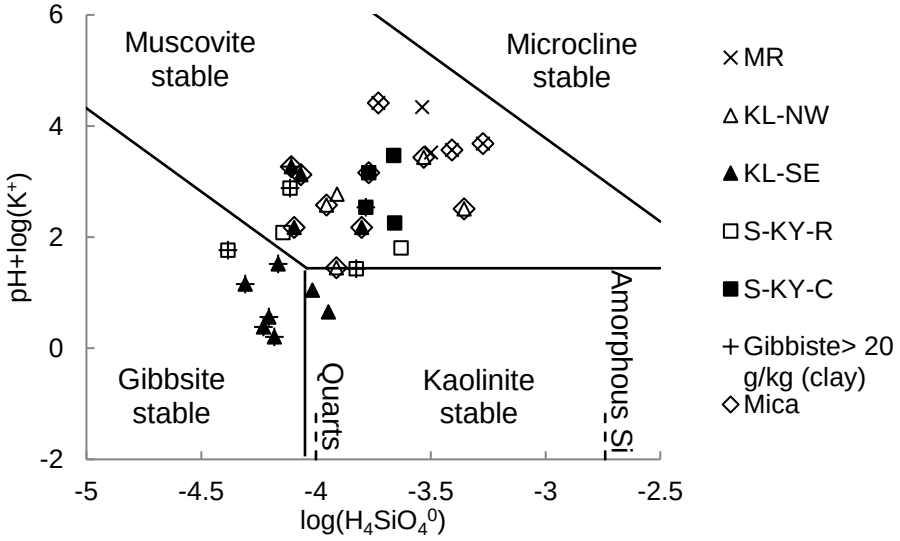

Fig. 2.8 Composition of the soil solution extracts of samples from different regions plotted on stability diagrams representing the relative stability of muscovite, microcline, kaolinite, and gibbsite

The stability diagram of gibbsite, kaolinite, and muscovite (Fig. 2.8) represented that samples from KL-NW, MR, and S-KY-C had high values of pH + log (K^+) and high $H_4SiO_4^0$ activities and were in the muscovite stability field. The samples including mica (Table 2.8) were all in the muscovite stability field. Mica that may be di-octahedral is stable under these soil solution conditions, though mica does not precipitate (neo-form) in soil solution.

2.4 Discussion

2.4.1 Parent Materials and Weathering Degree

The volcanic deposits of the regions in the northern highland (MR, KL-NW, and KL-SE) are similar (both in physical character and chemical composition) to one another but different from those of the regions in the southern highland (S-KY-C and S-KY-R). In the northern regions of Tanzania, the parent materials at the sites of KL-NW, KL-SE, and MR are intermediate or mafic; specifically, at the sites of MR, KL-NW, and KL-SE, the parent materials were close to phonolite or phono-tephrite based on total elemental analysis. The results are congruent with previous studies (Little and Lee, 2006, 2010). The Fe was concentrated in the soil with the desilication process. The total Fe content of each site is higher than the Fe contents of andesite (55 g kg^{-1}) (Best, 2003) (Table 2). At the sites in MR, the soils were rich in Ca and Mg, and the Al and Fe were relatively low compared to those in KL-NW and KL-SE (Fig. 2.2). The relatively high pH (H_2O) values (Table 5) at all the sites compared with soils in humid Asia, such as in Japan and Indonesia (Watanabe et al., 2006), might result in high amounts of primary mineral remaining.

In the southern regions of Tanzania, the parent materials at the sites of S-KY-R and S-KY-C are felsic. The result of the total elemental analysis showed that the soils at the sites of S-KY-R and S-KY-C are rich in Si, K, and Na, which indicates the parent materials in the S-KY-R and S-KY-C groups should be close to tephrite rather than basalt (Best, 2003). The total Fe and Mg contents of soils in S-KY-C (29 ± 8 and 1.7 ± 0.4, respectively) and S-KY-R (63 ± 25 and 1.3 ± 0.3, respectively) were relatively low, indicating the soils were more felsic compared with those in KL-NW, KL-SE, and MR (Table 2.2 and Fig. 2.2).

The high TRB values, high Fe activity ratio (Fe_o/Fe_d) and low ratio of free Fe oxides to total Fe (Fe_d/Fe_t) (Table 7) indicate the degree of weathering of the soils in the volcanic regions of Tanzania are relatively low (IUSS Working Group WRB, 2015). Specifically, the weathering degrees of the soils in MR and S-KY-C are lower than in KL-NW, KL-SE, and S-KY-R. The soils of S-KY-C had high TRB, which indicates a lower weathering degree than in the S-KY-R group that would be the most weathered (Table 2.7). The climatic condition would affect the degree of

weathering of the soils. The intensive rainfall and high temperature in S-KY-R (Table 2.1) would result in higher weathering. The high leaching rate should be the reason for the relatively high weathering degree at the sites of S-KY-C compared to that at MR, both of which have soils of similar age.

2.4.2 Distribution of Nanocrystalline Minerals

The distribution of nanocrystalline Al and Fe is mainly controlled by soil moisture and temperature in this study. At the sites of Mt. Kilimanjaro (KL-SE and KL-NW), where the weathering degree of the soils was higher than that at MR and S-KY-C, the soils from low elevation sites that had low EP (<500 mm) and low values of $Al_o + 1/2Fe_o$ (Fig. 2.4a). Within the high elevation sites (>1500 m asl), the soils from humid KL-SE contained higher values of $Al_o + 1/2Fe_o$ than the soils from KL-NW that had drier conditions. In addition, at the low moisture sites (EP < 500 mm), $Al_o + 1/2Fe_o$ increased with increasing EP. In contrast, at the high moisture sites (EP > 500 mm), no trend was found between $Al_o + 1/2Fe_o$ and EP (Table 6 and Fig. 2.4a). These results indicate that the drying of the soils would accelerate the crystallization of Al and Fe. Under dry conditions, the supply of Fe and Al along with Si to form new nanocrystalline Al and Fe is limited because of the restricted leaching (Georgoulias and Moustakas, 2010), and the extended dry period would also prevent the accumulation of organic matter, which would accompany the nanocrystalline Al and Fe.

In the regions with a lower weathering degree (MR and S-KY-C), EP still strongly influences the distribution of nanocrystalline Al and Fe even at the humid sites (EP > 500 mm) (Fig. 2.4a). The contents of nanocrystalline Al and Fe were relatively higher in S-KY-C than in MR. Considering all the sites of MR with S-KY-C, the contents of nanocrystalline Al and Fe were higher in high EP sites. These indicate that the high soil moisture caused by high EP would accelerate the dissolution of primary minerals and retard the crystallization, which creates a favorable condition for the formation of nanocrystalline Al and Fe at a relatively early stage of soil genesis.

The soil mineralogical parameters, such as Si_o, $Al_o + 1/2Fe_o$, and Fe_o/Fe_d, were positively

correlated with elevation and negatively with MAT for all the sites (Table 2.6 and Fig. 2.4c). The low MAT would retard the crystallization of nanocrystalline Al and Fe. At the sites that had relatively low weathering degree and sufficient moisture (EP > 500 mm), the temperature is the primary factor controlling the distribution of nanocrystalline minerals. In high-temperature soils, Fe oxides should be primarily crystalline, while nanocrystalline Fe oxides are dominant in low-temperature soils (Diaz et al., 2010). The conditions of my study had a rather narrow and low temperature range, but I still think high MAT at low elevations would accelerate the crystallization of Al and Fe oxides. High organic matter content at low temperature sites would also inhibit the crystallization of nanocrystalline minerals (Huang et al., 2018). In S-KY-R that had humid condition, the soils at high elevation sites had more Si_o, Al_o and Fe_o but were lower than those in KL-SE and S-KY-C. Enhanced weathering in the soils of S-KY-R would result in the crystallization of minerals.

2.4.3 Distribution of Crystalline Secondary Minerals

The formations of crystalline minerals (smectite, kaolinite, and gibbsite) are affected by soil solution compositions, which are mainly controlled by soil moisture and the elemental content of the parent materials. The absence of halloysite may be because of the significant seasonal drying and the moderate soil pH of the soils. The constant presence of water and low pH of soil promotes the formation of halloysite, whereas the kaolinite tends to form at sites with the alternation of moist and dry conditions, especially drying (Churchman et al., 2016; Churchman et al., 2010; Cunningham et al., 2016). The amount of kaolinite is negatively correlated with elevation (Table 2.6). The soils from low elevations have high kaolinite contents (Table 2.8). The kaolinite may form at the expense of nanocrystalline minerals because of the higher temperatures at the low elevation sites (Watanabe et al., 2017). The high $H_4SiO_4^0$ activities found in kaolinite stability field (Fig. 2.7) favor the formation of kaolinite.

In contrast, gibbsite is found in soils from the sites with high EP (Fig. 2.5), which have low $H_4SiO_4^0$ activities, and the gibbsite is more stability in the soils (Figs. 2.7 and 2.8) (Huang et al.,

2018). Gibbsite is detected in the soils of KL-SE where the weathering degree is relatively high and $H_4SiO_4^0$ activities are low. Gibbsite is absent in the S-KY-C group but present in the S-KY-R group (Table 8). This is probably because of the high primary minerals remaining (Fig. 2.3a and 2.3c) in the soils of S-KY-C, which leads to high $H_4SiO_4^0$ activities (Fig. 2.8). The high $H_4SiO_4^0$ activities would retard the formation of gibbsite (Huang et al., 2018; Karathanasis, 2018; Watanabe et al., 2006; Watanabe et al., 2017).

In this study, expandable 2:1 type minerals (smectite and vermiculite) are absent in all the soils. In dry condition, soils from andesite contain 2:1 crystalline minerals such as smectite and vermiculite in addition to kaolinite and nanocrystalline minerals (Rasmussen et al., 2010; Vingiani et al., 2004). The CEC of the soils at MR and KL-NW are high considering the contribution from organic matter (Table 2.5), which may result from the presence of 2:1 type minerals. In this study, however, the soils of KL-NW and MR, which have dry condition, have an absence of smectite. The reason for the absence may be that smectite is still in small crystals with less long-range ordered crystalline structure, which cannot be detected by X-ray diffractogram (van der Gaast et al., 1986). Other reasons might be the low Fe^{3+} and Mg^{2+} activities in the soil solution that retard the formation of smectite and the abundance of nanocrystalline Al minerals that may inhibit 2:1 minerals formation through the competition for available Al (Zehetner et al., 2003). For the transformation of vermiculite from mica, soil solutions at all the sites that contain mica are in the muscovite stability field (Fig. 2.8), and mica is stable and does not transform.

2.5 Conclusion

Both soil moisture and temperature are critical factors controlling the distribution of crystalline and nanocrystalline secondary minerals with weathering degrees in the volcanic regions of Tanzania. In the weakly weathered soils, Al_o and Fe_o are high and sensitive to the changes in moisture and temperature. Low EP would be favorable for the crystallization of nanocrystalline Al and Fe. At low moisture sites (EP < 500 mm), insufficient EP would limit the distribution of the nanocrystalline minerals. Moreover, low temperature would retard the crystallization of

nanocrystalline Al and Fe. At the sites with enough moisture (EP > 500 mm), the temperature is the primary factor controlling the distribution of nanocrystalline minerals. The low MAT with enough moisture would retard the crystallization of nanocrystalline Al and Fe, which leads to high $Al_o + 1/2Fe_o$ and high Fe_o/Fe_d values. If the soil is weathered (S-KY-R), Al_o and Fe_o are low, even if the soil has moist conditions.

The formation of crystalline secondary minerals (kaolinite and gibbsite) is controlled by the chemical compositions of soil solutions that reflect the moisture condition and Si content of the soils. The formation of kaolinite is favored at the sites that have high $H_4SiO_4^0$ activities caused by relatively low leaching rates with high MAT or high Si remaining from primary minerals or both. Meanwhile, the marked dry season promotes the formation of kaolinite but retards the formation of halloysite. In contrast, gibbsite is stable with low $H_4SiO_4^0$ activities, reflecting high leaching rates and high weathering degree.

This study clearly shows the importance of climate (temperature and precipitation) as the controlling factor for nanocrystalline and crystalline minerals distribution in volcanic soils. The comprehensive effect of climate and nanocrystalline minerals on soil organic carbon storage was discovered in this study and was further studied and discussed in the next chapter.

CHAPTER 3

SOIL ORGANIC CARBON POOLS CONTROLLED BY CLIMATE AND NANOCRYSTALLINE MINERALS IN TOPSOIL

3.1 General

Understanding the effects of controlling factors on SOC content is essential to make models that predict the change of SOC stocks under future climate conditions (Illiger et al., 2019; Yigini and Panagos, 2016). Some of these factors have been studied, while the controlling factors interact with each other and influence SOC simultaneously (Doetterl et al., 2015). On the other hand, SOC is not a homogenous whole body but consists of various functional pools that have different MRTs and are controlled by specific stabilization mechanisms (von Lützow et al., 2007). The labile SOC pool, which has a short MRT and consists of fresh organic matter, is highly dependent on environmental conditions (Gulde et al., 2008; Schlesinger, 1995). The labile SOC is essential for short-term C and N cycling and has been studied intensively owing to its sensitivity to climate change. However, not only the labile SOC, which is temperature-sensitive, is affected by climate variations, but also the stability of carbon with a relatively long MRT declines with the continuous warming (Davidson and Janssens, 2006; Rey and Jarvis, 2006). The temperature sensitivity of resistant SOC pools is similar to that of the labile pool, and both pools are expected to respond similarly to global warming (Fang et al., 2005). The awareness of the importance of mid–long MRTs carbon in the carbon cycle has been increasing in recent years. Still, the underlying mechanisms of SOC stabilization and the factors regulating the storage of SOC with mid–long MRTs are unclear. Thus, dividing SOC into different pools based on MRT and determining the effects of climatic and geochemical properties on the size, proportion, and MRT of each SOC pool could clarify the factors that control the storage and stability of SOC. Herein, partitioning SOC pools with the consideration of MRTs have been successfully done by fitting the multiple-pool first-order model to respired CO_2 with measurement of soil organic matter (SOM) fractions

(Collins et al., 2000; Tian et al., 2016; Wang et al., 2017).

Soils under natural forest and grassland are widely distributed and have a strong ability to stabilize C (Gong et al., 2013; Jobbagy and Jackson, 2000). Forest soils may hold as much as 70% of the global SOC stock and play a vital role in the global carbon cycle (Batjes, 2016; Lal, 2005; von Lützow and Kögel-Knabner, 2009). Declining SOC stability will dramatically influence soil carbon storage, especially in soils under natural and largely-undisturbed vegetation, including forests with a high SOC content. Previous studies focusing on the factors that control SOC storage and stability have mainly concentrated on soils in temperate regions, which are predicted to be sensitive to climate change (Li et al., 2017; Sanchez-Gonzalez et al., 2017). Compared to temperate regions, studies on SOC dynamics and its controlling factors in tropical regions, in which carbon cycles more rapidly, are much scarcer. The ability of nanocrystalline Al and Fe to stabilize SOC has been mentioned (Filimonova et al., 2016; Garrido and Matus, 2012; Wagai et al., 2015; Yu et al., 2017), whereas the effects of nanocrystalline minerals on individual SOC pools of tropical volcanic regions remain unclear. Therefore, the volcanic regions of Tanzania and Indonesia, where has diverse climates, similar parent materials, rich in nanocrystalline minerals, and dense cover of largely-undisturbed vegetation, are the ideal regions for studying these phenomena.

The objective of this study was to determine the factors (climatic and geochemical) that control the storages and stabilities of SOC pools. To achieve this objective, SOM fractionation was performed, and a three-pool first-order kinetic model was fitted to the SOC decomposition curve produced over long-term incubation, using soils from tropical volcanic regions. I hypothesized that climatic factors affect the labile SOC pool, while geochemical factors, especially nanocrystalline minerals influence more stable pools.

3.2 Materials and Methods

3.2.1 Study Sites and Soil Sampling

The study sites were located in tropical volcanic regions of Tanzania and Indonesia. A total of 24 sites were selected in two regions of each country with less human impact (Table 3.1). The map of sampling sites was prepared by using ArcGIS software (ESRI) (Fig. 3.1). In Indonesia, six sites were selected at Mt. Tengger, East Java (IJ) (340–1680 m asl.), and six sites at Mt. Sibyak, North Sumatra (IS) (220–1440 m asl.). In Tanzania, six sites each were selected from the southeast (TE) (1030–1910 m asl.), and the northwest slopes of Mt. Kilimanjaro (TW) (1470–2710 m asl.). All sites were selected at locations with good drainage conditions along the elevation gradient. The study sites were within a 50 km radius from the volcanic crater and were covered by natural or largely-undisturbed vegetation (mostly forest). The MAT at the sites ranged from 12 to 26°C, and MAP ranged from and 800 to 3300 mm (Fick and Hijmans, 2017). In Indonesia, the MAP in North Sumatra was higher than in East Java, and the soils were humid throughout the entire year at the sites of IS. The precipitation in Tanzania was lower than in Indonesia, and the MAP of the southeast slope was higher than that of the northwest slope due to the wind direction in the rainy season.

Table 3.1 Fundamental information on study sites

Region	Sites	Elevation	MAT [a]	MAP [a]	EP [a]	STR [b, c]	SMR [b, c]	Soil classification [c]	NPP [d]
	No.	m	°C	mm	mm				g C m^{-2} yr^{-1}
Java, Indonesia (IJ)	6	340–1680	17.3–24.7	1960–3280	620–2450	Isothermic (2) Isohyperthemic (4)	Ustic (1), Udic (5)	Andisols (6)	900–1030
Sumatra, Indonesia (IS)	6	220–1440	19.0–25.8	2220–2980	1100–1810	Isothermic (2) Isohyperthemic (4)	Udic (6)	Ultisol (1) Andisols (5)	950–1030
Southeast slope of Kilimanjaro, Tanzania (TE)	6	1030–1910	17.1–21.9	910–1690	−130–790	Isothermic (6)	Ustic (1), Udic (5)	Ultisols (2) Andisols (4)	330–770
Northwest slope of Kilimanjaro, Tanzania (TW)	6	1470–2710	12.2–19.0	800–1230	−50–600	Isomesic (2) Isothermic (4)	Ustic (2), Udic (4)	Alfisols (2) Andisols (4)	290–670

[a] MAT, mean annual temperature; MAP, mean annual precipitation; EP, excess precipitation.
[b] STR, soil temperature regime, SMR, soil moisture regime. [c] Soil temperature and moisture regime, and soil classification (Soil Survey Staff, 2014). [d] NPP, net primary production (potential).

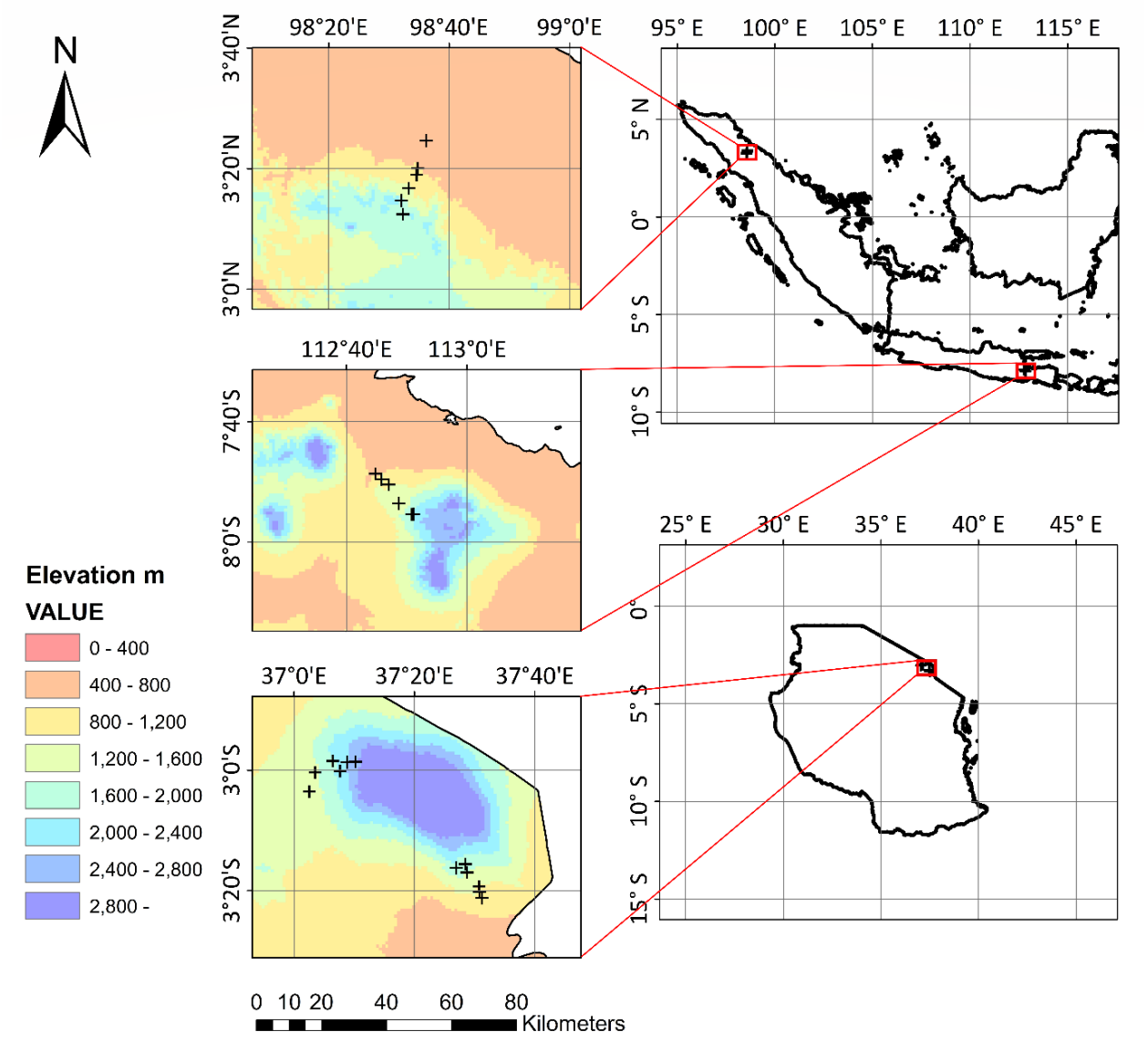

Fig. 3.1 The location of the study regions and the specific sampling sites

Due to the difficulties in making soil profile replicates in wild mountain forests, one shallow soil profile (1 m × 1 m, 50 cm depth) was made at a relatively flat and representative location (e.g., away from main roots, without apparent disturbance of wild animals, and average canopy cover) for each site. The same amount of surface soils (0–15 cm) were collected by trowel from each of four sides of the soil profile after removing the surface plant residues. The collected soils were carefully mixed as a composite sample for each site (Pennock et al., 2007). Each composite soil sample (1 kg per sample, n = 24) was separated into two parts: one of which was preserved in the refrigerator at 3°C, and the other of which was air-dried. All samples were sieved through a 2 mm

mesh and mixed well before incubation and analyses. The soils at the study sites were classified as Andisols, Ultisols, and Alfisols, according to USDA Soil Taxonomy (Soil Survey Staff, 2014). The soil moisture regimes ranged from ustic to udic, and the temperature regimes ranged from isohyperthermic to isomesic (Table 3.1).

3.2.2 Climate, Vegetation and Parent Material of Study Sites

Sumatra and Java generally possess a tropical climate with one primary rainy season (November to March), whereas Mt. Kilimanjaro generally exhibits an equatorial climate with both long (from March to May) and short (within November to February) rainy seasons as described in Chapter 2 (2.2.1). The driest period in Sumatra and Java runs from June to October, which is similar to the dry season in Mt. Kilimanjaro. The MAT, MAP, monthly mean temperatures, and precipitation at each study site were obtained from the WorldClim database (Fick and Hijmans, 2017). Excess precipitation per year (EP), which is used to evaluate the soil moisture, was calculated by subtracting potential evapotranspiration from precipitation (2.2.1).

Vegetation types were clarified according to field observations. For the IJ sites, the natural vegetation was woodland at elevations lower than 400 m asl., and this changed to rainforest at higher elevation sites. For the IS sites, the natural vegetation was rainforest. For the TE sites, the natural vegetation was deciduous wooded grassland at sites lower than 1100 m asl., and the natural vegetation was Afromontane dry transitional forest or rainforest at elevations higher than 1100 m asl. For the TW sites, the natural vegetation was deciduous wooded grassland at sites lower than 1600 m asl., and this changed to Afromontane forest. The most elevated site of TW (TW-6) was in the Montane Ericaceous belt (2710 m asl.), and this site had the lowest temperature of any site and was frequently exposed to fire disturbance (Newmark, 1991). All sampling sites were selected at locations not influenced by leguminous plants. The net primary production (NPP) for each site was calculated using the MAT and MAP values, with the consideration of vegetation types (Del Grosso et al., 2008).

The parent materials of Tanzanian sites were described in Chapter 2 (2.2.1 and 2.3.2). The

parent materials of Indonesian sites were based on a simplified geological map of Sumatra (Crow and Barber, 2005), and a previous study (Darman et al., 2000). The parent materials of the IS and IJ sites were andesitic tephra deposits, whereas the parent materials of all Mt. Kilimanjaro sites were tephritic to phonolitic tephra deposits. The latest major volcanic activities for all sites were within the Holocene and Late Pleistocene (Crow and Barber, 2005; Darman et al., 2000; Nonnotte et al., 2011; Nonnotte et al., 2008).

3.2.3 Physicochemical Properties

The exchangeable cations of soil (Ca^{2+}, Mg^{2+}, K^{+}, and Na^{+}) were extracted using 1 M ammonium acetate at pH 7.0. Exchangeable Ca^{2+} and Mg^{2+} were determined by flame atomic absorption spectroscopy, and exchangeable K^{+} and Na^{+} were determined by flame emission spectroscopy (AA-660, Shimadzu, Kyoto, Japan). The total C and total N contents of the soil samples were determined by the dry combustion method using a CN analyzer (EA IsoLink CN IRMS System, Thermo Fisher Scientific, MA, USA). The total C was a proper parameter to indicate the SOC content because these soil samples were carbonate free.

The Al_o and Fe_o, which indicate the content of nanocrystalline minerals, were extracted using ammonium oxalate (0.2 M, pH 3.0) by shaking samples in the dark for 4 h. Then, the mixed solutions were centrifuged at 2600 × *g* for 10 minutes, and the supernatants were filtered through a 0.45-μm pore membrane filter (Millipore) (Blakemore, 1987). The Al and Fe contents of the filtered solutions were then determined using an inductively coupled plasma atomic emission spectrometry (ICP–AES) (ICPE-9000, Shimadzu, Kyoto, Japan).

The methods of the other soil properties analyses, including soil pH, CEC, and soil texture, are described in Chapter 2 (2.2.1). The accuracy of measured physicochemical properties was confirmed by the additional known-value soil sample.

3.2.4 SOM Fractionation

Soil organic matter fractionation was performed to directly measure the quantity and quality of the different SOM fractions (representing different SOC stabilities). Air-dried soil (10 g) was used in SOM fractionation. Density fractionation was applied first using sodium iodide solution with a density of 1.6 g cm^{-3}. Soil samples were dispersed in sodium iodide solution, and mixed solutions were centrifuged at 2600 × *g* to separate the light (particles flowing on the supernatant, LF) and heavy fractions (sediment, HF) (Kadono et al., 2008). Both light and heavy fractions were washed by 0.01 M $CaCl_2$ then deionized water carefully to remove the iodide and were dried at 70°C. After that, five grams of the well-mixed dried heavy fraction was treated with 15 mL of 5 g L^{-1} sodium hexametaphosphate with 15 h of shaking for dispersion. Then, the occluded particulate organic matter in aggregates (oPOM) (>53 μm), and the mineral associated organic matter (≤53 μm) were separated from the dispersed solution by sieving (Cambardella and Elliott, 1992). Further, the mineral-associated organic matter (1 g, 70°C dried) was collected to determine the resistant fraction (non-hydrolyzable SOM fraction) by refluxing with 6 M HCl at 115°C for 16 h using a temperature-controlled digestion block (Paul et al., 2001b). Acid refluxed samples were washed three times with deionized water. After drying at 70°C and weighing, the carbon and nitrogen contents of each fraction were determined using a CN analyzer. The soil microbial biomass carbon (MBC) and nitrogen of fresh soils before incubation were estimated using the fumigation-extraction method (kEC = 0.45 and kEN = 0.54) (Joergensen, 1996). The organic C and total N of extracted solutions with and without fumigation were determined using a combustion catalytic oxidation method (TOC-L, Shimadzu, Kyoto, Japan).

3.2.5 Laboratory Incubation

Laboratory incubation was conducted for 343 days with the incubation temperature set at 25°C in the dark to evaluate the SOC decomposition. For each soil, three replicate samples (fresh soil, equivalent to 20 g oven-dry soil per sample) were weighed and placed in glass jars (225 mL, 7 cm diameter). The moisture of the soil samples was adjusted and maintained at 55% of the water

holding capacity through the addition of deionized H_2O at regular intervals (2 weeks). All the soil samples were pre-incubated for three days at 25°C after the moisture adjustment to equilibrate the disturbance. The released CO_2 was trapped in a 10 mL 1 M NaOH solution. The trapping solution was replaced with the same concentration of NaOH solution on days 7, 14, 21, 28, 42, 56, 77, 98, and 119, and at 4-week intervals for the later stage of incubation. The incubation jars did not remain closed for longer than two weeks at any point. To quantify CO_2 release, the replaced trapping solutions were titrated with 0.1 M HCl by an auto titrator (COM-1600, Hiranuma, Ibaraki, Japan) (Paul et al., 2001b). The cumulative CO_2 release curve was made based on the average CO_2 release of three replicate soil samples from each site across the whole incubation period.

3.2.6 Model Fitting for SOC Pools Partitioning for Each Site

Based on the cumulative CO_2 release curve for each site at the end of incubation, a first-order kinetic model was fitted to partition the SOC into three pools (labile, intermediate, and stable SOC pools) as following Equation (Paul et al., 2001b; Tian et al., 2016):

$$C_r = 1 - a_o \times e^{-K_L \times t} - b_o \times e^{-K_I \times t} - c_o \times e^{-K_S \times t} \quad (1)$$

where, C_r is the amount of cumulative CO_2 release at time t, which is expressed as a proportion (%) of total SOC; a_0, b_0, and c_0 are the proportions of the labile, intermediate, and stable SOC pools in SOC, respectively, ($a_0 + b_0 + c_0 = 1$); and K_L, K_I, and K_S (day^{-1}) are the mineralization rate constants, which were calculated as the reciprocals of the respective mean residence times (MRTs) of the labile, intermediate, and stable SOC pools, respectively.

The proportion of the non-hydrolyzable fraction C determined by the SOM fractionation was used as the c_0 in the model. Radiocarbon dating of the non-hydrolyzable fraction in northern Tanzania, southern Kenya, and Indonesia indicated that the residence time of this recalcitrant fraction was about a thousand years (Wattel- Koekkoek et al., 2003; Wiedemeier et al., 2012). The MRT of stable SOC pool ($1/K_S$) was high enough at the scale of hundreds to thousands of years, and the influence of stable SOC pool on modeling for the other pools was insignificant (Paul et al., 2001a; Paul et al., 2001b). Based on the previous studies (Paul et al., 2001b; Wattel- Koekkoek et

al., 2003; Wiedemeier et al., 2012) and to increase the accuracy of convergence fitting, it was assumed that the MRT of the stable carbon pool ($1/K_S$) in the field was 1000 yr. Furthermore, the MRT of SOC is regulated by the MAT due to the temperature sensitivity of the microbial respiration rate. To eliminate the influence of the difference in temperatures between the field and laboratory conditions, the laboratory-derived MRT of the stable carbon pool was adjusted from the assumed $1/K_S$ (field: 1000 yrs) using the following Equation (Paul et al., 2001b; Wang et al., 2017):

$$MRT_{lab} = MRT_{field}/Q_{10} \quad (2)$$

where, MRT_{lab} is the mean residence time in the laboratory, and MRT_{field} is the mean residence time in the field. Q_{10} is the temperature sensitivity coefficient, which was calculated using the MAT of the sampling sites ($Q_{10} = 2^{(25-MAT)/10}$) (Collins et al., 2000).

Equation (1) was fitted with nonlinear least-squares regression using the Universal Global Optimization (Auto2Fit 5.5, 7D-Soft High Technology Inc., China) algorithm. The a_0, K_L, and K_I values were estimated from the model. The b_0 was calculated by subtracting a_0 and c_0 from one. Nonlinearity regression analysis was conducted based on Equation (1) with the following limitations: $1/K_L = [1, 100]$, $1/K_I = [1000,100000]$ (root of mean square error < 0.001, sum squared residuals < 10^{-5}, $r > 0.999$, and $R^2 > 0.999$). The sizes of the labile, intermediate, and stable pools (C_L, C_I, and C_S, respectively) were calculated using the proportions of each pool (a_0, b_0, and c_0) and the total SOC content.

3.2.7 Statistical Analysis

The normality of the climatic data, elevation, and geochemical properties, SOM fractions data were tested, as well as model fitting results. Covariance structure analysis was applied to check the homogeneity of SOC quantities in different regions with multiple comparisons after Bonferroni adjustment. The Pearson product-moment correlation coefficient was applied to assess the correlation between climatic conditions and elevation, as well as the correlations between soil properties and SOC pools that passed the normality test. The Spearman's rank correlation was applied to other factors that did not pass the normality test even after logarithmic and root

conversions. One-way analysis of variance (ANOVA) and Tukey-Kramer post-hoc tests were applied to determine differences in soil physicochemical properties among regions. Kruskal-Wallis H tests were applied if the pre-conditions for ANOVA were not fulfilled. The significance level was set at 0.05. Partial correlation analyses (Spearman) were applied to determine the correlations between SOC pools (sizes and MRTs) and climate, or SOC pools and soil physicochemical properties, with the effect of related properties controlled. Additionally, path analysis was conducted to assess the effects (direction and contribution) of climatic and geochemical properties on SOC pools. The stepwise selection was applied to select optimal factors from factors that significantly correlated to the dependent variable for path analysis.

3.3 Results

3.3.1 Climate, Vegetation, and Soil Physicochemical Properties

The climate, vegetation, and soil classifications of the study sites are presented in Table 3.1. The spatial distribution of MAT and MAP, and their root-mean-squared error (RMSE) are presented in Fig. S3.1. The MAT and MAP differences caused by uncertainty (RMSE) is lower than their difference between sampling sites, which indicated the limited influences of potential errors on their statistical correlations. Mean annual temperature decreased with increasing elevation across all the sites ($r = -0.99$, $P < 0.01$). The moisture (EP) and MAT were both higher in the Indonesian sites than in the Tanzanian sites. Excess precipitation was lower at TW sites than TE sites at similar elevations, due to lower MAP. In terms of vegetation, the NPPs of IJ (900–1030 g C m^{-2} yr^{-1}) and IS (950–1030 g C m^{-2} yr^{-1}) were higher than those of TE (330–770 g C m^{-2} yr^{-1}) and TW (290–670 g C m^{-2} yr^{-1}).

The general physicochemical properties of the soils are presented in Table 3.2 and S3.1. The pH (H_2O) of the soils ranged from 4.6 to 7.0 across all sites (Table S3.1, Fig. S3.2), which is acidic to neutral. The pH (H_2O) of soils from TW sites was significantly higher than that from IS sites. The pH (H_2O) of soils from IS sites was lower than that from IJ sites at similar elevations. Sand content was higher in IJ (27 ± 13%) and IS (29 ± 12%) than in TW (8 ± 4%). Besides, the content

of exchangeable Ca at TW (28 ± 17 $cmol_c\ kg^{-1}$) was higher than that in other regions (Table 3.2).

Table 3.2 Physicochemical properties of the soils in different sampling regions

Region	pH (H_2O)	CEC	SOC	Total N	Clay	Sand	Ca_{ex} [c]	Al_o+1/2Fe_o [d]	oPOM C [e]
		$cmol_c\ kg^{-1}$	$g\ kg^{-1}$	$g\ kg^{-1}$	%	%	$cmol_c\ kg^{-1}$	$g\ kg^{-1}$	$g\ kg^{-1}$
IJ	6.0 ± 0.4 ab [ab]	25 ± 6 ab	44 ± 18	3.0 ± 1.2 ab	30 ± 14	27 ± 13 a	13 ± 5 b	16 ± 5	0.8 ± 0.4 b
IS	5.2 ± 0.2 b	30 ± 11 ab	86 ± 44	4.8 ± 1.8 ab	27 ± 12	29 ± 12 a	2.5 ± 2.2 b	36 ± 21	4.4 ± 2.9 a
TE	5.7 ± 1.0 ab	21 ± 4 b	46 ± 31	2.4 ± 1.7 b	28 ± 12	15 ± 7 ab	4.9 ± 4.7 b	19 ± 12	1.4 ± 0.9 b
TW	6.3 ± 0.4 a	40 ± 15 a	92 ± 68	8.1 ± 6.4 a	21 ± 6	7.7 ± 4.4 b	28 ± 17 a	28 ± 18	1.0 ± 0.9 b

[a] Mean ± standard deviation. [b] Different letters (small) indicate the means are statistically different at $P < 0.05$ among groups. [c] Ca_{ex}, exchangeable Ca. [d] Al_o+1/2Fe_o, the content of nanocrystalline minerals. [e] oPOM, occluded particulate organic matter in aggregates. IJ, Java (Indonesia); IS, Sumatra (Indonesia); TE, Southeast slope of Kilimanjaro (Tanzania); TW, northwest slope of Kilimanjaro (Tanzania).

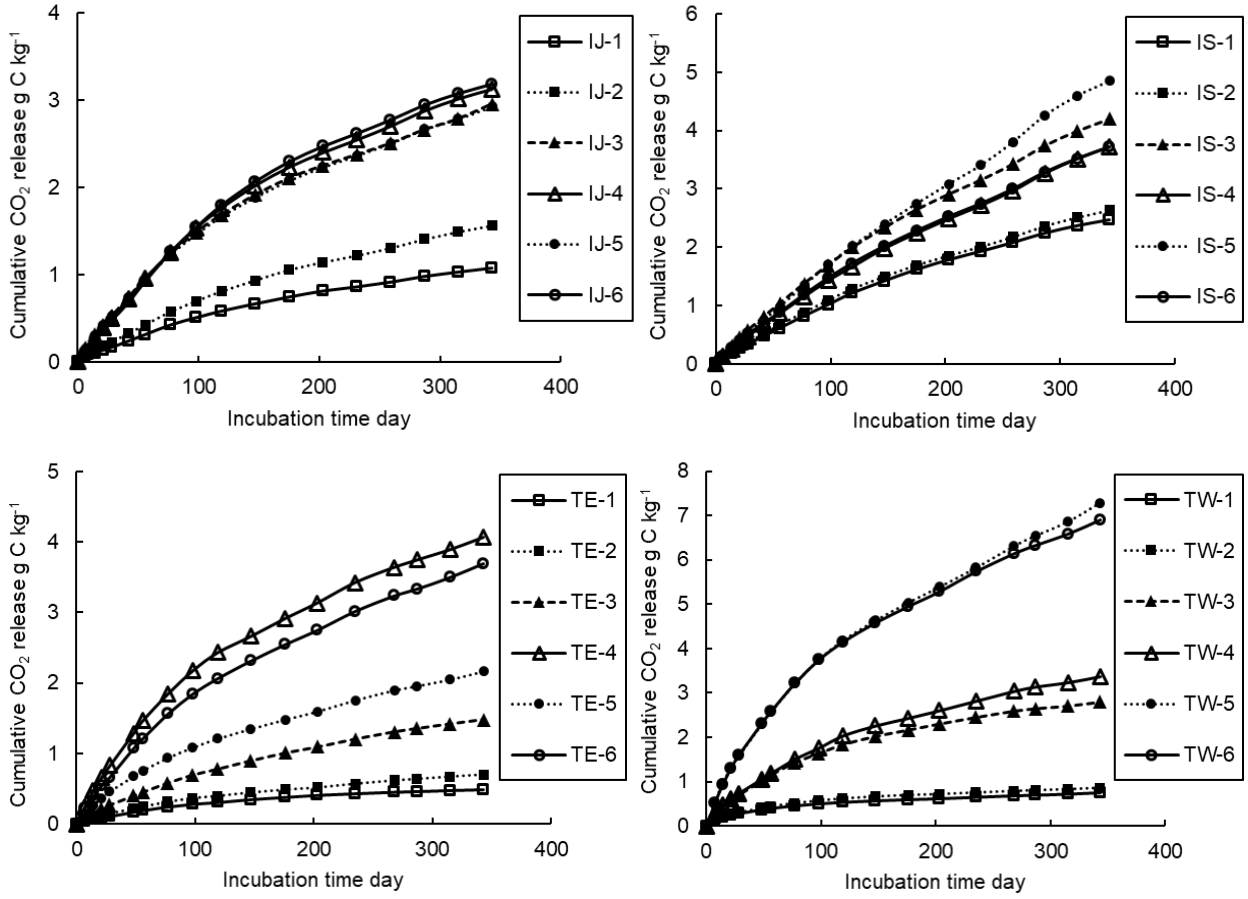

Fig. 3.2 Cumulative CO_2 release of the soil samples for each site during 343 days incubation at 25°C. Each point is the mean value of three replicates (n = 3). IJ, Java (Indonesia); IS, Sumatra (Indonesia); TE, southeast slope of Kilimanjaro (Tanzania), TW, northwest slope of Kilimanjaro (Tanzania). The numbers following site ID represent the elevation of the sampling site, being higher from 1 to 6

The SOC of the soils ranged from 10 to 180 $g\ kg^{-1}$ across all sites (Table S3.1, Fig. S3.2).

Total organic C recovery after density and particle size fractionations was 92 ± 8%, and the differences in recovery rates between study regions were not significant. Soil organic carbon generally increased with elevation (decreased with MAT) in each region, and the SOC of soils at IS sites that were humid throughout the year was higher than the other sites within a similar elevation. The oPOM carbon content of IS soils was abundant (4.4 ± 2.9 g kg^{-1}) and significantly higher than that at IJ, TE, and TW (Table 3.2 and S3.1). The total N content of TW soils was significantly higher, and the C/N ratio was significantly lower than that of TE soils.

The results of covariance structure analyses showed that, apart from IS (high oPOM), there were no significant differences in SOC contents between different regions. After adjusting the effects of oPOM, the SOC contents had no significant difference between either of the two regions.

The relationships between climate and geochemical properties across all sites are shown in Table S3.2. Soil pH (H_2O) was negatively correlated with EP ($r_s = -0.49$, $P < 0.05$). The CEC, which may mainly be contributed by organic matter, was negatively correlated with MAT and was positively correlated with $Al_o + 1/2Fe_o$. The contents of nanocrystalline minerals ($Al_o + 1/2Fe_o$) was negatively correlated with MAT ($r_s = -0.44$, $P < 0.05$) and pH ($r_s = -0.58$, $P < 0.01$).

3.3.2 Soil Incubation and SOC Pools

The cumulative CO_2 release for each site is presented in Fig. 3.2. Across all sites, the cumulative CO_2 release per dry soil increased intensively over the first three months, then became slower and steadily increased during the later stage of the incubation. The percentage of the total SOC decomposed during the entire incubation period for IJ, IS TE and TW were 5.8 ± 1.0%, 4.9 ± 1.7%, 4.3 ± 0.8%, and 3.8 ± 0.4%, respectively.

The SOC decomposition curve produced over incubation fitted the three-pool kinetic model well (root of mean square error < 0.001, sum squared residual < 10^{-5}, $r > 0.999$, $R^2 > 0.999$). The proportions, sizes, and MRTs of all sites are presented in Table 3.3. In the model, $1/K_S$, which is MRT of C_S (the non-hydrolyzable SOC fraction), was long enough, and variations of $1/K_S$ at the scale of hundreds to thousands of years did not much influence on estimations of other pools in

this and previous studies (Paul et al., 2001b; Tian et al., 2016). The C_I was mainly determined by C_S (non-hydrolyzable SOC fraction) due to the small proportions of the labile pool (1.9% ± 0.8%) across all sites. The MRTs of the labile pool ($1/K_L$) were within the incubation duration time, and C_L was correlated with and had similar contents to the MBC of the site (Table 3.3 and 3.4). Due to the high reliability of the C_L, $1/K_L$, and C_I estimates along with low contribution of C_S to the total cumulative CO_2 release (1.5% ± 0.7%), the $1/K_I$ estimates were also considered highly credible.

Table 3.3 The values of the parameters obtained by three-pool kinetic model for the soils at different sites

Site.	IJ-1	IJ-2	IJ-3	IJ-4	IJ-5	IJ-6	IS-1	IS-2	IS-3	IS-4	IS-5	IS-6
a_o [a] %	2.4	2.8	3.7	3.3	2.8	2.4	2.4	1.8	1.8	0.7	0.6	0.6
b_o %	64.2	51.0	48.0	47.7	48.0	56.4	63.1	63.6	51.0	39.3	34.8	44.7
c_o %	33.4	46.2	48.3	49.0	49.2	41.2	34.5	34.6	47.2	60.0	64.6	54.7
C_L [b] (g C kg^{-1})	0.54	0.65	1.58	1.64	1.56	1.63	0.81	0.86	1.26	1.89	0.60	0.87
C_I (g C kg^{-1})	14.50	12.04	20.42	23.69	26.88	37.86	21.07	29.80	36.68	41.07	35.15	68.08
C_S (g C kg^{-1})	7.55	10.93	20.55	24.36	27.51	27.64	11.51	16.22	33.89	51.52	65.11	83.46
$1/K_L$ [c] (days)	97	97	87	94	88	95	97	93	93	92	86	79
$1/K_I$ (days)	9000	4300	5000	5200	6700	7900	4000	5500	4100	3200	3400	8300

Site.	TE-1	TE-2	TE-3	TE-4	TE-5	TE-6	TW-1	TW-2	TW-3	TW-4	TW-5	TW-6
a_o %	1.7	1.4	1.5	2.3	1.7	2.1	2.1	1.9	1.5	1.7	1.7	1.8
b_o %	43.7	53.7	44.7	50.7	55.1	53.8	46.4	60.6	55.7	52.1	54.8	40.0
c_o %	54.6	44.9	53.8	47.0	43.2	44.1	51.5	37.5	42.8	46.2	43.5	58.2
C_L (g C kg^{-1})	0.26	0.28	0.45	0.67	0.85	1.46	0.47	0.43	2.41	1.65	2.68	3.36
C_I (g C kg^{-1})	6.81	10.88	13.08	14.67	27.34	36.97	10.47	14.11	73.50	51.31	85.91	73.71
C_S (g C kg^{-1})	8.51	9.08	15.73	15.93	21.48	30.35	11.64	8.75	43.32	45.44	68.16	107.18
$1/K_L$ (days)	62	49	50	54	56	60	30	35	47	43	53	44
$1/K_I$ (days)	9800	8900	4100	5800	7100	5600	9700	9600	9600	6000	9400	5300

[a] a_0, b_0, and c_0, portions of labile, intermediate and stable carbon pools, respectively.

[b] C_L C_I, and C_S, the sizes of labile, intermediate and stable carbon pools, respectively.

[c] $1/K_L$ and $1/K_I$, the mean residence times of labile and intermediate pools, respectively.

IJ, Java (Indonesia); IS, Sumatra (Indonesia); TE, southeast slope of Kilimanjaro (Tanzania); TW, northwest slope of Kilimanjaro (Tanzania). The numbers following site ID represent the elevation of the sampling site, being higher from 1 to 6.

The intermediate SOC pool contributed to 58 ± 11% of the cumulative CO_2 release, followed by the labile SOC pool (40 ± 11%) by the end of incubation (calculated by Eq. (S1)). The contribution of the stable pool to the cumulative CO_2 release (day 343) was low (1.5 ± 0.7%). The

C_L was the smallest of the three pools with the sizes from 0.54 to 1.64 g C kg^{-1} for IJ, 0.60 to 1.89 g C kg^{-1} for IS, 0.26 to 1.46 g C kg^{-1} for TE, and 0.43 to 3.36 g C kg^{-1} for TW (Table 3.3). The C_I and C_S were similar in content (33 ± 21 g C kg^{-1} and 33 ± 27 g C kg^{-1}, respectively). The C_I and C_S were larger at high elevation sites, with the exceptions of the intermediate pool of IJ-2 and IS-6, and the stable pool of TW-2. The C_I and C_S were relatively higher at IS than IJ sites at similar elevations. The MRTs of the labile pools ($1/K_L$) were relatively higher at IJ (87–97 days) and IS (79–97 days) than at TE (49–62 days) and TW (30–53 days). The MRTs of the intermediate pools ($1/K_I$) were within the range of thousands of days.

3.3.3 Relationship Between SOC Pools, Climatic and Geochemical Properties

Single correlation analysis was applied across all samples to analyze the sizes, portions, and MRTs of three SOC pools in relation to properties that include the climate, soil physicochemical properties, and SOM fractions (Table 3.4). For C_L, it was positively correlated with the EP (r_s = 0.44, $P < 0.05$) and was negatively correlated with the MAT ($r_s = -0.55$, $P < 0.01$). The contents of nanocrystalline minerals ($Al_o + 1/2Fe_o$) was also positively correlated with C_L ($r_s = 0.63$, $P < 0.01$). In terms of the intermediate pool, C_I was negatively correlated with the MAT ($r_s = -0.58$, $P < 0.01$). The C_I was also negatively correlated with pH ($r_s = -0.57$, $P < 0.01$) and was positively correlated to the $Al_o + 1/2Fe_o$ ($r_s = 0.86$, $P < 0.01$). The negative correlation between C_S and MAT was still found ($r_s = -0.57$, $P < 0.01$). The C_S was also negatively correlated with pH ($r_s = -0.57$, $P < 0.01$) and positively correlated with $Al_o + 1/2Fe_o$ ($r_s = 0.94$, $P < 0.01$), similarly to C_I. On the other hand, MBC increased with increases in C_L, and MBC contents almost equaled C_L. No direct correlations were found between EP and C_I or C_S. In addition, clay + silt contents and exchangeable Ca had no significant correlation with the sizes of the SOC pools.

Table 3.4 Correlations between soil carbon pools and related variables

	a_0 [a]	b_0	c_0	C_L	C_I	C_S	$1/K_L$	$1/K_I$
MAT [b]				−0.55**	−0.58**	−0.57**	0.62**	
EP				0.44*			0.77**	−0.57**
pH(H_2O)					−0.57**	−0.57**		

Al_o +1/2Fe_o [c]		−0.42*	0.46*	0.63**	0.86**	0.94**		
Clay + silt	−0.49*						−0.72**	0.48*
Ca_{ex} [d]								
CEC		−0.41*	0.43*	0.59**	0.70**	0.79**		
oPOM C [e]					0.63**	0.72**		−0.50*
oPOM C/SOC								
MBC [f]				0.83**	0.77**	0.80**		
MBC/SOC	0.45*			−0.43*	−0.74**	−0.74**		
C/N		−0.51*	0.49*	−0.52**	−0.44*			

** Correlation is significant at the 0.01 level (2-tailed). * Correlation is significant at the 0.05 level (2-tailed).
[a] a_0, b_0, and c_0, proportions of labile, intermediate, and stable SOC pools; C_L, C_I, and C_S, sizes of labile, intermediate, and stable SOC pools; $1/K_L$ and $1/K_I$, mean residence times of labile and intermediate pools. [b] MAT, mean annual temperature; EP, excess precipitation. [c] Al_o+1/2Fe_o, the content of nanocrystalline minerals. [d.] Ca_{ex}, exchangeable Ca. [e] oPOM C, occluded particulate organic matter in aggregates; oPOM C/SOC, content of occluded particle organic matter carbon in soil organic carbon. [f] MBC, microbial biomass carbon; MBC/SOC, content of microbial biomass carbon in soil organic carbon.

In detail, C_L, C_I, and C_S generally increased with increases in contents of nanocrystalline minerals for each region, though C_L was not significantly correlated with Al_o + 1/2Fe_o in IJ or IS soils (Fig. 3.3A). The relationships between the sizes of the pools and Al_o + 1/2Fe_o became stronger from the labile pool to the stable pool (Table 3.4, Fig. 3.3A). For TW sites, exchangeable Ca was higher than other regions (Table 3.2) and was positively correlated with the sizes of labile, intermediate, and stable pools (r = 0.91, P < 0.05, r = 0.91, P < 0.05 and r_s = 0.94, P < 0.05, respectively), if the most elevated site (TW-6, 2710 asl.) was excluded (Fig. 3.3B). For sites of IS, the oPOM, which represents the effect of aggregates, was relatively high and oPOM was positive correlated with C_I and C_S (r = 0.86, P < 0.05 and r = 0.94, P < 0.05, respectively) (Fig. 3.3C).

The proportion of labile pool (a_0) was positively correlated with MBC/SOC (r_s = 0.45, P < 0.05) and negatively correlated with the contents of clay + silt (r_s = −0.49, P < 0.05). The proportions of intermediate pool (b_0) was negatively correlated with Al_o + 1/2Fe_o and the ratio of C/N (r = −0.42, P < 0.05 and r = −0.51, P < 0.05, respectively).

The MRTs of labile pool ($1/K_L$) and intermediate pool ($1/K_I$) were not correlated with the sizes of SOC pools (C_L C_I and C_S), total N, C/N and MBC (Table 3.4). The $1/K_L$ was positively correlated with MAT and EP (r_s = 0.62, P < 0.01 and r_s = 0.77, P < 0.01, respectively). For the

other properties, $1/K_L$ was negatively correlated with clay + silt content ($r_s = -0.72$, $P < 0.01$). In contrast, $1/K_I$ was negatively correlated with EP ($r_s = -0.57$, $P < 0.01$), and was positively correlated with clay + silt content ($r_s = 0.48$, $P < 0.01$). Furthermore, the $1/K_I$ increased when oPOM content was relatively low ($r_s = -0.50$, $P < 0.05$).

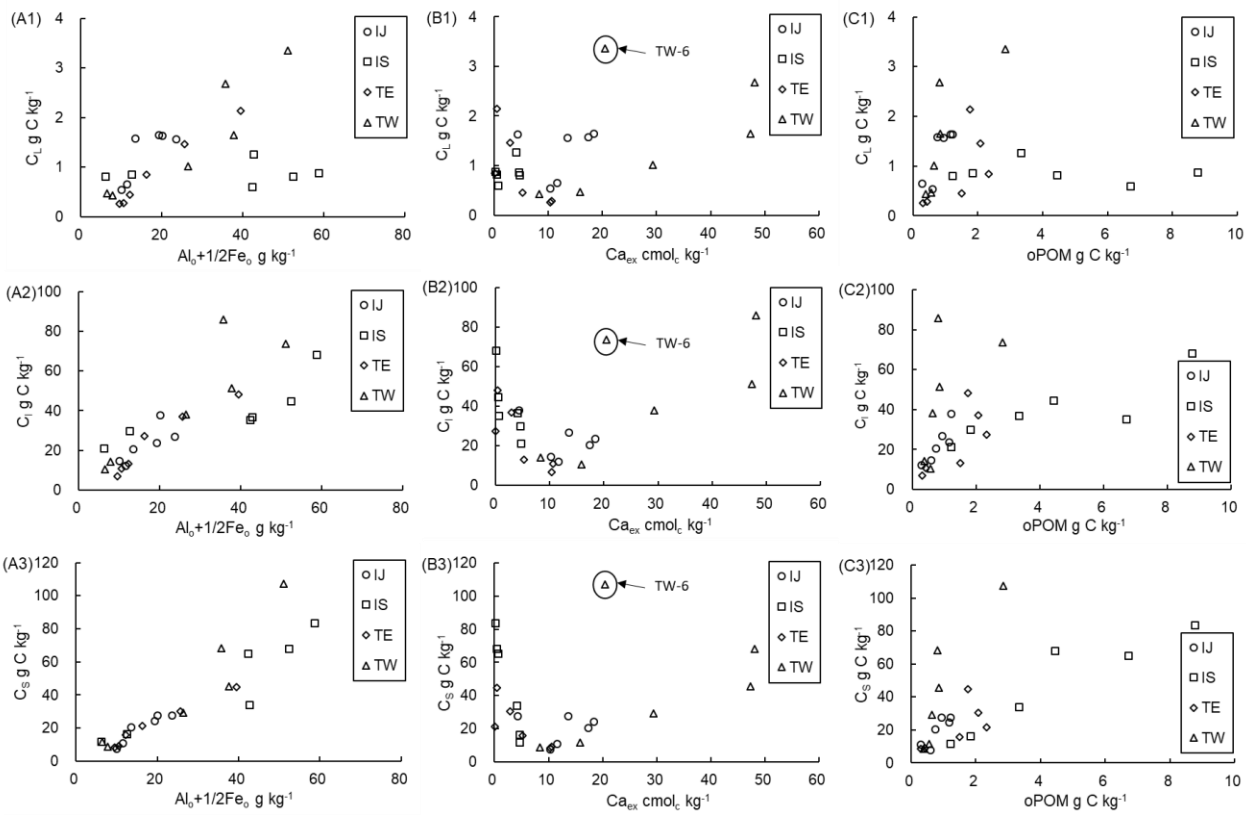

Fig. 3.3 The relationship of contents of nanocrystalline minerals (Al_o + 1/2Fe_o, A), exchangeable Ca (Ca_{ex}, B), and occluded particulate organic matter in aggregates (oPOM, C) and sizes of soil carbon pools (labile: C_L, 1; intermediate: C_I, 2; and stable: C_S, 3) for each site. IJ, Java (Indonesia); IS, Sumatra (Indonesia); TE, southeast slope of Kilimanjaro (Tanzania), TW, northwest slope of Kilimanjaro (Tanzania)

3.3.4 Partial Correlations Between Related Variables and SOC Pools

Using a single correlation coefficient will give misleading results when attempting to elucidate the numerical relationship between a certain factor and the SOC pools if another confounding factor related to both variables exists (e.g., the relationship among MAT, Al_o +1/2Fe_o, and C_L) (Fig. 3.4). Thus, partial correlation analysis (Spearman) was applied to find correlations

after controlling for confounding factors (Table 3.5) in order to clarify the direct or indirect effects of mutually-related factors on the sizes and MRTs of the three SOC pools. Variables were selected for partial correlation analyses based on the single correlations (Tables 3.4 and S3) between mutually-related factors and the three SOC pools (triangle relationship in Fig. 3.4). After controlling for Al_o + 1/2Fe_o, MAT negatively was correlated with the C_L, C_I, and C_S with a significance of 0.05 level, that is, $r_{MAT\text{-}CL\ (Alo+1/2Feo)} = -0.44$, $P < 0.05$, $r_{MAT\text{-}CI\ (Alo+1/2Feo)} = -0.43$, $P < 0.05$ and $r_{MAT\text{-}CS\ (Alo+1/2Feo)} = -0.51$, $P < 0.05$, respectively (Table 3.5). The Al_o +1/2Fe_o still strongly was correlated with the C_I and C_S after controlling for MAT, pH, or MAT and pH, while the significance level of the correlation between Al_o + 1/2Fe_o and C_L decreased to 0.05 even when only MAT was controlled for (Table 3.5). After controlling for Al_o +1/2Fe_o, no correlation was found between soil pH and the size of each SOC pool. For MRTs of labile and intermediate pools ($1/K_L$ and $1/K_I$), a substantial weakening of the correlation between $1/K_L$ and clay + silt was found when EP was controlled for. However, the correlation between $1/K_L$ and EP was significant even after controlling for clay + silt content.

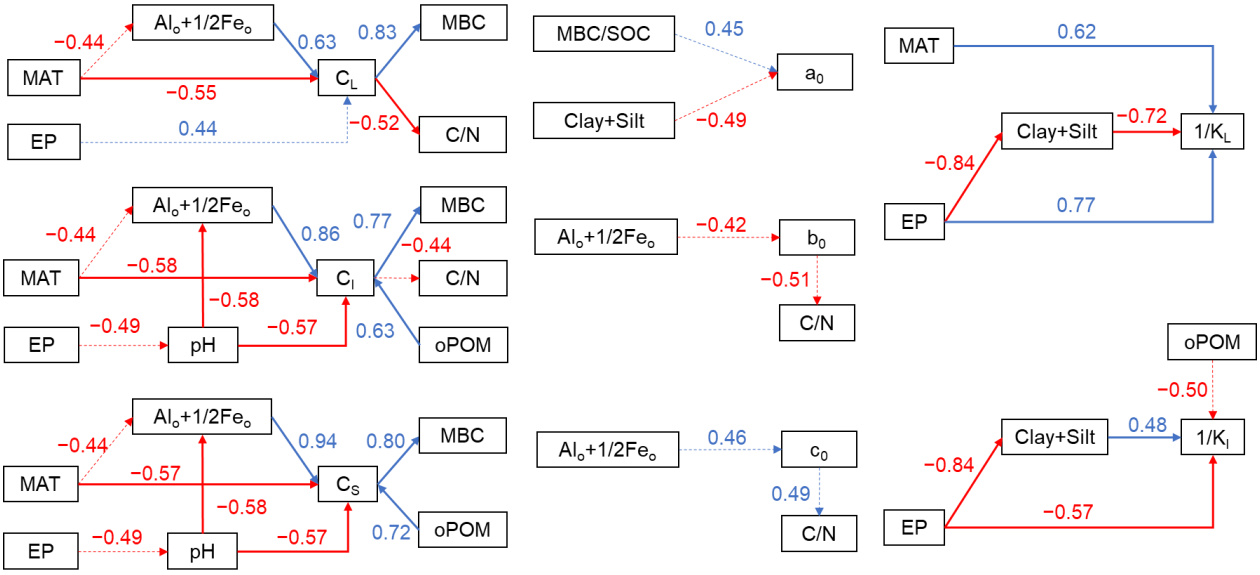

Fig. 3.4 Schematic diagram of single correlations for sizes (labile: C_L, intermediate: C_I, and stable: C_S), proportions (labile: a_0, intermediate: b_0, and stable: c_0), mean residence times (labile: $1/K_L$ and intermediate: $1/K_I$) of three carbon pools, and related properties including the climatic (MAT: mean annual temperature and EP: excess precipitation), geochemical properties, microbial biomass carbon (MBC) and occluded particulate organic matter in aggregates (oPOM). Arrow line type represents the significance of correlation, i.e., solid line: $P < 0.01$, and dotted line: $P < 0.05$. Number above an arrow shows the correlation coefficient.

Table 3.5 Partial correlation of mutually-related factors on soil carbon pools

	MAT [a]		$Al_o + 1/2Fe_o$				pH	
C_L [b]	−0.55**	−0.44*	0.63**	0.52*	–	–	–	–
C_I	−0.58**	−0.43*	0.86**	0.83**	0.79**	0.73**	−0.57**	−0.17
C_S	−0.57**	−0.51*	0.94**	0.94**	0.92**	0.90**	−0.57**	−0.06
	Zero-order	$Al_o + 1/2Fe_o$	Zero-order	MAT	pH	MAT & pH	Zero-order	$Al_o + 1/2Fe_o$
	Controlled factors							

	MAT	EP		Clay + silt	
$1/K_L$ [b]	0.62**	0.77**	0.43*	−0.72**	−0.23
$1/K_I$	−0.37	−0.57**	−0.35	0.48**	0.01
	Zero-order	Zero-order	Clay + silt	Zero-order	EP
	Controlled factors				

[a] MAT, mean annual temperature; EP, excess precipitation; $Al_o+1/2Fe_o$, the content of nanocrystalline minerals.

[b] C_L, C_I, and C_S, sizes of labile, intermediate, and stable SOC pools; $1/K_L$ and $1/K_I$, mean residence times of labile and intermediate pools.

The row above the "Controlled factors" shows the zero-order (without controlling any factors) and the factors being controlled for (or factors of which effect on correlation coefficient was removed). The number and asterisk show the correlation coefficient and significance, respectively, with or without controlled factors.

3.3.5 Contributions of Climatic and Geochemical Properties to SOC Pools

Path analysis was applied across all sites to identify the main controlling factors and their contributions to sizes, proportions, and MRTs of SOC pools (Fig. 3.5). The dominant factors that controlled C_L were the climatic properties: MAT and EP. Mean annual temperature negatively contributed to more than half the variation in C_L with a normalized direct path coefficient (r_p) of −0.74 ($P < 0.001$), and the remaining variation was due to EP ($r_p = 0.38$, $P < 0.05$). The $Al_o + 1/2Fe_o$ strongly and positively contributed to C_I ($r_p = 0.67$, $P < 0.001$), whereas MAT negatively contributed to C_I ($r_p = −0.35$, $P < 0.05$). Furthermore, the positive contribution of $Al_o + 1/2Fe_o$ to C_S ($r_p = 0.82$, $P < 0.001$) was more influential than its contribution to C_I ($r_p = 0.67$, $P < 0.001$), and the contribution of MAT to C_S and C_I was minor ($r_p = −0.22$, $P < 0.05$, and $r_p = −0.35$, $P < 0.01$, respectively). The contributions of EP to C_I and C_S were not significant. The $Al_o + 1/2Fe_o$, which was essential for the size of relatively stable pools (C_I and C_S), was negatively affected by MAT and pH, with normalized path coefficients of −0.42 and −0.49 at a significance level of 0.05 and 0.01, respectively.

The ratio of MBC/SOC, which was negatively affected by $Al_o + 1/2Fe_o$ ($r_p = -0.65$, $P < 0.001$), dominantly contributed to a_0 ($r_p = 0.65$, $P < 0.001$). A weak negative contribution of clay + silt content to a_0 was also found ($r_p = -0.36$, $P < 0.05$). The b_0, which was mainly determined by c_0 (almost in inverse proportion) and was negatively contributed by $Al_o + 1/2Fe_o$ ($r_p = -0.54$, $P < 0.01$). Meanwhile, climatic–properties predominantly contributed to $1/K_L$ and $1/K_I$. In detail, EP contributed to the variation in $1/K_L$ ($r_p = 0.70$, $P < 0.001$) along with MAT ($r_p = 0.45$, $P < 0.001$). In contrast, $1/K_I$ was negatively contributed by EP ($r_p = -0.50$, $P < 0.05$) (Fig. 3.5).

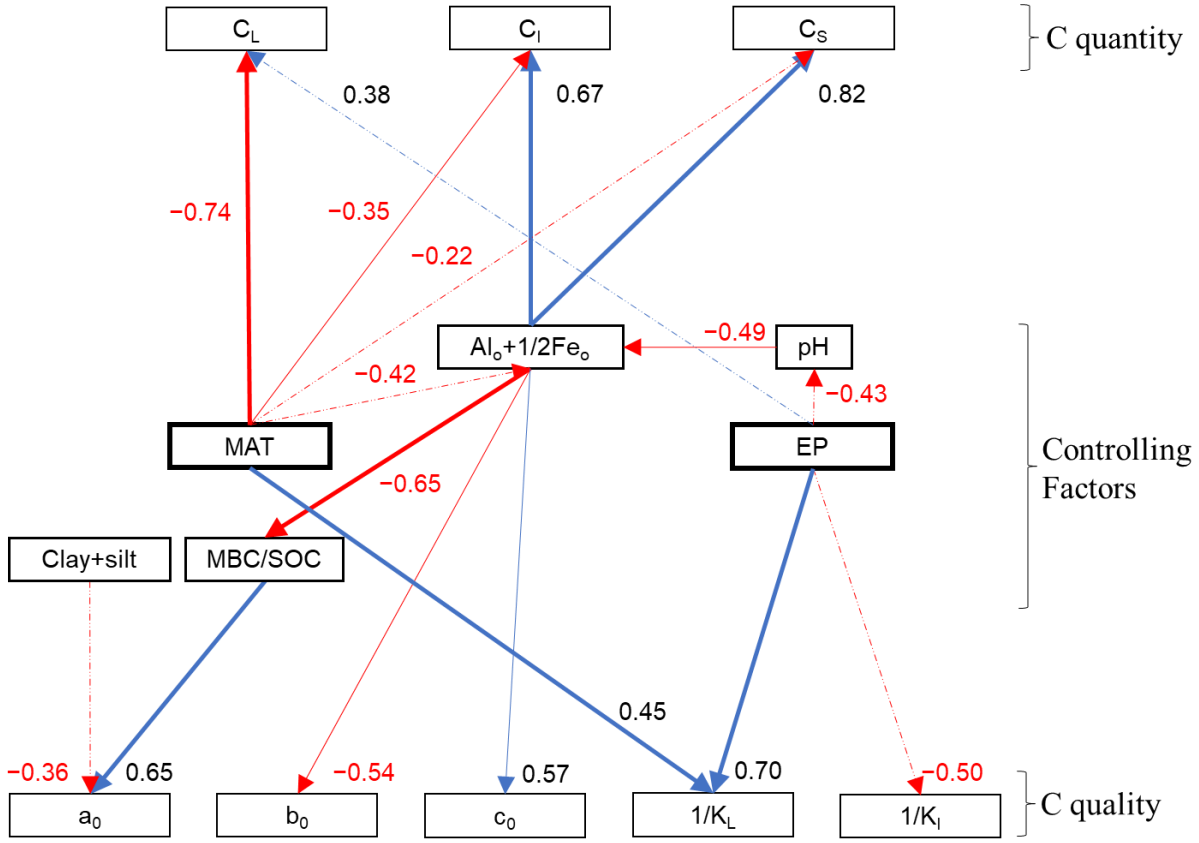

Fig. 3.5 A schematic diagram of the path analysis for clarifying the contributions of controlling factors on size (labile: C_L, intermediate: C_I, and stable: C_S), proportions (labile: a_0, intermediate: b_0, and stable: c_0), and mean residence times (labile: $1/K_L$ and intermediate: $1/K_I$) of soil carbon pools. Controlling factors include mean annual temperature (MAT), excess precipitation (EP), geochemical properties, and a proportion of microbial biomass carbon in SOC (MBC/SOC). Arrow line type represents significance of regression, i.e., thick solid line, $P < 0.001$; solid line, $P < 0.01$; dotted line, $P < 0.05$. Number above an arrow shows the normalized path coefficient

3.4 Discussion

3.4.1 Climate, Geochemistry, and SOC of the Sites

There was a significant positive correlation between MAT and elevation across all sites (Table S3.2), indicating that MAT and elevation were inversely proportional. However, the correlation between elevation and EP was not significant, which indicates that moisture was more strongly affected by the regional climate and higher MAP in Indonesia than in Tanzania. The relatively high NPP of IJ and IS (Table 3.2) are also due to high precipitation, which supports the growth of plants and contributes to higher primary production (Del Grosso et al., 2008).

Across all sites, the pH of soils was slightly acidic to neutral with the direct contribution from EP. The negative correlation between EP and soil pH indicates that higher EP results in progressive leaching and decreases the pH of soils (Guicharnaud and Paton, 2006). The exchangeable Ca was high under high pH conditions, especially at TW sites (Table 3.2 and S3.1). At the sites with relatively high soil pH, the positive effect of Ca^{2+} on SOC stabilization could be significant (Rowley et al., 2018). The contents of $Al_o + 1/2Fe_o$ was negatively correlated with MAT and soil pH. The low temperature at more elevated sites with sufficient moisture (EP) retards the crystallization and promotes the formation of nanocrystalline minerals in volcanic regions (Lyu et al., 2018). In addition, the CEC of the soil was positively correlated with $Al_o + 1/2Fe_o$ (Table S3.2). Nanocrystalline minerals can be the core of organo-mineral complexes that preserve organic matter and increase the CEC of soil (Parfitt et al., 1999; Wagai et al., 2015).

The quantity and quality of SOC were similar across the different study regions. The lack of significant differences in the covariance structure analysis with multiple comparisons indicates homogeneity in the quantity of SOC between the study regions. In detail, after adjusting for the oPOM carbon content, which represents the effect of aggregates, especially in IS, the difference in SOC content between each of two regions (IJ, IS, TE, and TW) was not significant. The proportions of the stable SOC pool, c_0 (45 ± 6%, 49 ± 12%, 48 ± 5%, and 47 ± 8% for IJ, IS, TE, and TW, respectively), indicate the similarity of SOC quality range between regions. Soil organic carbon varied along the elevation gradient and was relatively high in soils collected from high

elevation sites in each region (Fig. S3.2). The oPOM carbon contents were significantly higher at IS sites than TW sites, of which SOC contents were similar to IS sites (Table 3.2 and S3.1). The high oPOM at IS sites may be partially due to the positive effect of aggregation, which could be enhanced at the volcanic region with high soil moisture throughout the year (Lavee et al., 1996; Li et al., 2017). The relatively abundant $Al_o + 1/2Fe_o$ at IS sites (Table S3.1) can also positively affect the aggregation (Wagai et al., 2020) and enlarge the oPOM carbon. Meanwhile, the low C/N ratio of soils at TW indicates that the organic matter at TW that had high exchangeable Ca experienced some decomposition and was in a relatively stable form.

3.4.2 SOC Pools and Their Contributions to SOC Decomposition

The labile SOC pool influenced soil respiration in the early stage of SOC decomposition (Fig. 3.2), while the intermediate and stable pools represent the total SOC (Table 3.3). The cumulative CO_2 release at the end of incubation was primarily a product of the intermediate and labile SOC pools (58 ± 11% and 40 ± 11%, respectively). The intermediate SOC pool with MRTs of thousands of days predominantly controlled SOC decomposition at the scale of years, as indicated by the contribution of the intermediate pool to the cumulative CO_2 release (58 ± 11%) over the 343-day incubation. The stable SOC pool, which represents decomposition resistant SOC, made up 47 ± 8% of SOC but contributed to less than 3.2% of the cumulative CO_2 released over 343 days of incubation across all the sites (calculated by Eq. (S1)).

The C_I and C_S were relatively larger at IS, which had lower pH with higher soil moisture than other sites within similar elevations (Table 3.3). The higher C_I and C_S at more elevated sites (Table 3.3) may be because the low temperature at high elevation sites decreased microbial activity and resulted in high SOC stabilization by nanocrystalline minerals. The low pH at IS may have depressed the decomposition of organic matter by suppressing the activity of microbes, thus enlarging the intermediate and stable pools (Zhang et al., 2020).

The ratios (a_0 and b_0) and MRTs of the labile and intermediate SOC pools ($1/K_L$ and $1/K_I$) generally represent the stability and microbial usability of the organic matter within each pool

(Schimel and Weintraub, 2003). The MRTs of the labile and intermediate SOC pools were comparable with those reported in previous studies, which applied the same SOC pool partitioning method and the same assumption for MRTs. In detail, the MRTs of the labile and intermediate SOC pools in this study are generally longer than those of soils in the temperate agricultural field (Collins et al., 2000; Paul et al., 2001b) and soils under the forest of the temperate volcanic region (Tian et al., 2016), probably because of the difference in the contents of the nanocrystalline minerals, which can stabilize SOC as discussed below. The $Al_o + 1/2Fe_o$, should be much lower in Mollisols and Alfisols in the temperate agricultural field (Collins et al., 2000; Paul et al., 2001b) and may result in the lower MRTs of SOC pools. Meanwhile, the soils of the previous study conducted in the temperature volcanic region had lower $Al_o + 1/2Fe_o$ contents (Lampo et al., 1993) but comparable total SOC (Tian et al., 2016) to that of soils in this study. It indicates that the higher contents of nanocrystalline minerals ($Al_o + 1/2Fe_o$) in the soils of this study may stabilize SOC, resulting in the higher MRTs of the labile and intermediate SOC pools (higher SOC stability).

3.4.3 Dominant Controlling Factors and Their Effects on SOC Pools

The results of correlation and path analyses show that climatic and geochemical factors, directly and indirectly, control soil carbon pools in tropical volcanic regions (Table 3.5, Fig. 3.4 and 3.5). The SOC pools are predominantly controlled by temperature, moisture, and nanocrystalline minerals. First, the temperature directly affected the sizes of SOC pools. The correlations between the MAT and sizes of the three SOC pools (C_L, C_I, and C_S) were significant, even after controlling for $Al_o + 1/2Fe_o$ ($r_{MAT\text{-}CL\ (Alo+1/2Fe)} = -0.44$, $r_{MAT\text{-}CI\ (Alo+1/2Fe)} = -0.43$, and $r_{MAT\text{-}CS\ (Alo+1/2Fe)} = -0.51$, respectively), indicating a direct negative effect of temperature on all compositions of the SOC. Low temperature of the sites retarded the SOC decomposition by microorganisms in the soil and enlarged SOC content at sites with high elevation (Davidson et al., 2006; von Lützow and Kögel-Knabner, 2009). The direct path coefficients between MAT and the three SOC pools (Fig. 3.5) also support the hypothesis that the temperature controls the potential quantity of SOC pools. Besides the negative contribution of MAT to C_L ($r_p = -0.74$, $P < 0.001$),

the positive contribution of MAT on $1/K_L$ (r_p = 0.45, $P < 0.001$) represent the significant impact of temperature on the quality (MRT) of labile SOC pool. High MAT accelerates the decomposition of SOC in the labile pool by microorganisms, leaving behind partially decomposed materials that are more recalcitrant to mineralization during incubation (high $1/K_L$) (Fig. 3.5). The predominant contribution of MAT on labile SOC pool rather than the other factors (Fig. 3.5) suggests that the labile pool might be more vulnerable to climate change than the intermediate and stable pools (Parton et al., 1987; Qi et al., 2016). Meanwhile, the relatively weak but significant direct contribution of MAT to C_I and C_S (Fig. 3.5) also highlights the importance of temperature on the more stable SOC pools.

In addition to MAT, EP weakly contributed to C_L (r_p = 0.38, $P < 0.05$) and predominantly contributed to $1/K_L$ (r_p = 0.70, $P < 0.001$) (Fig. 3.5). The significant weakening of the correlation between $1/K_L$ and clay + silt when EP was controlled for also shows the strong effect of EP on potential MRTs of labile SOC pool (Table 3.5). Sufficient moisture can support the growth of ligneous plants to form a tree-dominated system, which has higher primary production (Del Grosso et al., 2008), and enlarge the labile pool by supplying fresh organic matter. At sites with high EP, the natural vegetations were forests with relatively high density. The residues from woody plants at high EP sites are relatively less able to be utilized by microorganisms than those from shrubs or grasses (Mack et al., 2001). Besides, the EP also negatively contributed to $1/K_I$ (Fig. 3.5). Within the materials of the intermediate pool, the partially decomposed materials might be enlarged at the sites with high EP and be potentially available for further decomposition (low $1/K_I$). Also, high EP decreased the soil pH (r_p = −0.43, $P < 0.05$) and created a preferable condition for the formation of nanocrystalline minerals (Chapter 2), which are expected to stabilize organic matter.

The nanocrystalline minerals (Al_o + $1/2Fe_o$), of which formation is promoted in the humid and cool condition, was the predominant factor for SOC stabilization (Fig. 3.4 and 3.5). The correlation between Al_o + $1/2Fe_o$ and the labile pool (C_L) was weak and was not significant in IJ and IS soils (Fig. 3.3(A1)), indicating that the labile pool is not strongly dependent on nanocrystalline minerals. The Al_o + $1/2Fe_o$ negatively contributed to MBC/SOC, which, in turn,

positively contributed to and had similar values with a_0 (Fig. 3.5), indirectly reflecting the stabilization of SOC by nanocrystalline minerals.

The strong correlation between $Al_o + 1/2Fe_o$ and C_I (or C_S) after controlling for MAT and pH ($r_{Alo+1/2Fe\text{-}CI\ (MAT\&pH)} = 0.73$ and $r_{Alo+1/2Fe\text{-}CS\ (MAT\&pH)} = 0.90$, $P < 0.01$; Table 3.5) and the significant contributions of $Al_o + 1/2Fe_o$ to C_I and C_S ($r_p = 0.67$, $P < 0.001$, and $r_p = 0.82$, $P < 0.001$, respectively; Fig. 3.5) suggest that the nanocrystalline Al and Fe content might be the crucial factor affecting the intermediate and stable pools, rather than MAT and pH. The related studies also indicate that the Al and Fe oxyhydroxides could be better predictors for SOC storages at the sites with high moisture and low pH (Rasmussen et al., 2018; Yu et al., 2017). Moreover, the coefficients between $Al_o + 1/2Fe_o$ and the size of the SOC pool increased from the intermediate to the stable pool (Fig. 3.3A and 3.5). Also, there were significant positive contributions of $Al_o + 1/2Fe_o$ to c_0 and negative contribution of $Al_o + 1/2Fe_o$ to b_0 (Fig. 3.5). These results indicate the strong ability of nanocrystalline minerals in stabilizing C as stable rather than intermediate SOC by forming stable organo-mineral complexes (Takahashi and Dahlgren, 2016). Hence the interaction between SOC and nanocrystalline minerals should be essential for the sizes of intermediate and stable SOC pools (C_I and C_S), which predominantly contribute to the decomposition resistance. The associations between Al and Fe ions in nanocrystalline minerals and organic functional groups via covalent bonds are abundant in Andosols (Asano and Wagai, 2014). At sites with high $Al_o + 1/2Fe_o$, previously inputted organic matter at the early stage of C accumulation is expected to associate with the mineral core (nanocrystalline minerals) directly and became stable (Filimonova et al., 2016; Kleber et al., 2007b). Possibly because of this direct association, the $Al_o + 1/2Fe_o$ predominant controls the size of stable SOC pool (C_S) (Table 3.5, Fig. 3.5). Then further inputted organic matters are likely to indirectly accumulate in the hydrophobic zone via hydrophobic interactions (active non-polar C chemically sorbs to the directly mineral-associated organic matter) as well as in the kinetic zone (organic matter weakly connects to organo-mineral complexes) of nanocrystalline Al and Fe (Zhao et al., 2020). These indirectly stabilized C are considered as intermediate SOC. The significant contribution of $Al_o + 1/2Fe_o$ in enlarging the sizes of

intermediate SOC pool (Fig. 3.5) and the possible effect of $Al_o + 1/2Fe_o$ in enhancing the stability of labile and intermediate SOC pools (as discussed in section 4.2) also proved the positive impact of nanocrystalline minerals on SOC accumulation by indirect stabilization. Early inputted C gradually covered by latterly inputted organic matters and remained as stable SOC. Both the stable and intermediate SOC pools are strongly affected by the nanocrystalline mineral core (Fig. 3.4 and 3.5). Thus, nanocrystalline minerals is the dominant factor that controls the whole SOC and its stability in tropical volcanic regions.

3.4.4 Additional Factors Related to SOC Pools

The contribution of soil texture to SOC pools was not significant. The negligible direct effect of clay + silt is supported by no correlation between clay + silt with the sizes of SOC pools (C_L, C_I, and C_S) (Table 3.4), the lack of the correlation between soil texture and $1/K_L$ or $1/K_I$ after controlling for EP (Table 3.5) and the weakly contribution by the clay + silt contents to a_0 (r_p = −0.36, $P < 0.05$) (Fig. 3.4 and 3.5). Regarding soil pH, although low pH is expected to retard the decomposition of SOC by microorganisms (Zhang et al., 2020), the significant correlation between soil pH and C_I or C_S (r_s = −0.57, $P < 0.01$ and r_s = −0.57, $P < 0.01$, respectively) disappeared after controlling for $Al_o + 1/2Fe_o$ (Table 3.5, Fig. 3.4). There was no significant direct contribution of pH to SOC pools according to path analysis as well (Fig. 3.5). The effect of soil pH is indirect, that is, contents of nanocrystalline Al and Fe ($Al_o + 1/2Fe_o$) is high under low pH or moist soils, which in turn contributes to the SOC pools. Thus, neither soil texture nor soil pH is one of the main factors controlling the SOC pools at the study sites.

The similar size of MBC and C_L and positive correlations between the proportion of MBC in SOC and a_0 (Fig. 3.4) represent the similarity between MBC and the labile pool. At sites with high a_0, the SOC is relatively fresh and supports a sizable microbial community. The high moisture and high $Al_o + 1/2Fe_o$ may enhance aggregate stability, which can preserve organic matters (Lavee et al., 1996; Wagai et al., 2020). The positive correlation between C_I (or C_S) and oPOM (Table 3.4, Fig. 3.3C) may indicate the possible contribution of aggregation to SOC stabilization, especially

in humid IS sites with high oPOM content (Table 3.2 and S3.1); or simply, oPOM carbon increases with the increase of total SOC. The direct measurement of aggregates and the organic carbon inside the aggregates need to be conducted to evaluate the impact of aggregation on SOC stabilization at study sites. Moreover, the exchangeable Ca positively contributed to the sizes of the three SOC pools, including the labile pool, at TW sites with relatively high soil pH (Fig. 3.3B, Table 3.2). The positive correlation between exchangeable Ca and the SOC pools at TW sites indicates that Ca^{2+} stabilizes the SOC through both inner-sphere (for the intermediate and stable pools) and outer-sphere (for the labile pool) connections in neutral to alkaline soils (Rowley et al., 2018).

3.5 Conclusion

Fitting the multiple pool first-order kinetic model to the SOC decomposition curves produced over long-term incubation and SOM fractionation is a feasible method of understanding the factors that control SOC pools with different decomposability. Within the three pools, the intermediate SOC pool, which comprised about 50% of the total SOC and 58% of the cumulative CO_2 release over one-year of incubation, predominantly controls the carbon stability of the topsoil at the scale of years to tens of years. The main factors that control SOC pools in tropical volcanic regions are the temperature, moisture, and content of nanocrystalline minerals. Climatic factors primarily affect the labile to intermediate SOC pools (control SOC stability for a short period). In contrast, geochemical factors affect intermediate to stable SOC pools (control the majority of SOC and C stabilization for middle to long period).

The nanocrystalline minerals, rather than soil texture or soil pH, is the dominant controlling factor of C_I and C_S. Carbon stabilization is promoted at sites with high contents of nanocrystalline minerals, which preferentially form under the low temperature and sufficient moisture condition. The MAT of the sites not merely predominantly controls the size and MRT of the labile pool but also affects the sizes of intermediate and stable SOC pools. Also, EP mainly controls the potential stabilities (MRTs) of the labile and intermediate SOC pools ($1/K_I$ and $1/K_S$). In addition to the main controlling factors, calcium-mediated carbon stabilization enlarged C_L as well as C_I and C_S

for the sites with near-neutral soil pH. These findings have important implications for understanding the mechanisms of SOC stabilization, which is an essential process of the carbon cycle in tropical volcanic soils.

CHAPTER 4

FACTORS CONTROLLING SOIL ORGANIC CARBON POOLS IN SUBSOIL AND DIFFERENCES OF CONTROLLING FACTORS, POOLS' SIZES AND STABILITIES BETWEEN TOPSOIL AND SUBSOIL

4.1 General

Besides the topsoil, subsoil has been recognized as the crucial reservoir for C stocks in recent years (Chabbi et al., 2009; Cotrufo et al., 2019; Wordell-Dietrich et al., 2017). Moreover, the subsoil may still have the ability to stabilize more C due to the low SOC content (Torn et al., 1997). The studies focused on SOC stock in topsoil has been comprehensively conducted, while the mechanisms controlling SOC turnover in subsoil is still unclear.

The subsoil SOC has a high mean residence times (MRTs) of thousands of years measured by ^{14}C age dating (Kogel-Knabner et al., 2008; Paul et al., 2001a; Trumbore and Zheng, 1996; Wiedemeier et al., 2012), which appear to be resistant to climate change and has a low risk for decomposition. However, the high radiocarbon age of subsoil SOC can also represent the meager accumulation rates, which may occur due to the limitation of substrate input (Salome et al., 2010). Carbon input in subsoil should be mainly by root exudates and dissolved organic matter from the upper horizon, which is highly different from the topsoil (Rasse et al., 2005). A large amount of SOC, which has degradable chemical nature but resisted for an extended period, was found in subsoils (Parfitt et al., 1999; Salome et al., 2010). The energy limitation for microbial communities due to the restricted fresh C input could retard organic matter decomposition, then preserved as relatively stable SOC (Fontaine et al., 2007). In this case, environment change would directly and intensively influence the substrate quantity and quality that would regulate the SOC pools of subsoil. Recent studies on the effects of a year to decade scale changes in vegetation on SOC pools of subsoils also supported this hypothesis (Leuschner et al., 2014; Steinmann et al., 2016).

Elucidation of factors that control subsoil SOC storage and stability is required to respond to

the changing environment. Low mean annual temperature (MAT) at high elevations directly retards the microbial activities, reduces the organic matter decomposition, and enlarges the labile SOC pools (Garten Jr, 2011). Carbon input, which may be an essential factor for SOC storage in subsoils, is directly influenced by potential net primary production (NPP). High moisture would lead to a high NPP and high leaching of dissolved organic carbon as the carbon input to subsoil. Meanwhile, for the geochemical properties, soil minerals can associate and preserve organic matter for both topsoil and subsoil (Kleber et al., 2015). The clay, as well as silt fractions, may contribute to SOC stabilization simultaneously (Curtin, 2002). The nanocrystalline minerals (active Al and Fe) also stabilize SOC by forming organo-mineral complexes and microaggregates, significantly but not only for volcanic soils (Takahashi and Dahlgren, 2016; Wagai et al., 2020; Yu et al., 2017; Zhao et al., 2020). The effect of organo-minerals interaction on SOC stabilization, as one essential mechanism, would be more predominant in subsoil with more active sorption sites due to the lower SOC saturation than topsoil (Kaiser and Guggenberger, 2003). Besides, the metabolic of soil microorganisms is also influenced by microbial N availability, contributing to the SOC spatial distribution (Neff et al., 2002; Waring et al., 2014). As an example, the deficiency of N may decrease the stability of organic matter in subsoil due to microbial N mining (Chen et al., 2014). Moreover, the climatic, geochemical, and biotic factors interact with each other and control SOC storage and stability simultaneously (Doetterl et al., 2015). For instances, high moisture decreases soil pH, which declines the microbial activities (Zhang et al., 2020), and also promotes the formation of nanocrystalline minerals (Lyu et al., 2018), then the lowered microbial activity and the formed nanocrystalline minerals retard the SOC decomposition; the temperature and moisture control the potential NPP with the influence of vegetation type, then contributes to carbon input (Del Grosso et al., 2008).

In the previous study (Chapter 3), I emphasized the necessity of SOC partitioning based on their decomposability (labile, intermediate, and stable) to clarify factors and mechanisms that control the turnover of each SOC pool. It was revealed that climate affects relatively labile SOC pools that control the short-term stability of SOC, and the geochemical factors affect more stable

pools that control the total C stabilization in topsoil. In detail, the nanocrystalline minerals are the predominant factor of sizes of intermediate and stable SOC pools, which control the stability of total SOC; temperature affects all of three SOC pools and predominantly controls the labile SOC pool; moisture contributes to MRTs of labile and intermediate SOC pool. However, the factors that control the SOC pools in subsoil are still not well-known and should be different from topsoil. Also, studies on SOC dynamics and its controlling factors in tropical subsoils are much scarcer compared to the temperate soils.

The objectives of this study were:1) to figure out the factors that control the SOC pools in the subsoil of tropical volcanic regions; 2) to compare the difference of SOC pools and the controlling factors between the subsoil and topsoil. I hypothesized that climatic and biotic factors control the labile SOC pool, while geochemical factors influence more intermediate and stable pools in subsoil. Compared to topsoil, the sizes and stability of stable SOC pools would be more related to geochemical factors, especially the contents of nanocrystalline minerals. The labile and intermediate SOC pools of subsoil would be more related to biotic factors than topsoil. Also, all SOC pools in subsoil would significantly be affected by climatic properties.

4.2 Materials and methods

4.2.1 Study Sites and Soil Sampling

The study sites were same as Chapter 3, which were in tropical volcanic regions of Tanzania and Indonesia. Details of the climate, vegetation, and parent material of study sites and sampling method are described in the Chapter 3. Same amount of subsoils (20–40 cm) were collected from four sides of each profile after removing the surface plant residues. The soils collected from each site were carefully mixed as a composite sample and sieved pass through a 2 mm mesh. The composite sample for each site (1 kg per sample, n = 23) was separated into two parts: one part was preserved in the refrigerator at 3°C (fresh), and the other was air-dried. All samples were homogenized again before incubation and analyses.

4.2.2 Physicochemical Properties and SOM Fractionation

Physicochemical analyses and SOM fractionation applied for the subsoil were similar to that for the topsoil (Chapter 3, 3.2.3 to 3.2.4).Soil dissolved organic carbon (DOC) and dissolved total nitrogen (DTN) were extracted by 0.5 mol L^{-1} K_2SO_4 and were determined using the combustion catalytic oxidation method and catalytic thermal decomposition method, respectively (TOC-L, Shimadzu, Kyoto, Japan). Instead of measuring aggregate weight diameter, the ratio of oPOM to LF was used as the aggregation index (Haddix et al., 2020).

The methods of the other analyses are described in Chapter 3 (3.2.3 to 3.2.4).

4.2.3 Soil Incubation and SOC Pools Partitioning

Same incubation setting and methods for SOC pools partitioning were applied for the subsoil as the topsoil (Chapter3, 3.2.5 and 3.2.6). Generally, long-term soil incubation was conducted for around one year (343 days) with a constant temperature at 25°C in the dark condition to obtain the cumulative CO_2 release curve. A first-order kinetic model was fitted to partition the SOC into three pools (labile, intermediate, and stable SOC pools), which based on the cumulative CO_2 release

curve for each site as following:

$$C_r = 1 - a_o \times e^{-K_L \times t} - b_o \times e^{-K_I \times t} - c_o \times e^{-K_S \times t}$$

Where, C_r is the amount of cumulative CO_2 release at day t of incubation, which is expressed as a proportion (%) of total SOC; a_0, b_0, and c_0 are the proportions of the labile, intermediate, and stable SOC pools in SOC, respectively, ($a_0 + b_0 + c_0 = 1$); and K_L, K_I, and K_S (day^{-1}) are the mineralization rate constants, which were calculated as the reciprocals of the respective mean residence times (MRTs) of the labile, intermediate, and stable SOC pools, respectively. The sizes of the labile, intermediate, and stable SOC pools (C_L, C_I, and C_S, respectively) were calculated using the proportions of each pool (a_0, b_0, and c_0) and the total SOC content of each site.

4.2.4 Statistical Analysis

The normality tests of the climatic, biotic, and geochemical properties and SOC fractions data were conducted, as well as SOC pool data from the model fitting by normal probability plot and Shapiro–Wilk test. Due to the low passing rate of normality tests on related properties, the Spearman's rank correlation was applied to all factors. The t-test was applied to evaluate the significance of the difference between the topsoil and subsoil. One-way analysis of variance (ANOVA) and Tukey-Kramer posthoc tests were applied to determine differences in soil physicochemical properties among regions. Kruskal-Wallis H tests were applied if the pre-conditions for ANOVA were not fulfilled. The significance level was set at 0.05 (two-tailed). Partial correlation analyses (Spearman) were applied to determine the correlations between pool data and related climatic, geochemical, and biotic properties, when the confounding variables were controlled. Additionally, path analyses were conducted to evaluate the direction and contribution of climate, geochemical, and biotic properties on SOC pools and MRTs. The stepwise selection was applied to select optimal factors from variables that significantly correlated to the dependent variable for path analysis.

4.3 Results

4.3.1 Climatic, Geochemical, and Biotic Properties

The climate, soil classification, vegetation, and soil properties are shown in Table 4.1, 4.2, and S4.1. The uncertainties of MAT and MAP were lower than their difference between sampling sites and had low influences of potential errors on their statistical results (Fig. S3.1). The mean annual temperature across all sites decreased with elevation, while the EP was not correlated with elevation, which indicates the regional precipitation intensively affects the soil moisture. Net primary production was relatively high at the sites with high precipitation and dense vegetation (Table 4.1). The high moisture primarily promoted the growth of woody plants and increased the primary production of the sites (Breshears and Barnes, 1999; Del Grosso et al., 2008).

Table 4.1 Basic information of sampling sites and selected physicochemical properties of subsoil (20–40 cm)

Region	Sites	Elevation	MAT [a]	MAP [a]	Soil classification [b]	Vegetation types	NPP [c]	pH (H_2O)	SOC [d]
	No.	m	°C	mm			g C m^{-2} yr^{-1}		g kg^{-1}
Java, Indonesia	6	340–1680	17.3–24.7	1960–3280	Andisols (6)	Woodland (1); Rainforest (5)	900–1030	6.0 ± 0.2 ab [ef]	21.5 ± 9.3
Sumatra, Indonesia	6	220–1440	19.0–25.8	2220–2980	Ultisols (1); Andisols (5)	Rainforest (6)	950–1030	5.3 ± 0.1 b	42.9 ± 23.4
Southeast slope of Kilimanjaro, Tanzania	6	1030–1910	17.1–21.9	910–1690	Ultisols (2); Andisols (4)	Wooded grassland (1); Afromontane forest (3); Rainforest (2)	330–770	5.6 ± 0.6 ab	23.3 ± 13.5
Northwest slope of Kilimanjaro, Tanzania	5	1470–2480	13.9–19.0	800–1180	Alfisols (2); Andisols (3)	Wooded grassland (2); Afromontane forest (3)	290–670	6.3 ± 0.6 a	49.5 ± 35.9

[a] MAT, mean annual temperature; MAP, mean annual precipitation. [b] Soil classification based on USDA soil classification (Soil Survey Staff, 2014). [c] NPP, net primary production (potential). [d] SOC, soil organic carbon. [e] mean ± standard deviation. [f] Different small letters show the means are statistically different at $P < 0.05$ among study regions.

Table 4.2 Geochemical and biotic properties of subsoil (20–40 cm) at each study region

	Clay+silt	Al_o + 1/2Fe_o	Si_o	Ca_{ex}	MBC	MBC /SOC	DON+MBN	DOC +MBC /DON+MBN	Aggregation Index
	%	g kg^{-1}	g kg^{-1}	$cmol_c$ kg^{-1}	g kg^{-1}		g kg^{-1}		
IJ [a]	77 ± 20 ab	22 ± 14	6.6 ± 5.8 ab	7.7 ± 2.8 ab	0.14 ± 0.07 a	7.3 ± 4.1	0.05 ± 0.01 b	6.4 ± 0.6	0.78 ± 0.58 ab
IS	63 ± 13 b	61 ± 42	24 ± 17 a	0.6 ± 0.5 b	0.14 ± 0.05 a	5.0 ± 4.1	0.12 ± 0.03 a	7.8 ± 2.9	1.56 ± 0.64 a
TE	85 ± 8 ab	21 ± 16	4.4 ± 7.9 b	5.9 ± 5.1 b	0.19 ± 0.14 ab	7.7 ± 2.3	0.08 ± 0.05 ab	7.1 ± 0.9	1.21 ± 0.85 ab
TW	93 ± 3 a	28 ± 21	6.5 ± 5.7 b	18 ± 14 a	0.43 ± 0.33 a	11.8 ± 6.3	0.11 ± 0.05 ab	6.8 ± 1.0	0.33 ± 0.17 b

[a] IJ, Java (Indonesia); IS, Sumatra (Indonesia); TE, southeast slope of Kilimanjaro (Tanzania); TW, northwest slope of Kilimanjaro (Tanzania).

[b] NPP, net primary production (potential); Al_o, Fe_o, and Si_o, oxalate extractable Al, Fe, and Si; Ca_{ex}, exchangeable Ca; MBC, microbial biomass carbon; MBC/SOC, the content of microbial biomass carbon in soil organic carbon, DTN+MBN, dissolved total nitrogen and microbial biomass nitrogen; Aggregation Index, an index showing the degree of aggregation obtained dividing oPOM C by light fraction C.

[c] Different small letters show the means are statistically different at $P < 0.05$ among study regions.

The soil pH (H_2O) was acidic to neutral across all sites, ranged from 5.1 to 6.8 (Table S4.1). The soil pH at IS sites was significantly lower than that at TW (Table 4.1). The soil pH at IS sites was lower than that at IJ sites at a similar elevation (Table S4.1). The contents of nanocrystalline minerals (Al_o + 1/2Fe_o) had no significant difference between regions. The exchangeable Ca were high at TW sites, where soil pH is relatively high (Table 4.1, 4.2, and S4.1).

The quantity of SOC of the subsoil has no significant difference among the study regions (Table 4.1). The SOC contents of the soils ranged from 10 to 100 g kg^{-1} across all sites. Total organic C recovery after density and particle size fractionations was 90 ± 8%, and the differences in recovery rates between study regions were not significant. The SOC contents generally increased with elevation in each study region (Fig. S4.1). The contents of the MBC had no significant difference between two of the four regions (Table 4.2). The available N for microbes (DTN + MBN) were significantly higher at IS sites than IJ sites. Meanwhile, the aggregation index (oPOM/LF) was relatively higher at IS sites, which indirectly represented the more enhanced aggregation (Table 4.2).

The relationships of climatic, geochemical and biotic properties are represented in Table S4.2. The contents of nanocrystalline minerals (Al_o + 1/2Fe_o) was positively correlated with EP (r_s = 0.52, P < 0.05) and negatively correlated with soil pH (r_s = −0.48, P < 0.05). Also, Al_o +1/2Fe_o positively correlated to DTN + MBN (r_s = 0.64, P < 0.01) and negatively correlated to MBC content in SOC (MBC/SOC) (r_s = −0.61, P < 0.01). The exchangeable Ca positively correlated to soil pH and clay + silt (r_s = 0.68 and 0.58, respectively, P < 0.01). Meanwhile, MBC/SOC was also high at the sites with high clay + silt and exchangeable Ca (r_s = 0.60 and 0.55, respectively, P < 0.01).

4.3.2 SOC Decomposition and SOC Pools

The SOC decomposition curves across all sites of the entire incubation period are shown in Fig. 4.1. The intensive respiration appeared in the first four weeks, then getting slower across all sites. Over the 343-days incubation, 2.3 ± 0.7% of the total SOC was decomposed, and the difference between study regions was not significant. Each of the SOC decomposition curves (Fig. 4.1), was fitted Eq. 1 well. The mean square error roots were lower than 0.001; sum squared residuals were lower than 10^{-5}; r > 0.995; R^2 > 0.995.

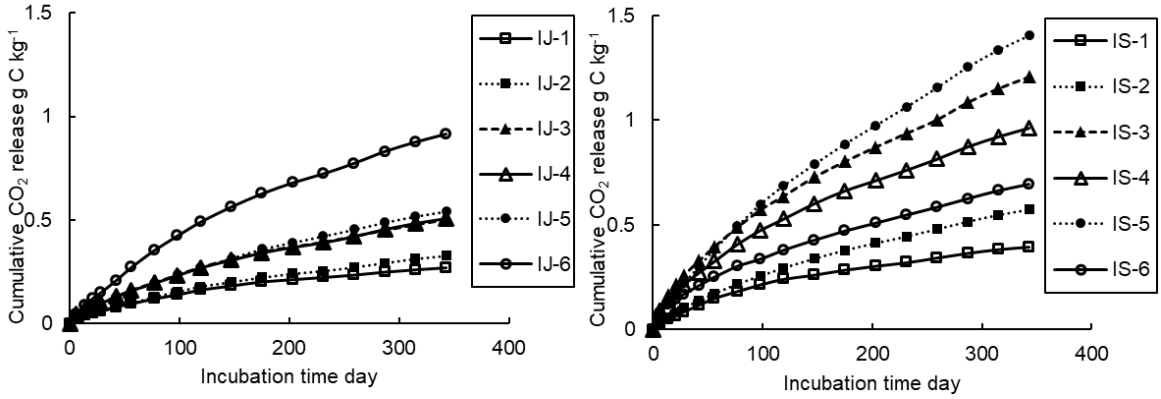

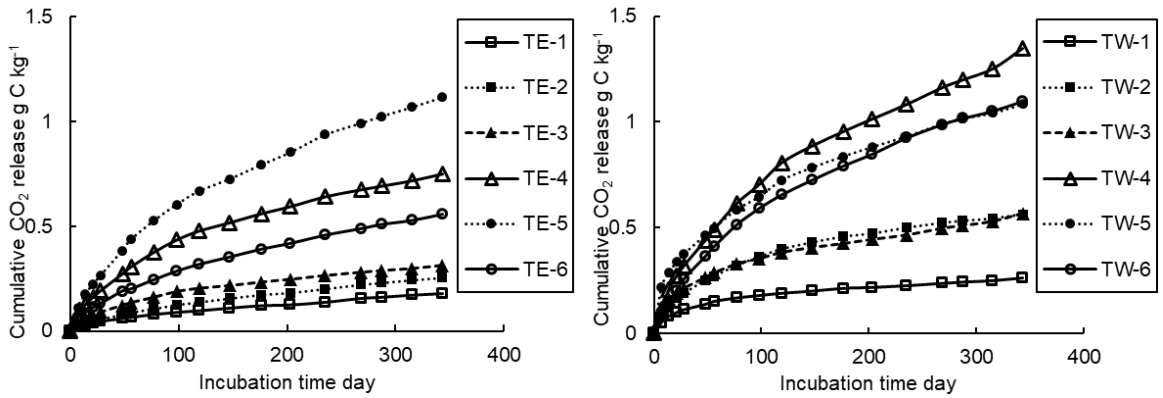

Fig. 4.1 SOC decomposition curve of the subsoils (20–40 cm) for each site over 343 days incubation at 25°C. Each point is the mean value of three replicates. IJ, Java (Indonesia); IS, Sumatra (Indonesia); TE, southeast slope of Kilimanjaro (Tanzania), TW, northwest slope of Kilimanjaro (Tanzania). The following numbers represent the elevation gradient of the site, getting higher from 1 to 6

Table 4.3 Sizes, proportions and mean residence times of subsoils (20–40 cm)

Site.	IJ-1 [a]	IJ-2	IJ-3	IJ-4	IJ-5	IJ-6	IS-1	IS-2	IS-3	IS-4	IS-5	IS-6
a_o [b]	1.1%	0.9%	1.0%	0.6%	1.3%	0.5%	1.7%	0.9%	1.0%	0.6%	0.3%	0.6%
b_o	73.8%	62.2%	56.4%	60.4%	54.0%	70.4%	71.8%	79.6%	68.4%	64.0%	66.0%	69.7%
c_o	25.1%	36.9%	42.6%	39.0%	44.7%	29.1%	26.5%	19.5%	30.6%	35.4%	33.7%	29.8%
C_L (g C kg^{-1})	0.13	0.12	0.17	0.15	0.37	0.16	0.19	0.18	0.38	0.46	0.20	0.36
C_I (g C kg^{-1})	8.29	8.06	9.72	14.63	15.20	24.75	7.98	16.59	25.29	40.17	42.96	43.59
C_S (g C kg^{-1})	2.82	4.78	7.34	9.43	12.59	10.23	2.95	4.06	11.33	21.79	21.92	18.63
$1/K_L$ (days)	58	62	53	51	79	64	62	60	43	51	25	18
$1/K_I$ (days)	19700	13200	10200	12700	9400	25400	13200	14200	10400	22500	30400	26000

Site.	TE-1	TE-2	TE-3	TE-4	TE-5	TE-6	TW-1	TW-2	TW-3	TW-4	TW-5
a_o %	0.6%	0.6%	1.1%	1.0%	0.6%	0.9%	1.1%	1.9%	1.0%	0.8%	0.4%
b_o %	38.6%	41.1%	51.5%	61.0%	66.4%	69.7%	44.9%	64.3%	55.2%	58.0%	54.2%
c_o %	60.9%	58.3%	47.4%	38.0%	33.0%	29.4%	54.0%	33.8%	43.8%	41.1%	45.3%
C_L (g C kg^{-1})	0.06	0.08	0.15	0.45	0.19	0.25	0.14	0.31	0.55	0.50	0.44
C_I (g C kg^{-1})	3.90	5.20	6.97	26.98	21.07	19.17	6.18	10.45	31.29	35.11	54.48
C_S (g C kg^{-1})	6.16	7.38	6.41	16.79	10.45	8.07	7.43	5.50	24.83	24.87	45.52
$1/K_L$ (days)	31	34	44	41	37	37	22	34	44	25	46
$1/K_I$ (days)	11800	10000	14700	13900	20000	15100	19300	13500	14400	21500	31500

[a] IJ, Java (Indonesia); IS, Sumatra (Indonesia); TE, southeast slope of Kilimanjaro (Tanzania); TW, northwest slope of Kilimanjaro (Tanzania). The following numbers represent the elevation gradient of the site, getting higher from 1 to 6.

[b] a_0, b_0, and c_0, portions of labile, intermediate and stable carbon pools, respectively; C_L C_I, and C_S, the sizes of labile, intermediate and stable carbon pools, respectively; $1/K_L$ and $1/K_I$, the mean residence times of labile and intermediate pools, respectively

The sizes, proportions, and MRTs of pools were represented in Table 4.3. Low contribution of the stable pool to cumulative CO_2 release by the end of incubation (2.7 ± 1.6%) indicates the influence of the stable pool on the SOC decomposition curve was not significant. Moreover, MRT of C_S was long enough (assumed as 1000 years), and variations of $1/K_S$ at the scale of hundreds to thousands of years did not much influence on estimations of other pools in this and previous studies (Paul et al., 2001b, Tian et al., 2016). The $1/K_L$ was within 80 days, which was significantly shorter than the incubation duration, and C_L had similar contents to the MBC of the site. Thus, a_0 and $1/K_L$ had high credibility. The b_0 was primarily determined by c_0, which was the proportion of directly measured non-hydrolyzable SOM fraction, due to the small proportions of the labile pools (a_0, 0.9 ± 0.4%) across all sites. The high credibility of the a_0, $1/K_L$, and b_0 estimates, along with the negligible effects of the stable pool, proved the reliability of $1/K_I$ estimates.

The intermediate SOC pool, which took 61 ± 11% of total SOC, contributed to 59 ± 8% of the cumulative CO_2 release, followed by the contribution of labile SOC pool (38 ± 8%) by the end of incubation (calculated by Eq. S1). The contribution of the stable pool to cumulative CO_2 release by the end of incubation is limited (2.7 ± 1.6%). The intermediate SOC pool was the largest among three pools with the sizes from 3.90 to 54.48 g C kg^{-1}across all sites (21 ± 14 g C kg^{-1}), followed by the stable SOC pool (13 ± 10 g C kg^{-1}). The labile pool size was the smallest among the three pools (0.26 ± 0.14 g C kg^{-1}) (Fig. 4.2). The MRTs of the labile pool ranged from 18 to 79 days across all sites. The MRTs of the intermediate pools were within the range of tens of years (9400 to 30400 days) (Table 4.3).

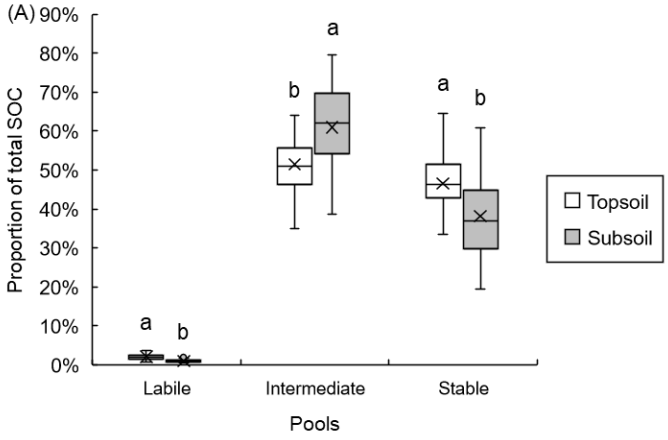

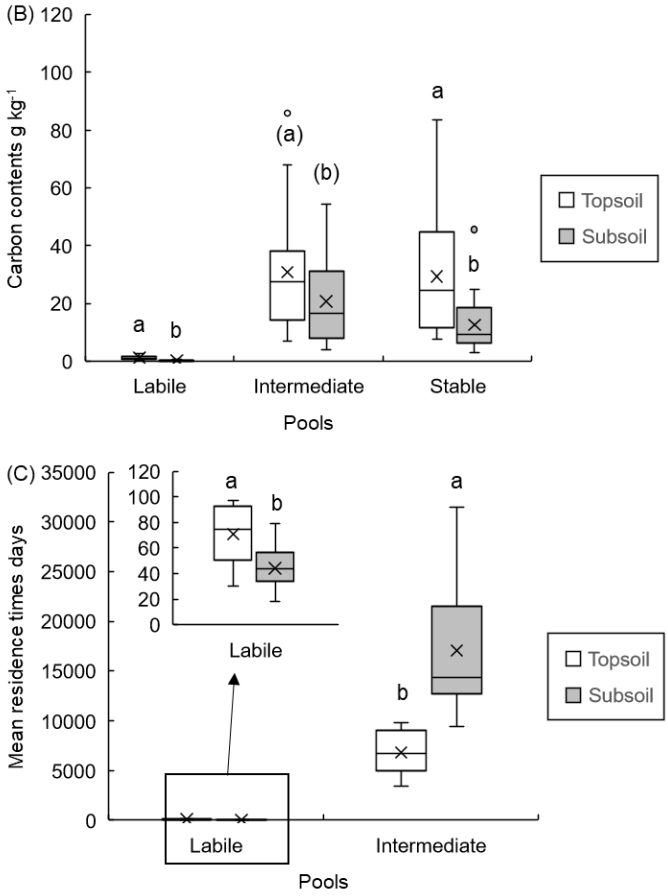

Fig. 4.2 Box plots of proportions (A), sizes (B), and mean residence times C) of SOC pools in topsoil and subsoil across all sites. Small letters above the plots show the significance of difference, a and b represent the significance at 0.01 level, (a) and (b) represent the significance at 0.05 level.

Compared with topsoil (0–15 cm), the a_0 and c_0 of the subsoil were significantly lower, while the b_0 was significantly higher than that of topsoil across all sites (Fig. 4.2A). The sizes of three pools were all significantly larger in the topsoil than in subsoil, while the significance level of the difference in C_I between the topsoil and subsoil was relatively lower than other pools (Fig. 4.2B). The MRTs of the labile pools were significantly lower, while the MRTs of the intermediate pools were significantly higher in the subsoil than topsoil (Fig. 4.2C).

4.3.3 Single Correlations Between SOC Pools Data, Climate, Geochemical and Biotic Properties

The results of single correlation analysis, which represents the relationship between SOC

pools, climate, geochemical and biotic properties, across all samples is shown in Table 4.4. In terms of the labile pool, the C_L was negatively correlated with the MAT ($r_s = -0.55$, $P < 0.01$), and was positively correlated with contents of nanocrystalline minerals ($Al_o + 1/2Fe_o$) ($r_s = 0.67$, $P < 0.01$). The available N for microbes (DTN + MBN) was positively correlated with C_L ($r_s = 0.87$ and 0.67, respectively, $P < 0.01$), which has similar contents with MBC of the soil. For the intermediate pool, C_I was also negatively correlated with MAT ($r_s = -0.50$, $P < 0.01$), while the significance dropped compared with the labile pool. In contrast, the C_I was strongly positively correlated with $Al_o + 1/2Fe_o$ ($r_s = 0.89$, $P < 0.01$). Besides, the exchangeable Ca contents and MBC/SOC were relatively low at the sites with high C_I. ($r_s = -0.44$ and -0.45, respectively, $P < 0.05$). The significant coefficient between C_I and DTN + MBN ($r_s = 0.79$, $P < 0.01$) was relatively lower than that between C_L and DTN + MBN. In terms of the stable pool, C_S was still negatively correlated with MAT and positively correlated with $Al_o + 1/2Fe_o$ ($r_s = -0.70$ and 0.81, respectively, $P < 0.01$). The DTN + MBN was also positively correlated with C_S, and the coefficient was lower than that of the labile and intermediate pools.

Table 4.4 Correlations between carbon pools and related properties for subsoil (20–40 cm)

	C_L [a]	C_I	C_S	$1/K_L$	$1/K_I$
MAT [b]	-.55**	-.50*	-.70**		
EP				.60**	
Clay + silt					
$Al_o + 1/2Fe_o$ [d]	.67**	.89**	.81**		.43*
Ca_{ex}		-.44*			
MBC/SOC [e]		-.45*			
DTN + MBN	.87**	.79**	.67**		
(DOC + MBC)/ (DTN + MBN)					
C/N					
Aggregation Index [f]			-.50*		

[a] C_L, C_I, and C_S, sizes of labile, intermediate, and stable SOC pools; a_0, b_0, and c_0, proportions of labile, intermediate, and stable SOC pools; $1/K_L$ and $1/K_I$, mean residence times of labile and intermediate pools

[b] MAT, mean annual temperature; EP, excess precipitation. [c] NPP, net primary production (potential). [d] $Al_o + 1/2Fe_o$, the content of nanocrystalline minerals; Ca_{ex}, exchangeable Ca. [e] MBC/SOC, the content of microbial biomass carbon in soil organic carbon; DTN + MBN, dissolved total nitrogen plus microbial biomass nitrogen. [f] Aggregation Index, an index showing the degree of aggregation obtained dividing oPOM C by light fraction C.

Furthermore, the relationships between $Al_o + 1/2Fe_o$ and the sizes of three SOC pools were represented in Fig. 4.3. The correlation coefficient between $Al_o + 1/2Fe_o$ and C_S were lower in the subsoil ($r_s = 0.81$, $P < 0.01$) than that in topsoil ($r_s = 0.94$, $P < 0.01$, Chapter 3). The ratios of C_I and C_S to $Al_o + 1/2Fe_o$, which represents the carbon saturation degree of nanocrystalline minerals, were lower in the subsoil (Fig. 4.3). On the other hand, excess precipitation, C/N ratio of available sources for microbes ((DOC + MBC)/(DTN + MBN)), and clay + silt had no significant correlation with the sizes of SOC pools.

The proportion of the labile pool (a_0) was negatively correlated with $Al_o + 1/2Fe_o$ and positively correlated with MBC/SOC ($r_s = -0.50$, $P < 0.05$ and $r_s = 0.71$, $P < 0.01$, respectively). For b_0, it was positively correlated with EP and aggregation index ($r_s = 0.51$and 0.55, respectively, $P < 0.05$), and negatively correlated with clay + silt and exchangeable Ca contents ($r_s = -0.51$ and -0.47, respectively; $P < 0.05$). In terms of MRTs of pools, $1/K_L$ and $1/K_I$ were not correlated with C_L, C_I and C_S, MAT, clay + silt, exchangeable Ca, MBC, DTN + MBN and aggregation index. The $1/K_L$ was positively correlated with EP ($r_s = 0.60$, $P < 0.01$), while the $1/K_I$ was positively correlated with $Al_o + 1/2Fe_o$ (Table 4.4).

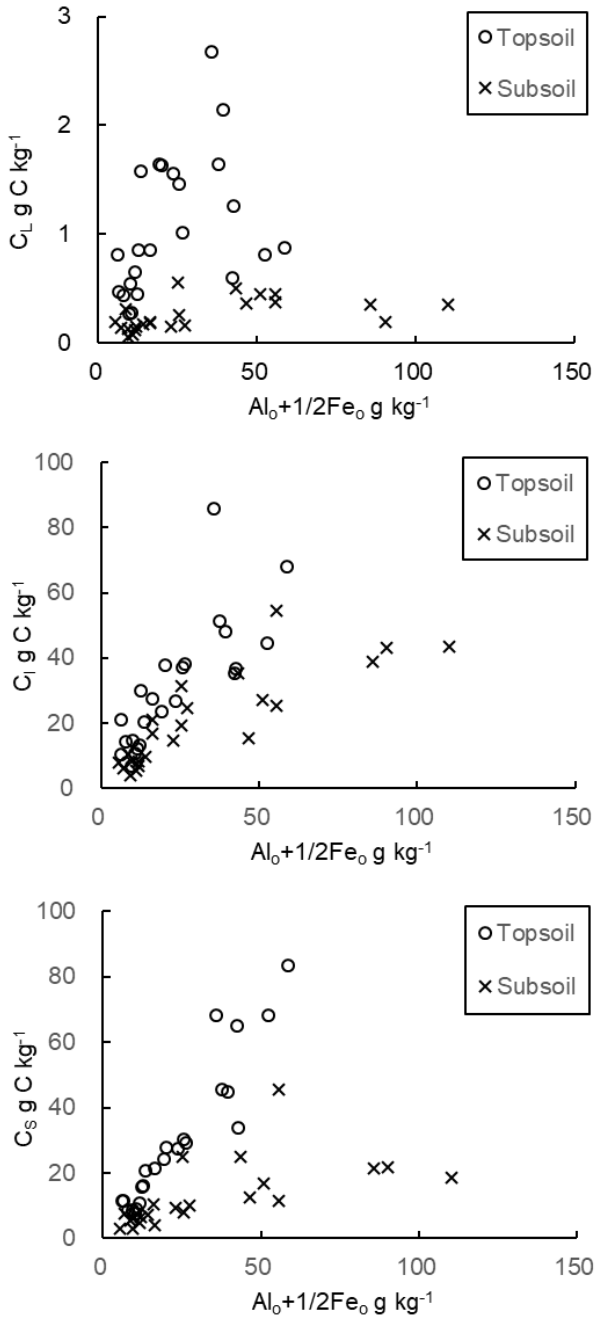

Fig. 4.3 The relationship of contents of nanocrystalline minerals (Al_o + 1/2Fe_o) and sizes of soil carbon pools (labile: C_L, intermediate: C_I, and stable: C_S) for each site. The data of topsoil is from Chapter 3.

4.3.4 Partial Correlations and Path Analyses on SOC Pools and Related Properties

Partial correlation is a possible method to elucidate the correlations between one of the mutually related variables (from single correlation analyses, Table S4.2) and an individual SOC pool across all sites. Thus, partial correlation analyses (Spearman) were applied to clarify

relationships between data of SOC pools and related properties after controlling for the confounding factors (e.g., the triangular relationships among MAT, $Al_o + 1/2Fe_o$, and sizes of SOC pools, Fig. S4.2). Variables for partial correlation analyses were selected based on the triangular relationships from previously identified single correlations (Fig. S4.2).

Table 4.5 Partial correlation of related properties on carbon pools of subsoil (20–40 cm)

(A)	MAT [a]		$Al_o + 1/2Fe_o$ [b]				DTN + MBN [c]		MBC/SOC		Aggregation Index [d]	
C_L [e]	–0.55**	–0.44*	0.67**	0.59**	0.29	–	0.87**	0.77**	–	–	–	–
C_I	–0.50*	–0.40	0.89**	0.87**	0.81**	0.86**	0.79**	0.61**	–0.45**	–0.21	–	–
C_S	–0.70**	–0.70**	0.81**	0.83**	0.68**	–	0.67**	0.32	–	–	–0.50*	–0.17
a_0	–	–	–0.50*	–	–	–0.13	–	–	0.71**	0.59**	–	–
	Zero-order	$Al_o + 1/2Fe_o$	Zero-order	MAT	DTN + MBN	MBC/SOC	Zero-order	$Al_o + 1/2Fe_o$	Zero-order	$Al_o + 1/2Fe_o$	Zero-order	MAT
	Controlled factors											

(B)	Ca_{ex} [b]		Clay + silt			EP [a]	
b_0 [e]	–0.47*	–0.25	–0.51*	–0.26	–0.33	0.50*	0.24
c_0	0.46*	0.23	0.52*	0.26	0.35	–0.52*	–0.24
	Zero-order	Clay + silt	Zero-order	EP	Ca_{ex}	Zero-order	Clay + silt
	Controlled factors						

[a] MAT, mean annual temperature; EP, excess precipitation. [b] $Al_o + 1/2Fe_o$, the content of nanocrystalline minerals; Ca_{ex}, exchangeable Ca. [c] DTN + MBN, dissolved total nitrogen plus microbial biomass nitrogen; MBC/SOC, the content of microbial biomass carbon in soil organic carbon. [d] Aggregation Index, an index obtained dividing occluded particle organic matter C by light fraction C. [e] C_L, C_I, and C_S, sizes of labile, intermediate, and stable SOC pools; a_0, b_0, and c_0, proportions of labile, intermediate, and stable SOC pools.
The row above the "Controlled factors" shows the zero-order (without controlling any factor) and the confounding factors being controlled. The number and asterisk show the correlation coefficient and significance, respectively, with or without controlled factors.

After controlling $Al_o + 1/2Fe_o$, the MAT was still negatively correlated with C_L and C_S ($r_{MAT\text{-}CI\ (Alo\ +1/2Feo)} = -0.44$, $P < 0.05$ and $r_{MAT\text{-}CS\ (Alo\ +1/2Feo)} = -0.70$, $P < 0.01$). The contents of nanocrystalline minerals primarily controlled C_I and C_S, even after controlling the MAT or DTN + MBN (Table 4.5A). When MBC/SOC was controlled for, $Al_o + 1/2Fe_o$ also strongly positively affected the C_I with a coefficient of 0.86 at 0.01 level. For DTN + MBN, after controlling $Al_o + 1/2Fe_o$, it was still correlated with C_L and C_I but not C_S. In terms of the effect of MBC/SOC, the

correlation between MBC/SOC and C_I disappeared when Al_o+1/2Fe_o was controlled for. The correlation between aggregation index and C_S disappeared when the MAT was controlled for (Table 4.5A).

In terms of proportions and MRTs of SOC pools, a_0 was not correlated with Al_o+1/2Fe_o after controlling MBC/SOC (Table 4.5A), while a_0 was correlated with MBC/SOC after controlling Al_o+1/2Fe_o ($r_{MBC/SOC\text{-}a0\ (Alo\ +1/2Feo)}$ = 0.59, $P < 0.01$). The b_0, which was largely determined by c_0, was not correlated with any related climatic, geochemical, or biotic properties after controlling confounding variables.

In addition to partial correlation analyses, path analysis was applied to find the controlling factors and their contributions to size, proportion, and MRT of each SOC pool across all sites (Fig. 4.4). Predominant factors that controlled the sizes of SOC pools were MAT, Al_o + 1/2Fe_o, and DTN + MBN. The available N for microbes (DTN + MBN) contributed to more than half of the variation in C_L with a normalized path coefficient (r_p) of 0.67 at 0.001 level, followed by a minor contribution from MAT (r_p = −0.33, $P < 0.05$). The contents of nanocrystalline minerals dominantly controlled C_I (r_p = 0.60, $P < 0.001$). The DTN+MBN positively contributed to C_I, and MAT negatively contributed to C_I (r_p = 0.30 and −0.30, respectively; $P < 0.01$). In terms of C_S, the positive contribution of MAT to C_S (r_p = −0.55, $P < 0.001$) was more influential than its contribution to C_I and C_L (r_p = −0.30, $P < 0.01$ and r_p = −0.33, $P < 0.05$, respectively). The positive contribution of Al_o + 1/2Fe_o to C_S was also found (r_p = 0.47, $P < 0.01$) but weaker than that to C_I (r_p = 0.60, $P < 0.001$). The Al_o + 1/2Fe_o, which was essential for C_I and C_S, was negatively affected by pH (Fig. 4.4).

Proportions and MRTs (quality) of labile SOC pool were mainly contributed by biotic and climatic properties, while geochemical properties contributed to intermediate and stable pools (Fig. 4.4). The proportion of the labile pool (a_0) was dominantly positively contributed by MBC/SOC (r_p = 0.69, $P < 0.001$), which was negatively affected by Al_o + 1/2Fe_o and positively affected by exchangeable Ca (r_p = −0.48, $P < 0.01$ and r_p = 0.41, $P < 0.05$, respectively). Whereas, the b_0 and c_0 were contributed by clay +silt and aggregation index (Fig. 4.4). In terms of MRTs, EP and

Al_o+1/2Fe_o positively contributed to $1/K_L$ and $1/K_I$, respectively (r_p = 0.55 and r_p = 0.58, respectively; $P < 0.01$).

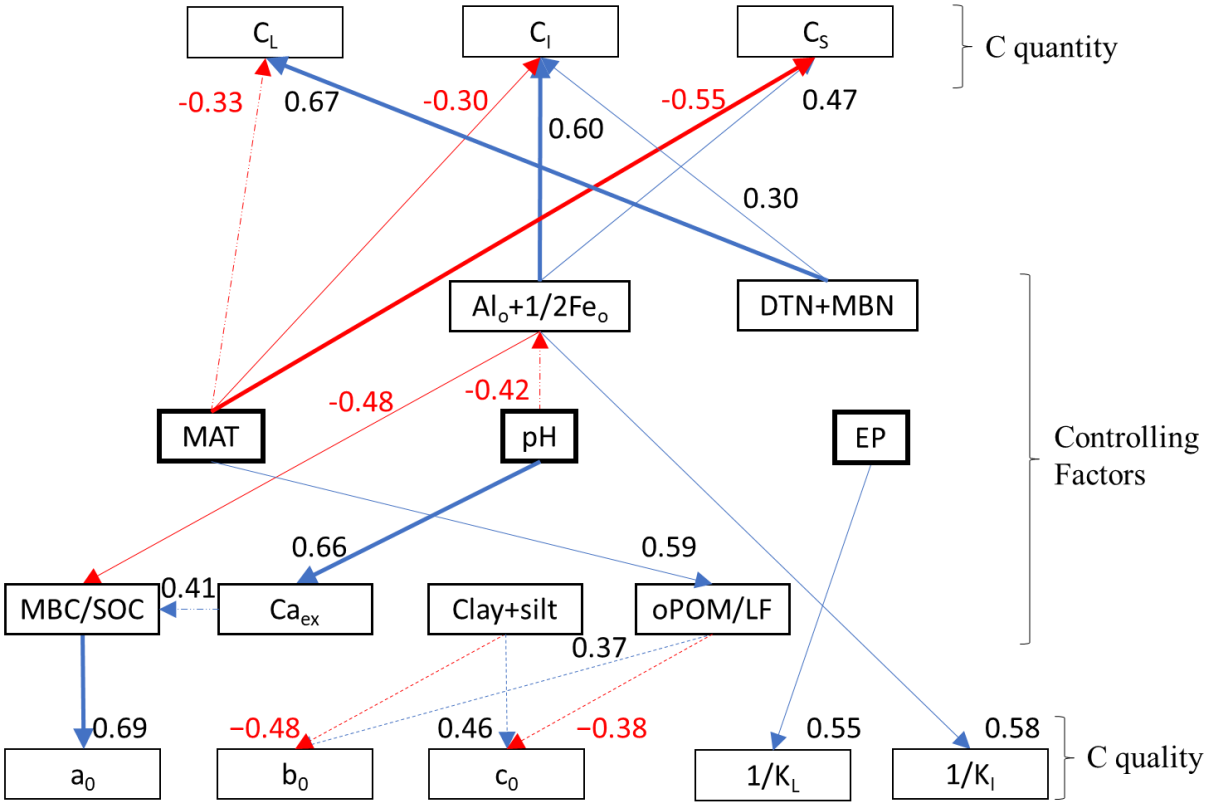

Fig. 4.4 A schematic diagram of the path analysis of subsoil (20–40 cm) for representing the contributions of each dominant factor on size (labile: C_L, intermediate: C_I, and stable: C_S), proportions (labile: a_0, intermediate: b_0, and stable: c_0), and mean residence times (labile: $1/K_L$ and intermediate: $1/K_I$) of soil carbon pools. Controlling factors include mean annual temperature (MAT), excess precipitation (EP), geochemical properties, dissolved total nitrogen and microbial biomass nitrogen (DTN + MBN), a proportion of microbial biomass carbon in SOC (MBC/SOC) and aggregation index (oPOM/LF). Type of arrow line represents significance of regression, i.e., thick solid line, $P < 0.001$; solid line, $P < 0.01$; dotted line, $P < 0.05$. Number above an arrow is the normalized path coefficient.

4.4 Discussion

4.4.1 Total SOC, Climatic, Biotic, and Geochemical Properties of the Sites

The quantities of SOC in subsoils have no significant difference across all regions (Table 4.1). The lack of significant differences in one-way analysis of variance with multiple comparisons indicates similarity in the quantity of SOC across study regions. The SOC content varied along the

elevation of sampling sites and was high at high elevation sites in each region (Table 4.2, Fig. S4.1). The stability of aggregates, which can trap and stabilize organic matter, is enhanced at high soil moisture sites over a year (Lavee et al., 1996; Six and Jastrow, 2002). The higher SOC content at IS site than that at the other sites within similar elevations (Fig. S4.1) would be partly because of the enhanced aggregation, indicated by a high aggregation index (Table 4.2 and S4.1). The relatively low soil pH can retard the activity of microbes and may also be a possible reason for high SOC content at IS sites (Table 4.2 and S4.1).

For the geochemical properties, soil pH was acidic to neutral and relatively low at the sites of high soil moisture (Table S4.1). The exchangeable Ca, which can have positive effects on carbon stabilization (Carmeis Filho et al., 2017; Rowley et al., 2018), was high at sites with relatively high pH ($r_s = 0.68$, $P < 0.01$). The content of nanocrystalline minerals, which is high in volcanic regions, was positively correlated with EP (Table S4.2). Sufficient soil moisture at the sites promotes the dissolution of parent material and retard further crystallization, simultaneously enriching the nanocrystalline minerals (Chapter 2). Meanwhile, the significant negative correlation between $Al_o+1/2Fe_o$ and MBC/SOC ($r_s = -0.61$, $P < 0.01$) may indicate that nanocrystalline minerals reduce the available substrate for microbes (Yang et al., 2020).

4.4.2 SOC Pools and Dominant Controlling Factors of SOC Pools

The intermediate SOC pool (61 ± 11% of SOC) predominantly controls SOC decomposition at the scale of years, which is indicated by the MRTs (Table 4.3) and contribution of the intermediate pool to the cumulative CO_2 release (59 ± 8%) by the end of incubation. The stable SOC pool was resistant to decomposition, which made up 38 ± 11% of SOC but had limited contribution to cumulative CO_2 release (2.7 ± 1.6%). Thus, the intermediate and stable SOC pools control long-term SOC stability. Whereas the labile pool contributed to 38 ± 8% of cumulative CO_2 release over the incubation, and the contribution concentrated in the first one or two months of the incubation (Fig. 4.1 and Table 4.3). The small proportion (0.9 ± 0.4% of SOC), high contribution of the labile pool to cumulative CO_2 release, and concentrated contribution at the

early stage of SOC decomposition indicate the labile SOC pool controls the short-term SOC stability for the subsoil (Table 4.3).

The results of correlation and path analyses represent that climate and geochemical factors, as well as biotic factors, control SOC pools in the subsoil directly and indirectly (Tables 4.4 and 4.5, Fig. 4.4 and S4.2). The sizes of SOC pools were significantly controlled by MAT, $Al_o + 1/2Fe_o$, and DTN + MBN (Fig. 4.4). The temperature directly influenced the sizes of three SOC pools. The MAT was positively correlated with sizes of three SOC pools (Fig. S4.2), and after controlling for $Al_o + 1/2Fe_o$, MAT was still correlated with C_L and C_S (Table 4.5A). Also, MAT widely contributed to C_L, C_I, and C_S (Fig. 4.4). These results indicate the negative effect of temperature on SOC pools: Low MAT reduces activities of microorganisms, which retards the decomposition of SOC and maintains SOC at high elevation sites with low MAT (von Lützow and Kögel-Knabner, 2009). Moreover, the significant direct contribution of MAT to C_S ($r_p = -0.55$, $P < 0.001$) was even higher than that to C_L ($r_p = -0.33$, $P < 0.05$), which emphasizes importance of temperature on the size of stable SOC pool (Fig. 4.4). The temperature sensitivity of the stable pool could be high in subsoil, and both labile and stable SOC would respond similarly to global warming (Fang et al., 2005; Yan et al., 2017). Hence, the significant impact of temperature on C_S suggests that the stable pool might also be vulnerable to climate change besides the labile pool for subsoil.

Nanocrystalline minerals control the sizes of intermediate and stable SOC pools, which occupied most composition and significantly affected the long-term stability of total SOC. A strong correlation was still existing between Alo+1/2Feo and C_I (and C_S) when confounding factors were controlled for. Also, the significant contributions of $Al_o+1/2Fe_o$ to C_I and C_S ($r_p= 0.60$, $P < 0.001$ and $r_p= 0.47$, $P < 0.01$, respectively) (Fig. 4.4) indicate the content of nanocrystalline minerals is the direct crucial factor affecting the intermediate and stable pools, rather than soil texture and pH. Whereas, the low soil pH, due to high soil moisture, represented a preferable condition for the formation of nanocrystalline minerals ($r_p = -0.42$, $P<0.05$) (Chapter 2). The covalent bonds between metal ions (i.e., Al and Fe) and functional groups of organic matter, as well as hydrophobic interactions, are abundant and form organo-mineral complexes to stabilize SOC in

Andosols (Wagai et al., 2020; Wagai et al., 2015; Zhao et al., 2020). As a result, at sites with high Al_o + 1/2Fe_o, inputted organic carbon would be stabilized as organo-mineral complexes and enlarge the intermediate and stable pools. Meanwhile, the $1/K_I$, which is an index of intermediate pool stability that predominantly controlled whole SOC decomposition, was positively contributed only by Al_o + 1/2Fe_o (Fig. 4.4). The inputted organic matters for the subsoil are expected to have potentially labile structures and associate with the mineral core first (nanocrystalline minerals) (Filimonova et al., 2016; Sokol and Bradford, 2019), hence the nanocrystalline minerals controls the stability of intermediate SOC pool. Thus, the nanocrystalline mineral is a predominant factor that controls the SOC content and its stability. Besides, the disappearance of correlation between C_L and Al_o+1/2Fe_o after controlling DTN + MBN (Table 4.5) and the negligible contribution of Al_o + 1/2Fe_o to C_L (Fig. 4.4) indicates none of the direct effects of Al_o + 1/2Fe_o on the size of the labile pool.

The available N for microbes (DTN + MBN) significantly controls the relatively labile carbon contents in the subsoil. DTN + MBN was positively correlated with C_L and C_I even after controlling Al_o +1/2Fe_o (Table 4.5A). The direct path coefficients between DTN + MBN and C_L or C_I, showed a significant positive contribution of DTN + MBN to C_L and C_I (Fig. 4.4). Under the condition that the N is sufficient for microbes, the extracellular enzymes released for obtaining N from relatively stable organic matter is consistently suppressed (Craine et al., 2007). Thus, the energy consumption, which is provided by labile organic matter, would be reduced at the N sufficient condition and enlarges the labile SOC pool, then gradually stabilized as the intermediate SOC pool.

For the C quality, the biotic properties (i.e., MBC/SOC) and EP control the proportions and MRTs of the labile pool, while geochemical properties control the relative stable pools. The significant correlation between MBC/SOC and a_0 (Table 4.5A), as well as the predominant contribution of MBC/SOC to a_0 (Fig. 4.4), represent the proportion of labile SOC pool was relatively high at the sites with sizeable microbial community. Moreover, the negative contribution of Al_o + 1/2Fe_o to MBC/SOC (Fig. 4.4) reflects the indirect effect of nanocrystalline minerals on

SOC stabilization by reducing microbial community (activity), which may occur due to the Al toxicity (Takahashi and Dahlgren, 2016). In contrast, the positive contribution from exchangeable Ca to MBC/SOC (Fig. 4.4) represents the positive effect of Ca cation in enlarging labile C input from plants and buffering pH, which is essential for maintaining a large microbial community (Carmeis Filho et al., 2017; Narendrula-Kotha and Nkongolo, 2017; Rowley et al., 2018). The climatic factor, EP, significantly contributed to $1/K_L$ rather than $1/K_I$. The high moisture would promote the leaching of soluble labile carbon from the topsoil and enlarged the C input as root exudates. This high carbon input may accelerate carbon replenishment (Tian et al., 2016), left behind partially decomposed materials, making the SOC in the labile pool more recalcitrant to decomposition during incubation. Moreover, the possible positive effect of clay and silt in stabilizing C and enlarging stable carbon pool was partially proved by the weak positive contribution of clay + silt to c_0 and negative contribution of clay + silt to b_0 (r_p = 0.46, P<0.05 and r_p = −0.48, P<0.05, respectively). In contrast, the aggregation index (oPOM/LF) negatively contributed to c_0 and positively contributed to b_0. The enhanced aggregation may enlarge the intermediate pool, which is expected to be decomposable at the scale of years, by physical trapping and hydrophobic interaction with relative labile C (John et al., 2005).

4.4.3 Comparing SOC Pools and Controlling Factors Between Topsoil and Subsoil

Soil organic carbon of subsoil could be more fragile to climate change than that of topsoil for a mid to long period due to the intermediate pool dominated pool composition (Fig. 4.2). The significantly higher proportion of intermediate SOC pool and lower proportion of stable SOC pool represents the SOC of the subsoil would be easier to decompose than topsoil (Fig. 4.2A). The carbon input is much lower in the subsoil than the topsoil, hence significantly smaller pools in the subsoil (Fig. 4.2B). The lower MRTs of the labile SOC pool may indicate the more labile nature of C input in the subsoil than topsoil (Fig. 4.2C). While SOC of the topsoil contains more vegetation related plant residues, the sources of SOC of the subsoil are more root exudates and movable microbially processed materials from topsoil (Vancampenhout et al., 2012). The

significantly higher contents of LF (mainly partially decomposed plant residues) (von Lützow et al., 2007) in the topsoil than that in the subsoil also supported this hypothesis (Fig. S4.3). Then, the root exudates and microbially processed organic matter would be stabilized by minerals directly and efficiently (Sokol and Bradford, 2019), which would still be exposed to oxidization and extracellular enzymes due to the low SOC saturation in the subsoil (Fig. 4.3). As a result, the inputted relative labile C was stabilized by nanocrystalline minerals and enlarged the intermediate SOC pool, which can be decomposed within a middle to long period (Fig. 4.2A and 4.4). In contrast, topsoil can contain chemically recalcitrant aliphatic organic matter from plant residues, which would be stable even associated in the kinetic zone (weak association) of nanocrystalline minerals (Zhao et al., 2020), which could be considered as a part of the stable pool (Eusterhues et al., 2005).

Temperature widely controls all SOC pools, including intermediate and stable pools, for both topsoil and subsoil, while the sizes of the stable SOC pool is more related to temperature in the subsoil than topsoil. The contribution of MAT on C_S was higher and more significant in the subsoil ($r_p = -0.55$, $P < 0.001$, Fig. 4.4) than in the topsoil ($r_p = -0.22$, $P < 0.05$, Chapter 1). The SOC in the stable pool of the subsoil could be more sensitive to temperature change due to the labile chemical nature (Angst et al., 2018; Matus et al., 2014). Also, different from topsoil, organic matter source (quantity and chemical nature) of the subsoil is not only controlled by the type and density of vegetation, which is significantly affected by precipitation. Low MAT would retard the decomposition of labile organic matter in the topsoil (enlarge the labile SOC pool), high EP would promote the C leaching, then increase the input of movable microbially processed C from topsoil to subsoil (Rizinjirabake et al., 2019; Stergiadi et al., 2016). The significant effect of EP on the stability of labile SOC pool in the subsoil was proved by the predominant contribution of EP on $1/K_L$ (Fig. 4.4). The enhanced C input positively affects the stability of labile SOC pool (subsoil) during incubation by promoting carbon replenishment, as discussed above (4.2).

The nanocrystalline minerals control intermediate and stable SOC pools for both topsoil and subsoil. The $Al_o + 1/2Fe_o$ was more related to the intermediate pool than the stable pool for the subsoil. The organic matter stabilized by minerals was more similar to the original litter input in

topsoil, while there were more labile root exudates and microbially processed materials in subsoil (Rumpel et al., 2012). Also, intermediate SOC pool of subsoil would mainly be contributed by mineral-associated labile C with high carboxyl functions (Parfitt et al., 1999). In contrast, the intermediate pool of topsoil could also be contributed by the hydrophobic, kinetic interacted, or aggregate-trapped partially decomposed residues (Semenov et al., 2019; Zhao et al., 2020). It can be proved by the predominant contributions of Al_o+1/2Fe_o on both the size and MRT of intermediate SOC pool in the subsoil of this study (Fig. 4.4). Consequently, the mineral core (mainly nanocrystalline Al and Fe in volcanic soils) rather than the chemical structure of organic matter, primarily controls the intermediate pool for subsoil. Whereas, for a deeper understanding of nanocrystalline minerals' effect on C stabilization, the chemical composition of SOC (with and without mineral association) should be focused on for further studies.

On the other hand, because of the relatively high ratio of Al_o to Si_o in topsoil than that in the subsoil for most of the sites (Fig. S4.4), the Al was more saturated with SOC (Fig. 4.3), forming organo-Al complex and left less extra Al to react with Si to form allophane in topsoil (Garrido and Matus, 2012). Thus, the subsoil had a low C saturation, and the mineral phase connected SOC is expected to be barely covered by latterly added organic matters and remain as a long-term decomposable SOC. The higher proportion of the intermediate pool in the subsoil than that in topsoil also supports this hypothesis. Meanwhile, this directly stabilized intermediate SOC pool had higher resistance for decomposition (higher $1/K_I$) than the intermediate SOC pool in the topsoil composed of the trapped residues or indirectly stabilized organic matter (Fig. 4.2C).

Besides, the available N for microbes (DTN + MBN) also controls the labile and intermediate pools of the subsoil (Fig. 4.4), while the effect of DTN + MBN was negligible for the topsoil (Fig. 3.5). The available N was more abundant for topsoil than subsoil across all sites, indicated by significantly higher DTN + MBN in the topsoil (0.24 ± 0.16 g kg^{-1}) than that in the subsoil (0.09 ± 0.05 g kg^{-1}). Nitrogen sources would not be the limiting factor for soil carbon storage, especially when the available N is sufficient (Neff et al., 2002).

4.5 Conclusion

Partitioning of soil organic carbon pool was conducted based on SOM fractionation and first-order model fitting to the SOC decomposition curve. This approach works well in identifying the predominant pool for whole SOC stability and factors that control the labile, intermediate, and stable SOC pools in subsoil. For the subsoil of tropical volcanic regions, the intermediate SOC pool is the predominant pool that controls the SOC stability within tens of years. The crucial factors that control sizes of SOC pools are the temperature, nanocrystalline minerals, and available N for microbes. Temperature negatively affects the sizes of all three pools, including intermediate and stable pools. Instead of soil texture and pH, the content of nanocrystalline minerals predominantly and positively controls the sizes of the intermediate and stable pools, as well as MRTs of the intermediate pool. The biotic and climatic factors, including microbial biomass, available N for microbes and EP, controls labile SOC pool.

Comparing with the topsoil, SOC in subsoil could be more sensitive to climate change. The higher proportion of intermediate pool (rather than the stable pool) in the subsoil than topsoil indicates the lower stability of SOC for a scale of tens of years. The stabilized organic matters by nanocrystalline minerals were more in the intermediate rather than stable SOC pool, and the effect of temperature on stable SOC pool was more substantial in the subsoil than that in the topsoil. Changes in excess precipitation would partially regulate the stabilities of labile and intermediate SOC pool for both subsoil and topsoil, which control the SOC decomposition at the scale of days to years. Meanwhile, the labile and intermediate SOC pools in the subsoil are partially controlled by DTN + MBN. Moreover, the low SOC saturation of nanocrystalline minerals in the subsoil indicates a potential capacity to stabilize more C. These findings deepened our understanding of the SOC stabilization mechanisms and emphasized the high climate-dependence and mineral-dependence of SOC with biotic influences in subsoil of tropical volcanic regions.

CHAPTER 5

CONTROL OF CLIMATE ON SOIL CHARGE CHARACTERISTICS THROUGH ORGANIC MATTER AND SOIL MINERAL DISTRIBUTIONS

5.1 General

The cation exchange capacity (CEC), which is widely applied to represent the surface charge characteristics of soils, is an essential component of soil properties. The CEC of the soil is a vital environmental indicator of elemental cycling and is commonly used in agricultural activities as an index of soil quality. The CEC represents soil surface ability in holding the exchangeable cations, mainly Ca^{2+}, Mg^{2+}, K^{+}, Na^{+}, and NH_4^{+}, which are critical for plant growth and reproduction. Meanwhile, soils with high CEC also have a high buffering capacity against soil acidification. The CEC is an inherent soil property that can change with the soil pH, clay and organic matter contents, and clay mineralogy. The variable charge from soil organic matter associated with the mineral phase and the constant charge from crystalline clay minerals are the main contributors to the CEC (Chorover et al., 2004; Wisawapipat et al., 2010).

The variable charge of the soil is based on the reactions of surface functional groups (e.g., the carboxyl group of organic matter and hydroxy group of nanocrystalline minerals) with ions in solution and depends on the pH and ionic strength of the soil solution (Naidu et al., 1994). In soils with low pH, the dissociation of cations by H^{+} from the variable charge sites leads to low CEC (Sharma et al., 2015). The nanocrystalline minerals can influence the variable charge of soil, while the strength and direction of this influence are regulated by soil pH. The points of zero charge of Al and Fe oxides or hydroxides and allophane (nanocrystalline minerals), which can provide variable charge, are generally high (pH 7.7–10.4 and 5.5–6.9, respectively (Mc Bride, 2018; Zelazny et al., 2018) when compared to the carboxy group of organic matter. Hence, the variable charge of soil is expected to be mainly contributed by soil organic matter (SOM) in acidic to neutral soils. The soil organic matter in the form of humic substances has a high variable charge density

of around 300 $cmol_c\ kg^{-1}$ (Klamt and Sombroek, 1988). The CEC can be controlled predominantly by the organic matter contents for both A and B horizon volcanic soils, as noted in New Zealand (Parfitt et al., 1995).

The content of soil organic matter, which provides a high variable charge, is affected by climatic and geochemical properties. The mean annual precipitation and temperature control the net primary productivity (Del Grosso et al., 2008). In forested areas, enough precipitation enhances the carbon input to the soil and promotes carbon sequestration via plant material (Cleveland et al., 2011; Running et al., 2000). The decomposition of soil organic matter is sensitive to soil temperature changes and moisture (Davidson and Janssens, 2006; Ise and Moorcroft, 2006). Low temperature retards the SOC decomposition by microbes and enlarges SOC content in the soil (Davidson et al., 2006; von Lützow and Kögel-Knabner, 2009). The exchangeable Al, which is toxic for soil microbes, increases with the decrease of pH in soils (pH < 6) under enhanced leaching conditions. The low pH and the contents of exchangeable Al adversely affect the microbial activities and affect the mineralization of soil organic matter. Notably, the nanocrystalline Al and Fe (active Al and Fe), which are rich in volcanic regions, have a strong ability to accumulate and stabilize C through the formation of organo-mineral complexes and microaggregates (Filimonova et al., 2016; Takahashi and Dahlgren, 2016; Wagai et al., 2020). The low temperature with enough moisture (EP) retards the crystallization and promotes the formation of nanocrystalline minerals (Chapter 2). Meanwhile, the bridging by Ca^{2+} between the mineral surface and organic matter can also promote soil organic matter at the sites with neutral to alkaline soil pH (Rowley et al., 2018).

The constant charge from crystalline clay minerals also contributes to CEC, especially for soils with low organic matter content such as some soils in India (Lal, 2004b). The permanent isomorphic substitutions of ions in soil clay mineral structures with those having different valences result in the constant charge (Chorover and Sposito, 1995). The constant charge from crystalline minerals is stable irrespective of the soil pH and has a strong affinity to NH_4^+ and K^+, especially in mica and vermiculite. The 2:1 type of crystalline clay minerals generally have high constant charge density; mica, smectite, and vermiculite have a constant charge density of 10–40, 70–90,

and 100–150 $cmol_c\ kg^{-1}$, respectively. Kaolin minerals have a relatively low constant charge density of 3–15 $cmol_c\ kg^{-1}$, while gibbsite has almost no constant charge (Buol et al., 2011; Sharma et al., 2015).

The distribution of crystalline clay minerals (e.g., 2:1 type clay minerals and kaolin minerals) would be affected by the moisture condition of the soil. Drier condition with less leaching causes high $H_4SiO_4^0$ activity in soil solution, which is favorable for the formation of halloysite other than allophane and imogolite in volcanic soils (Churchman and Lowe, 2011). In more developed soils, high pH and high $H_4SiO_4^0$ activity under alternating wet and dry conditions promote the formation of smectite, which has high CEC (Righi et al., 1999; Vingiani et al., 2004). In contrast, humid condition retards the crystallization of nanocrystalline minerals (Chapter 2). The 2:1 type of clay minerals and kaolinite would be unstable under intensive leaching and perudic conditions (Van Ranst et al., 2008), and gibbsite, which has almost no surface charge, exists in soils with intensive leaching (Kleber et al., 2007a).

Ascertaining factors that control the CEC of soil is complicated because of the confounding effects of both constant and variable charges. The climatic factors can control mineral and SOM distributions, which are assumed as the predominant contributors for constant and variable charges, respectively, as described above. Whereas, how climate affects the size of CEC through organic matter and clay mineral distributions is still unclear, especially for the relatively dry tropical volcanic regions. With less human interference, Mt. Kilimanjaro is an ideal study site to investigate the effects of climate and soil properties on the soil CEC. The soil pH of Mt. Kilimanjaro is slightly acidic to neutral (Chapter 2). Thus, the soil CEC of study sites should be contributed by the constant charge from crystalline clay minerals and the variable charge from SOM with negligible influence from the variable charge from nanocrystalline minerals because of their points of zero charge ranging slightly acidic to alkaline (Mc Bride, 2018; Zelazny et al., 2018). The soils have developed from homologous and pyroclastic volcanic deposits (tephra) under well-drained conditions (Chapter 2). The climate for Mt. Kilimanjaro is classified as tropical savanna to oceanic type (Aw to Cwb and Cfb), according to Köppen-Geiger climate classification (Peel et al., 2007). The

climatic condition for this site differs from those of other volcanic sites, such as in eastern and southeastern Asia where precipitation is intensive, that were studied previously (Nieuwenhuyse and vanBreemen, 1997; Van Ranst et al., 2008). In Mt. Kilimanjaro, the slope and elevation variation leads to a continuous change in temperature and precipitation. This difference in climate results in a diversity of SOM contents and crystalline clay minerals that determine the soil CEC.

The objective of this study was to 1) to clarify the contribution of constant charge and variable charges on soil CEC in Mt. Kilimanjaro; 2) and to figure out the effects of climate on the soil CEC through the distributions of soil minerals and organic matter in the relatively dry tropical volcanic region. Fifteen sites were selected to investigate the soil CEC, constant and variable charge densities, as well as the physicochemical and mineralogical properties. All the sites were divided into groups according to their climate, influenced by the slope, aspect, and elevation. I assumed that the soil CEC is both affected by the distribution of soil crystalline clay minerals (constant charge) and organic matter (variable charge), which are affected by temperature and moisture. I hypothesized that the variable charge contributions are higher in humid regions where organic matter is stabilized by nanocrystalline minerals, while the constant charge contributes more in dry regions where clay minerals are more crystallized.

5.2 Materials and Methods

5.2.1 Study sites and soil sampling

The study sites were located at the Mt. Kilimanjaro, Tanzania, which is same as Chapter 2. Fifteen sites with less human interference were selected at the northwest and southeast slopes of Mt. Kilimanjaro. Specifically, five sites were selected at the northwest slope (W) (1400–2440 m asl.), six sites at the high elevation region (≥ 1500 m asl.) of the southeast slope (EH), and four sites at the low elevation region (< 1500 m asl.) of the southeast slope (EL). The study sites were selected at locations with good soil drainage along the elevation gradient, ranging from 910 to 2800 m asl.

Soils from the A (A) and B horizons (B) were used for the primary soil analyses. Buried II A horizon was found in the profiles (deeper than 50 cm) of the highest two sites at the northwest slope. Totally, 30 soil samples were used for further analyses (five samples, W-A; five samples, W-B; six samples, EH-A; six samples, EH-B; four samples, EL-A; four samples, EL-B). All the samples were air-dried and sieved through a 2 mm mesh before the analyses. The soils at the study sites were classified as Andisols and Alfisols, according to the USDA soil taxonomy (Soil Survey Staff, 2014). The soil moisture regimes ranged from ustic to udic, and the temperature regimes ranged from isohyperthermic to isomesic (Table 5.1).

The vegetation, parent material and climate of study sites were described in Chapter 2 (2.2.1)

Table 5.1 Fundamental information of study sites in Mt. Kilimanjaro

Region	Site No.	Elevation m	MAT [a] °C	MAP [a] mm	EP [a]	STR [b, c]	SMR [b, c]	Soil classification [c]
Northwest slope (W)	5	1400–2440	13.2–19.2	750–1180	−120–510	Isothemic (2) Isomesic (3)	Ustic (3), Udic (2)	Haplustalfs (3), Hapludalfs (1), Hapludands (1)
High elevation of southeast slope (EH)	6	1530–2800	13.2–18.9	1200–1420	440–690	Isothemic (2), Isomesic (4)	Udic (6)	Hapludands (6)
Low elevation of southeast slope (EL)	4	910–1430	19.5–22.5	720–1640	−370–760	Isohyper-thermic (1), Isothemic (3)	Ustic (2), Udic (2)	Haplustalfs (2) Hapludands (2)

[a] MAT, mean annual temperature; MAP, mean annual precipitation; EP, excess precipitation.

[b] STR, soil temperature regime; SMR, soil moisture regime.

[c] Soil temperature and moisture regime, and soil classification (Soil Survey Staff, 2014).

5.2.2 Physicochemical properties

Exchangeable Al and H were extracted using 1 M KCl. Exchange acidity (Al + H) was determined by titration with 0.01 M NaOH to pH 8.3 using phenolphthalein as an indicator. The exchangeable Al was determined by back titration to pH 8.3 with 0.01 M HCl after the addition of a 4% NaF solution to release OH^- from $Al(OH)_3$. The content of exchangeable H was determined by subtraction (Funakawa et al., 2010). The sampling sites contain little or no carbonates. Hence, total C indicates the organic carbon content.

The methods of the other analyses including pH, exchangeable cations, soil texture and total elemental content are described in Chapter 2 (2.2.3 to 2.2.4), method for total C and N is described in Chapter 3 (3.2.3).

5.2.3 Mineralogical properties

The collected clay fraction was further fractionated to fine clay (< 0.2 μm) and coarse clay fractions (0.2–2 μm) by centrifugation. Then, both fine and coarse clay samples were treated as follows: K saturated and dried at 25 °C, K saturated and dried at 350 °C, K saturated and dried at 550 °C, Mg saturated and dried at 25 °C, and Mg saturated and dried at 25 °C then solvated in glycerol. The mineral composition of the saturated clay fraction was determined using an X-ray diffractometer (XRD) (Miniflex 600, Rigaku, Tokyo, Japan), which generates Cu-Kα radiation under a voltage of 40 kV and current of 15 mA. The peaks in the X-ray diffractograms were classified into four categories: dominant (height is more than twice of other peaks), clear, unclear (height is higher than three but lower than five times that of background noise), and not detected.

The constant charge density ($cmol_c\ kg^{-1}$ soil) was measured by the Cs absorption method (Chorover and Sposito, 1995; Zelazny et al., 2018). Briefly, the air-dried soil sample was saturated with Cs at pH 7 and dried at 65 °C for 48 hours. After drying, the cesium saturated soil sample was

shaken once with 0.01 M LiCl to displace Cs from weaker adsorption sites. Finally, the soil residue was shaken four times with 1 M ammonium acetate, and the extracted Cs, which is assumed to be adsorbed on to permanent charge sites, was measured with flame atomic absorption spectroscopy (AA-660, Shimadzu, Kyoto, Japan). The variable charge was calculated as CEC minus constant charge density. Because the points of zero charge of Al and Fe oxides and nanocrystalline Al and Fe minerals are generally high (pH 7.7–10.4 and 5.5–6.9, respectively) (Mc Bride, 2018; Zelazny et al., 2018), instead of Al and Fe oxides and nanocrystalline Al and Fe, soil organic matter would mainly contribute to the variable charge of soil.

The methods of the other mineralogical properties including ammonium oxalate extractable Al, Fe and Si (Al_o, Fe_o and Si_o), free iron oxides (Fe_d) and calculation of weathering indices (TRB and Fe_d/Fe_t) are described in Chapter 2.

5.2.4 Statistical Analysis

The normality of the climatic data, elevation, physiochemical and mineralogical properties, and charge characteristics was tested using the normal probability plot and Shapiro–Wilk test for A and B horizon soils separately before undertaking the correlation analysis. The Pearson product-moment correlation coefficient was applied to assess the correlation between climatic conditions and elevation. The Spearman rank correlation was applied to factors that did not pass the normality test even after logarithmic and root conversions. One-way analysis of variance (ANOVA) with Tukey–Kramer posthoc test was applied to find the difference in the total elemental contents and physicochemical properties between groups. Mann–Whitney U test was applied if the pre-conditions for ANOVA were not fulfilled. T-test was applied to find the difference between the properties of A and B horizons in the same region. The significance level of all the analyses was 0.05. All analyses were undertaken using the software IBM SPSS Statistics version 20.0.

5.3 Results

5.3.1 Climate and parent material

The MAT, MAP, and EP of the study sites are shown in Table 5.1. MAT decreased with increase in elevation for all sites ($r = -0.98$, $P < 0.01$). The correlation between MAP and elevation was not significant. Excess precipitation was positively correlated with elevation for all sites ($r = 0.62$, $P < 0.05$). The W and EL sites were relatively dry, and the EH sites were relatively humid. The EP ranged from −120 to 510 mm for the W sites, which was relatively lower than those for the EH sites (440 to 690 mm) with a similar elevation due to the relatively low MAP. For the EL sites (< 1500 m asl.), the EP was lower than that at the EH sites because of the higher potential evapotranspiration (−370 to 760 mm).

Table 5.2 shows the total elemental contents of the soil samples from different sites and different horizons. The contents were generally similar among regions and horizons. There was no significant difference in Fe and Al contents between the three groups. The Si content at W sites, which have low EP, was higher than that at EH sites. The Si content in the B horizon soil of EL sites was also higher than that at EH sites. The basic cations (K^+, Na^+, and Ca^{2+}) were relatively high at W sites, which were relatively dry. For the A and B horizons in the same region, all element contents were similar except for Al at W sites (Table 5.2).

Table 5.2 Total elemental contents of soil samples in different sampling regions

Region-horizon	Site no.	Fe	Al	Si	K	Na	Ca	Mg	TRB [a]	Fe_d/Fe_t [b]
					g kg^{-1}				$cmol_c$ kg^{-1}	
W-A	5	94 ± 33 [c]	103 ± 11 B [d]	160 ± 26 a	4.9 ± 2.0	3.7 ± 1.5 a	11 ± 4 a	5.0 ± 1.6	130 ± 33 a	0.36 ± 0.12
EH-A	6	120 ± 26	110 ± 24	95 ± 31 b	3.0 ± 1.3	1.9 ± 1.0 ab	2.8 ± 1.0 b	4.9 ± 1.5	70 ± 18 b	0.30 ± 0.03 B
EL-A	4	140 ± 38	110 ± 14	110 ± 25 b	4.6 ± 1.4	1.6 ± 0.5 b	4.8 ± 1.2 b	5.2 ± 2.5	88 ± 27 b	0.25 ± 0.04
W-B	5	99 ± 19	130 ± 10 A	160 ± 13 a	6.6 ± 2.1 a	3.1 ± 1.5 a	6.9 ± 5.8	4.0 ± 1.0	98 ± 45	0.43 ± 0.09 ab
EH-B	6	100 ± 39	130 ± 10	88 ± 22 b	3.4 ± 1.1 b	1.9 ± 0.9 ab	3.5 ± 1.7	4.1 ± 1.4	68 ± 17	0.51 ± 0.10 a A
EL-B	4	130 ± 29	130 ± 23	140 ± 14 a	3.1 ± 0.7 b	0.9 ± 0.4 b	3.2 ± 0.6	5.9 ± 1.8	77 ± 11	0.30 ± 0.11 b

[a] TRB, total reserve of bases. [b] Fe_d, dithionite citrate extractable Fe; Fe_t, total Fe. [c] Mean ± standard deviation.
[d] Different capital letters indicate the means in the same region are statistically different at $P < 0.05$ between A and B horizon. Different small letters indicate the means of A or B horizon are statistically different at $P < 0.05$ among groups.

5.3.2 General physicochemical properties

The general physicochemical properties of the soils are shown in Table 5.3. The pH (H_2O) ranged from 4.8 to 7.3 for all the sites. The pH (H_2O) at EH sites were significantly lower than that at W and EL sites. While the pH (H_2O) of A and B horizon soils were negatively correlated with EP (r_s = −0.58, P < 0.05 and r_s = −0.65, P < 0.01, respectively), the pH (KCl) showed negative correlation with EP for A horizon soils (r_s = −0.60, P < 0.05). The TC at EH-A (120 ± 68 g kg^{-1}) was higher than that at other sites (Table 5.3), and TC of A horizon soils was higher than B horizon soils for all the sites (Fig. 5.1). The TC increased with increase in elevation for both A and B horizon soils (r_s = 0.88, P < 0.01 and r_s = 0.79, P < 0.01, respectively). While it was negatively correlated with the MAT for both A and B horizon soils (r_s = −0.83, P < 0.01 and r_s = −0.69, P < 0.01, respectively), it was positively correlated with EP for both A and B horizon soils (r_s = 0.63, P < 0.05 and r_s = 0.71, P < 0.01, respectively). The clay content in W-B (49 ± 20%) and EL-B soils (52 ± 7%) was higher than that in EH-B (29 ± 12%).

Table 5.3 Physicochemical properties of the soils in different sampling regions

Region-horizon	pH(H_2O)	pH(KCl)	Total C g kg^{-1}	Total N g kg^{-1}	Clay %	Silt %	Sand %
W-A	7.0 ± 0.3 a [ab]	6.0 ± 0.4 a	54 ± 36 b	5.0 ± 4.3 ab	35 ± 6	54 ± 6 a	11 ± 3
EH-A	5.1 ± 0.4 b	4.3 ± 0.4 b B	120 ± 68 a	7.9 ± 4.4 a	35 ± 12 A	44 ± 6 b	21 ± 9
EL-A	6.8 ± 0.4 a	5.7 ± 0.3 a	25 ± 16 b	1.5 ± 1.5 b	49 ± 8	38 ± 8 b	13 ± 8
W-B	6.9 ± 0.4 a	5.4 ± 0.5 a	29 ± 29 ab	2.9 ± 3.4	49 ± 20 a	44 ± 20	7 ± 1 b
EH-B	5.7 ± 0.7 b	4.8 ± 0.2 b A	60 ± 43 a	3.9 ± 2.4	24 ± 6 b B	47 ± 12	29 ± 12 a
EL-B	6.6 ± 0.2 a	5.3 ± 0.2 ab	13 ± 6 b	1.1 ± 0.6	52 ±7 a	36 ± 5	12 ± 6 b

[a] Mean ± standard deviation. [b] Different capital letters indicate the means in the same region are statistically different at P < 0.05 between A and B horizon. Different small letters indicate the means of A or B horizon are statistically different at P < 0.05 among groups.

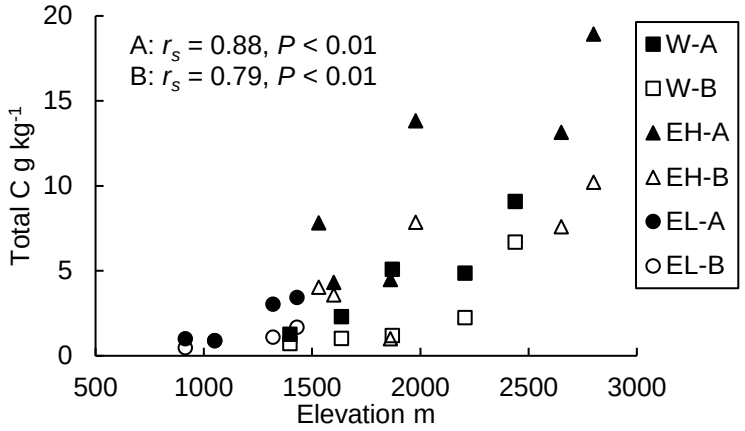

Fig. 5.1 Total carbon contents of the samples from each site at different elevations. W, EH, and EL mean northwest, high elevations of south-east, and low elevations of south-east slopes of Mt. Kilimanjaro, and A and B mean A and B horizons

5.3.3 Mineralogical properties

The TRB values (a weathering index) of all the sites were relatively high (> 40 $cmol_c\ kg^{-1}$) (Table 5.2). The TRB value recorded for the W-A sites (130 ± 33 $cmol_c\ kg^{-1}$) was higher than that noted for sites at EH-A and EL-A. The difference in the TRB between A and B horizon soils for the same region was not significant. The ratio of free Fe oxides to total Fe (Fe_d/Fe_t) (another weathering index) for the A horizon soils was similar across different sites (Table 5.2). B horizon soils at EL sites showed lower Fe_d/Fe_t values than those at EH sites, which may occur due to the limited weathering under the drier condition at EL sites. The relatively high Fe_d/Fe_t in the B horizon soils than the A horizon soils at EH sites may reflect the recent addition of volcanic ash at high elevation sites.

The results of selective extraction (Al_o, Fe_o, and Si_o) are shown in Table 5.4. The contents of Al_o+1/2Fe_o at EH sites (1500 to 2800 m asl.) and high elevation sites of W (> 2000 m asl.) were mostly higher than 20 g kg^{-1}, which is one of the criteria of Andic soil properties (Soil Survey Staff, 2014). Specifically, the contents of Al_o+1/2Fe_o ranged from 26 to 55 g kg^{-1} and 14 to 110 g kg^{-1} for A and B horizon soils at EH sites, respectively. The contents of Al_o+1/2Fe_o were lower at W and EL sites compared with sites at EH (Table 5.4). Further, the contents of Al_o+1/2Fe_o was found to be relatively high at elevated sites with low temperatures (Chapter 2). Excess precipitation

and Al_o+1/2Fe_o were significantly correlated for both A and B horizon soils (r_s = 0.75, P < 0.01

Table 5.4 Mineralogical properties of the soil for each site

Site	Elevation m	Selective extraction				Detection by XRD [a]							
		Fe_o	Al_o	Al_o+1/2Fe_o	Si_o	Coarse clay fraction				Fine clay fraction			
		g kg^{-1}				Kaolin	Mica	Vermi-culite	Gibbsite	Kaolin	Mica	Vermi-culite	Gibbsite
W-1A	2440	20.9	40.4	50.9	12.0	−	−	−	−	−	−	−	−
W-2A	2210	22.6	9.8	21.1	2.2	++	−	−	−	++	−	−	−
W-3A	1870	19.9	6.1	16.1	2.8	+	+	−	−	++	−	−	−
W-4A	1640	12.3	4.9	11.0	1.7	++	−	−	−	++	−	−	−
W-5A	1400	11.2	3.7	9.4	1.4	−	++	−	−	++	−	−	−
EH-1A	2800	36.9	30.2	48.6	2.5	−	−	±	−	−	−	++	−
EH-2A	2650	28.9	40.5	54.9	5.5	−	−	−	++	−	−	−	−
EH-3A	1980	27.6	39.2	53.0	5.3	−	−	−	++	−	−	−	−
EH-4A	1860	23.8	13.8	25.7	1.7	−	−	±	++	++	−	−	−
EH-5A	1600	19.9	34.6	44.5	10.1	−	−	±	++	−	−	−	−
EH-6A	1530	23.0	42.5	54.0	11.5	−	−	±	++	−	−	−	−
EL-1A	1430	10.4	12.0	17.2	4.1	+	−	−	+	+	−	−	+
EL-2A	1320	15.3	4.3	11.9	2.2	−	−	−	−	++	−	−	−
EL-3A	1050	10.8	4.5	9.9	1.0	+	+	−	+	++	−	−	−
EL-4A	910	10.8	3.8	9.2	1.1	+	+	−	−	++	−	−	−
W-1B	2440	24.0	62.7	74.7	26.1	−	−	−	−	++	−	−	−
W-2B	2210	18.0	13.5	22.5	2.9	−	−	−	−	++	−	−	−
W-3B	1870	16.0	4.9	13.0	1.9	−	++	−	−	++	−	−	−
W-4B	1640	9.1	6.0	10.5	0.7	−	++	−	−	++	−	−	−
W-5B	1400	7.2	2.3	5.9	1.3	−	++	−	−	++	−	−	−
EH-1B	2800	28.8	94.8	109.2	25.5	−	−	++	−	−	−	−	−
EH-2B	2650	29.6	89.3	104.1	24.7	−	−	±	−	−	−	−	−
EH-3B	1980	27.8	61.6	75.6	12.2	−	−	−	++	−	−	−	++
EH-4B	1860	15.8	6.2	14.1	0.9	−	−	−	++	−	−	−	++
EH-5B	1600	20.0	41.0	51.0	10.9	+	−	−	+	−	−	−	−
EH-6B	1530	22.3	43.1	54.2	11.2	−	−	−	++	−	−	−	++
EL-1B	1430	8.1	9.2	13.2	1.8	−	−	−	++	+	−	−	+
EL-2B	1320	10.2	3.4	8.5	1.5	−	−	−	−	++	−	−	+
EL-3B	1050	6.9	3.6	7.1	0.8	++	+	−	−	++	−	−	−
EL-4B	910	7.4	3.7	7.5	0.6	++	+	−	−	++	−	−	−

[a] XRD detection significance: ++, dominant; +, clear; ±, not clear; –, not detected.

and $r_s = 0.73$, $P < 0.01$, respectively), and the correlation was stronger than that between MAP and $Al_o+1/2Fe_o$ ($r_s = 0.62$, $P < 0.05$ and $r_s = 0.56$, $P < 0.05$, respectively). The significant positive correlation between $Al_o+1/2Fe_o$ and TC was found for both A and B horizon soils across all sites ($r_s = 0.89$, $P < 0.01$ and $r_s = 0.95$, $P < 0.01$). The ratio of TC to $Al_o+1/2Fe_o$ was relatively high in the A horizon than the B horizon soils (Fig. 5.2).

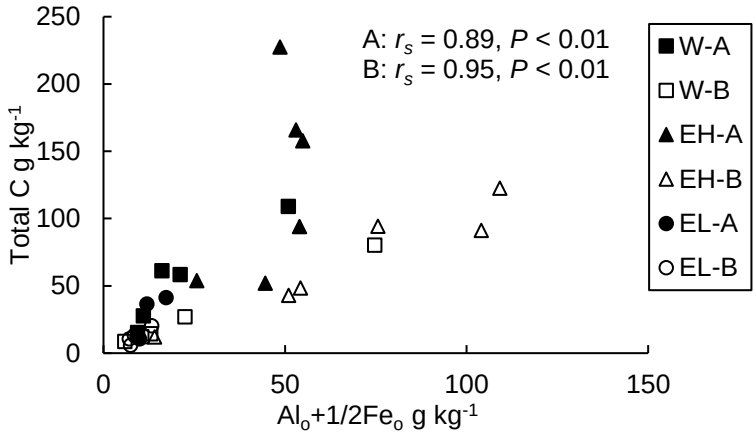

Fig. 5.2 Relationship between total carbon and nanocrystalline Al and Fe ($Al_o+1/2Fe_o$) in soil samples from each site. W, EH, and EL mean northwest, high elevations of south-east, and low elevations of south-east slopes of Mt. Kilimanjaro, and A and B mean A and B horizons

The results recorded using the XRD for crystalline clay minerals are shown on the right side of Table 5.4. The peaks of kaolin minerals (0.7-nm peak) were clear for A and B horizon soils at low elevation sites of W and EL, especially for the fine clay fraction. Gibbsite was detected in the soils of the lower elevation sites at EH and higher elevation sites at EL. Gibbsite was dominant in the fine clay fraction of B horizon soils at the low elevation sites of EH. The peak of mica (1.0-nm peak) appeared in coarse clay fractions of low elevation sites at W and EL. Meanwhile, vermiculite was detected at the highest site of EH (EH-1B, 2800 m asl.), especially in the fine clay fraction, but the peak was not clear in A horizon of the low elevation sites of EH. Smectite, which has a high constant charge, was not detected at any of the sites for both coarse and fine clay fractions.

5.3.4 Soil exchangeable cations and charge characteristics

The correlation for soil physicochemical and charge characteristics of A and B horizon soils

are shown in Table 5.5. The exchangeable Ca increased with the increase in pH (H_2O) for A and B horizon soils (r_s = 0.82, P < 0.01 and r_s = 0.85, P < 0.01, respectively) (Table 5.5). The exchangeable Al showed a negative correlation with pH (H_2O) for A horizon soils (r_s = −0.80, P < 0.01). While there was no correlation between the exchangeable Ca and TC, the exchangeable Al was positively correlated with TC for A horizon soils (r_s = 0.52, P < 0.05). Further, for the A horizon soils, the exchangeable Al also showed a positive correlation with Al_o+1/2Fe_o (r_s = 0.65, P < 0.01). In the case of weathering indices (TRB and Fe_d/Fe_t), a positive correlation between TRB and exchangeable Ca was found for both A and B horizon soils. Furthermore, the positive correlations were found between exchangeable Al and Fe_d/Fe_t (Table 5.5). The soil CEC was relatively high in soils with high TC (Table 5.5, Fig. 5.3) at high elevation sites. The CEC showed positive correlation with elevation and TC in the A horizon soils (r_s = 0.78, P < 0.01).

Table 5.5 Correlation matrix (Spearman) for soil physicochemical and charge characteristics of A and B horizon soils (15 sites)

A horizon	pH (H_2O)	pH (KCl)	TC	Clay	Al_o+1/2Fe_o	TRB	Fe_d/Fe_t
Ca_{ex} [a]	0.82**	0.86**				0.75**	
Al_{ex} [a]	−0.80**	−0.82**	0.52*		0.65**	−0.77**	0.59*
CEC			0.78**		0.54*		
CCD [b]	0.67**	0.71**				0.73**	
VCD [b]			0.95**		0.82**		

B horizon	pH (H_2O)	pH (KCl)	TC	Clay	Al_o+1/2Fe_o	TRB	Fe_d/Fe_t
Ca_{ex} [a]	0.85**	0.84**				0.57*	
Al_{ex} [a]		−0.53*					0.64*
CEC							
CCD [b]	0.55*					0.53*	
VCD [b]							

** Correlation is significant at the 0.01 level (2-tailed). * Correlation is significant at the 0.05 level (2-tailed).

[a] Ca_{ex}, exchangeable Ca; Al_{ex} exchangeable Al. [b] CCD, constant charge density; VCD, variable charge density.

The ratio of exchangeable cations (Ca^{2+}, Mg^{2+}, K^+, and Na^+) to CEC was relatively high at W and EL sites (Fig. 5.4), where the soil pH was high, and EP was low. The ratio of exchangeable cations to CEC reached one for the A horizon soils at W and EL (dry sites). On the contrary, the ratio of exchangeable cations to CEC was close to zero for the soils at EH (humid sites). The ratio

of CEC to TC ($cmol_c\ g^{-1}$, shown as the slope in Fig. 5.3) of EH-A and EH-B sites was constant (0.2 to 0.4 $cmol_c\ g^{-1}$). This ratio for the W and EL sites was higher than EH, especially those of the B horizon soils of W (about one $cmol_c\ g^{-1}$). The high CEC/TC ratio indicates that the CEC is not contributed by organic matter alone.

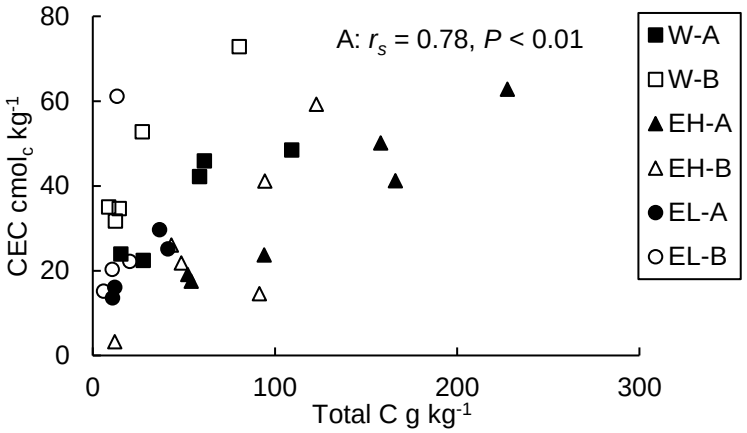

Fig. 5.3 Relationship between CEC and total carbon in the soil samples from each site. W, EH, and EL mean northwest, high elevations of south-east, and low elevations of south-east slopes of Mt. Kilimanjaro, and A and B mean A and B horizons

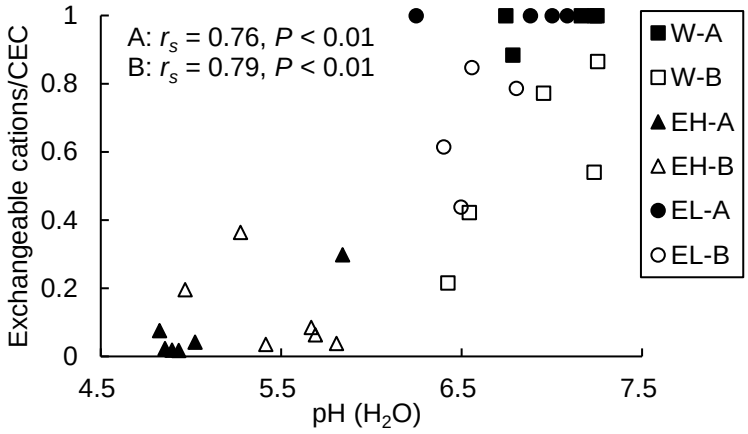

Fig. 5.4 Relationship between degree of base saturation and pH (H_2O) of the soil samples from each site. W, EH, and EL mean northwest, high elevations of south-east, and low elevations of south-east slopes of Mt. Kilimanjaro, and A and B mean A and B horizons

The relationships of CEC to variable charge density and constant charge density are shown in Fig. 5.5a and 5.5b, respectively. The variable charge density, which is derived mainly from organic matter, was positively correlated with CEC for both A and B horizon soils. (r_s = 0.78, P < 0.01 and r_s = 0.95, P < 0.01, respectively) (Fig. 5.5a). The variable charge density was also

positively correlated with TC and $Al_o+1/2Fe_o$ (r_s = 0.95, P < 0.01 and r_s = 0.82, P < 0.05, respectively) for the A horizon soils. The CEC increased with the increase of constant charge density for the dry sites of W and EL (Fig. 5.5b). The ratio of variable charge density to CEC was much higher at the humid sites (EH) than the dry sites (W and EL) (Fig. 5.5a).

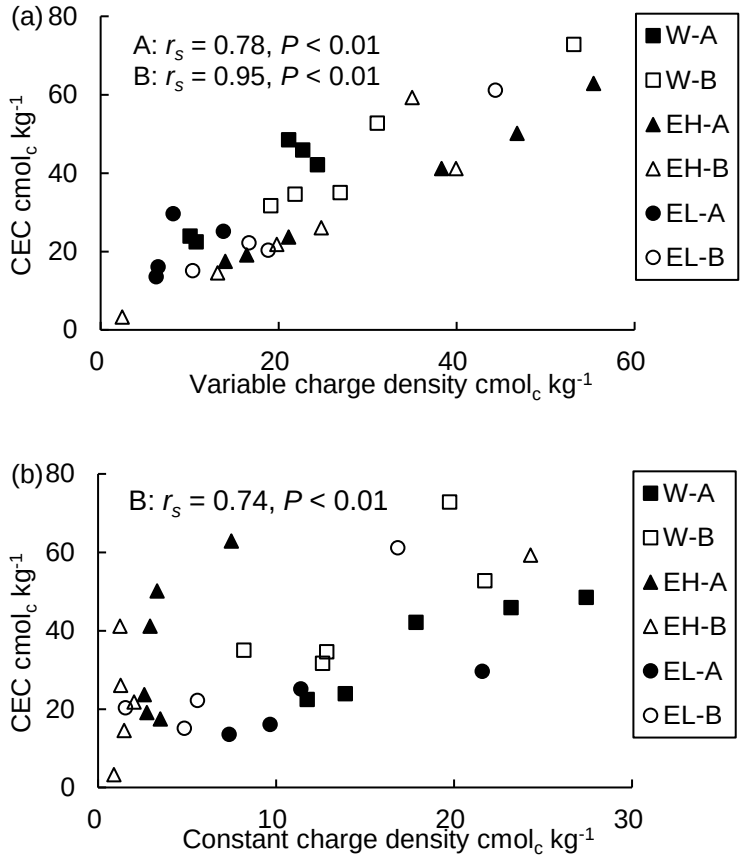

Fig. 5.5 Relationship between CEC and variable charge density (a), and relationship between CEC and constant charge density (b) at the soil samples from each site. W, EH, and EL mean northwest, high elevations of south-east, and low elevations of south-east slopes of Mt. Kilimanjaro, and A and B mean A and B horizons

The relationships of constant charge density to elevation and clay contents are shown in Fig. 5.6a and 6b, respectively. The constant charge density in the A horizon soils was higher than B horizon soils for the same site at EL and EH, except for the highest site of EH (Fig. 5.6a). There was no correlation between constant charge density and clay content for A and B horizon soils (Fig. 5.6b), although the reliable measurement of clay content in volcanic soils is generally difficult.

The constant charge density per clay in the soils at W sites was much higher than that at EH sites with similar elevation (Fig. 5.6b).

The contributions of variable charge and constant charge to CEC varied among the groups (Figs. 5 and 7). For the dry sites of W and EL, about 55% (52 ± 6% for W-A, 58 ± 11% for EL-A) of the CEC was contributed by the constant charge in A horizon soils and about 30% (34 ± 8% for W-B, 23 ± 11% for EL-B) in B horizon soils. For the humid sites of EH, the CEC was dominantly contributed by the variable charge. In detail, about 14% (12 ± 5% for EH-A, 16 ± 15% for EL-B) of the CEC was contributed by the constant charge. As a particular case, at the highest site of EH where the vermiculite was detected (Table 5.4), the constant charge contributed 41% of the CEC in B horizon soils (EH-1B).

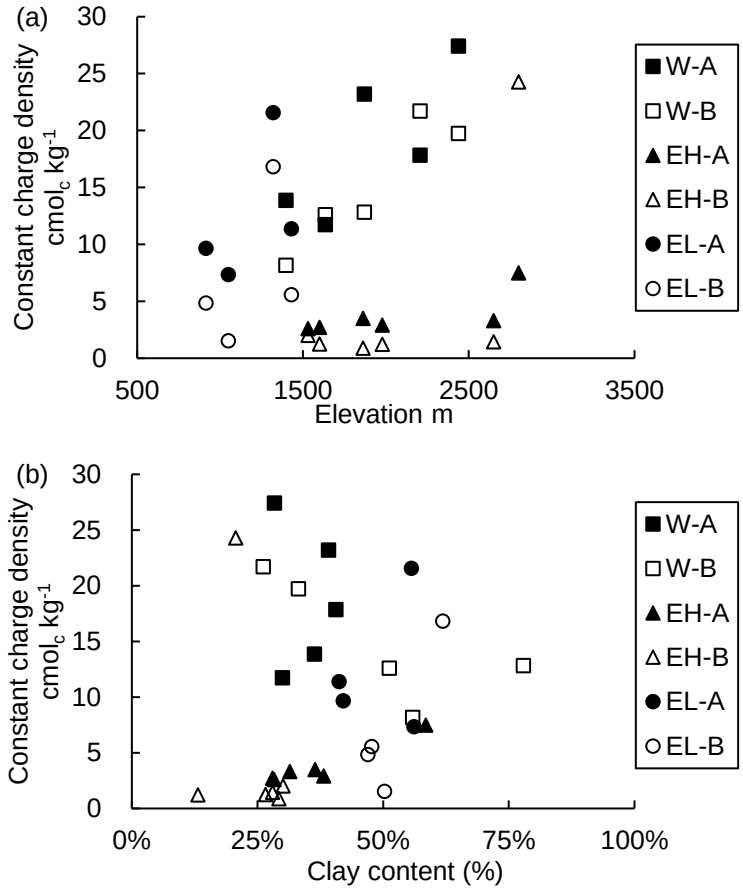

Fig. 5.6 Distributions of constant charge density along with elevation (a) and relationship between constant charge density and clay content (b) in the soil samples from each site. W, EH, and EL mean northwest, high elevations of south-east, and low elevations of south-east slopes of Mt. Kilimanjaro, and A and B mean A and B horizons

5.4 Discussion

5.4.1 Parent material and weathering degree

The soils of W, EH, and EL sites were developed from mafic volcanic tephra. The parent materials are mafic, specifically phonolitic tephra for both northwest and southeast slope of Mt. Kilimanjaro (Little and Lee, 2006; Wilkinson et al., 1986). The chemical compositions of the studied soils in W, EH, and EL sites were similar (Table 5.2), suggesting that the parent materials are identical. The indistinguishable chemical composition and soil texture also suggest that the parent materials for A and B horizons at a given site are the same. Greater EP (> 500 mm) leads to low Si contents at the EH sites due to the desilication process.

The weathering degree of the soils at W sites was slightly lower than that at EH and EL. The generally high TRB (Table 5.2) and low Fe_d/Fe_t (Table 5.2) of both the northwest and southeast slopes indicate the low weathering degree of the soils in Mt. Kilimanjaro (IUSS Working Group WRB, 2015). The weathering index Fe_d/Fe_t at W and EH sites were similar in the same elevation range. On the other hand, the relatively high TRB suggests more weatherable primary minerals, which indicates that the weathering degree of W-A is lower than EH-A and EL-A. The relatively high TRB at W sites may result from the low leaching at the sites with low EP (Watanabe et al., 2017). The weathering degree of A and B horizon soils were comparable within site (Table 5.2).

5.4.2 The soil pH, TC, and exchangeable cations

The pH of soils is slightly acidic to neutral and directly controlled by EP in the northwest and southeast slopes of Mt. Kilimanjaro. The positive correlation between EP and pH (pH (H_2O) and pH (KCl) (Table 5.2) indicates that the high EP leads to intense leaching, which decreases the soil pH and base cation content (Guicharnaud and Paton, 2006). The TC is relatively high in the soils at high elevation sites. The TC of the soils increases with an increase in EP and decrease in MAT along the elevation gradient. Low temperature decreases the microbial activities and retards carbon mineralization (Davidson and Janssens, 2006). Additionally, high precipitation can support the growth of indigenous plants, which have high primary production and hence can enhance the

carbon input. The significant positive correlation between the contents of Al_o+1/2Fe_o and TC (Fig. 5.2) indicates that the nanocrystalline Al and Fe have a strong ability to stabilize carbon in the soil (Filimonova et al., 2016; Wagai et al., 2020; Yu et al., 2017). Organic matter input in the form of root exudates and products of primary decomposition may be stabilized quickly by nanocrystalline Al and Fe (Wiseman and Puttmann, 2006).

The distribution of exchangeable cations is mainly affected by EP. The exchangeable bases were abundant at W and EL sites, which had low leaching (low EP) and high pH (Fig. 5.4). The exchangeable Ca was relatively high at W sites, but the bridging effect (Rowley et al., 2018) in stabilizing organic matter is unlikely to be significant for both A and B horizon soils as there was no correlation between exchangeable Ca and TC (Table 5.2). Low pH under high EP conditions, as seen in the soils at EH (pH < 6.0), enhances the release of Al^{3+} from minerals as exchangeable Al.

5.4.3 Distribution of soil minerals

The distributions of nanocrystalline Al and Fe and crystalline minerals are controlled by soil moisture and temperature in Mt. Kilimanjaro. The low temperature and high EP at the EH sites retard the crystallization of secondary minerals and result in higher nanocrystalline Al and Fe contents than the other sites. The low temperature with enough moisture at the high elevation sites retards the crystallization of nanocrystalline minerals such as allophane and ferrihydrite (Chapter 2). The retardation of crystallization at the high elevation sites enlarged the contents of nanocrystalline Al and Fe and formed the organo-mineral complexes to stabilize SOC (Matus et al., 2014; Takahashi and Dahlgren, 2016). Also, instead of crystalline phyllosilicate, the formation of nanocrystalline minerals is favored in volcanic soil, especially from tephra materials with high Al and Fe but low Si contents (EH sites, Table 5.2) (Harsh, 2011).

The kaolin minerals were the predominant crystalline clay minerals in the studied sites, especially in the soils at low elevation sites of W and EL (dry sites). Kaolin minerals would form in the soil when dry and moist conditions alternate (Churchman and Lowe, 2011) in A and B

horizon soils at W and EL. Halloysite was not included in the analyses, as it is not found in the study area because the marked dry season promotes the formation of kaolinite but retards the formation of halloysite (Chapter 2). Gibbsite was detected at the sites with high EP (low elevation sites of EH and high elevation sites of EL). Gibbsite is stable in soils where leaching is high, and Si activity is low (Huang et al., 2018). Mica at the low elevation sites of W and EL may have been carried by the wind from the surrounding areas where the parent materials are other than volcanic deposits (Lowe, 1986). Vermiculite was clearly found only in the highest site (EH-1) close to the snowline (Table 5.4), a site where may have significant weathering (Reynolds, 1971). Vermiculite could have been formed from mica under low pH conditions (Watanabe et al., 2006) and increase the constant charge density of the soil. Though smectite is expected to be formed in soils under alternating wet and dry seasons (Righi et al., 1999; Vingiani et al., 2004) and has been reported in the nearby volcanic areas (van der Gaast et al., 1986), I did not find smectite in this study. Soil solution composition indicates that smectite could have been formed in the northwest slope of Mt. Kilimanjaro, where it is relatively dry (Chapter 2). The absence of the smectite peak in the coarse and fine clay fractions for W sites may be because of the fine crystal size and the curved shape of the smectite, which are beyond the XRD detection capacity (van der Gaast et al., 1986).

5.4.4 Controlling factors for CEC

In Mt. Kilimanjaro, both variable and constant charges of the soil contribute to the CEC. The variable negative charge, which is mainly provided by the soil organic matter, positively affects the CEC. The points of zero charge of nanocrystalline Al and Fe minerals are generally high (neutral to alkaline) as described before (Mc Bride, 2018; Zelazny et al., 2018), resulted in the negligible effect of nanocrystalline minerals on CEC at slight acid to neutral conditions. The correlation between TC and CEC indicates that the CEC is strongly affected by the variable charge from organic matter (Table 5.5, Fig. 5.5). The enhanced growth of woody plants by high EP promotes the carbon input (Cleveland et al., 2011), and low MAT retards the decomposition of inputted organic matter by microbes (von Lützow and Kögel-Knabner, 2009); as a consequence, SOC content is expected to be enlarged at sites with high elevation (Fig. 5.1). For the A horizon

soils, the low pH with high exchangeable Al (high moisture), which is toxic for microbes, retards the mineralization of inputted organic matter and maintains a high TC content at the EH sites (Table 5.5). Meanwhile, the inputted organic matter is expected to be stabilized by nanocrystalline Al and Fe (organo-mineral complexes), significantly enlarged the CEC for all the soils in the study sites. The low temperature and humid condition at the high elevation sites enhanced the contents of nanocrystalline minerals by retarding the crystallization (Harsh, 2011; Lyu et al., 2018). Consequently, more organic matter is stabilized by more concentrated nanocrystalline Al and Fe (Fig. 5.2) (Rasmussen et al., 2018; Takahashi and Dahlgren, 2016; Zhao et al., 2020), resulting in higher CEC of the soils at the high elevation sites. On the other hand, the crystallization of nanocrystalline minerals is promoted for sites with higher temperatures (EL) and lower moisture (W and EL) (Chapter 2). Thus, the variable charge natures, which are highly related to the organo-mineral complexes, are getting weaker due to the progressive crystallization.

The constant charge from crystalline clay minerals significantly contributes to the soil CEC of dry sites (Fig. 5.6). The constant charge density would be enhanced by expandable 2:1 type minerals, high contents of kaolin minerals, and mica (Sharma et al., 2015). The ratio of constant charge density to clay content of the soil is higher at W than EH sites (Fig. 5.6b), which indicates that the clay in W sites (dry sites, Table 5.1) has more constant charges than other sites. In the case of W sites, although smectite was not detected by the XRD in both coarse and fine clay fractions, fine smectite, which beyond the detection of XRD, may exist and contribute to the constant charge, especially for elevated W sites (sites with wet and dry alternation) (Table 5.1, Fig. 5.6a). Relatively dry conditions with higher pH and Si activities enhance the formation of 2:1 crystalline minerals with a constant negative charge, such as smectite, in volcanic soils (Hodder et al., 1993; van der Gaast et al., 1986). At low elevation sites of W and EL, formations of kaolin minerals are promoted. Although the kaolin minerals have relatively low constant charge density (Buol et al., 2011), the high content of kaolin minerals at W and EL sites (Table 5.4) can partially explain the relatively high constant charge. Besides, at the dry sites with high pH and TRB, the contamination with eolian mica from the surrounding areas retains and would contribute to the constant charge for

both W and EL sites with low weathering degree (Table 5.4 and Fig. 5.6). Whereas, in general, kaolinite and mica have low CEC of about 1 to 5 $cmol_c\ kg^{-1}$ and 5 to 15 $cmol_c\ kg^{-1}$, respectively (Thompson and Ukrainczyk, 2002; White and Dixon, 2002). Hence, 2:1 type crystalline minerals (smectite and/or vermiculite), which were not detected in the X-ray diffraction analysis, could have been present in the soils of the elevated sites in dry regions (W and EL), considering their high constant charge density (> 10 $cmol_c\ kg^{-1}$) (Fig. 5.6a). On the other hand, for the humid sites (EH), high EP promotes gibbsite formation, which has almost no constant charge, instead of 2:1 and/or kaolin minerals (Chapter 2).

The contribution of variable charge and constant charge to CEC varies in different groups (different climatic conditions) and horizons (Fig. 5.7). The soil organic matter contributes to the high CEC of the soils at all the sites (Figs. 3 and 7). The CEC for the humid sites (EH) is controlled by the variable charge from organic matter (Figs. 5 and 7). The organic matter input is relatively high at the high elevation sites at EH due to the high net primary productivity (high EP) and low decomposition rate (low MAT and pH with high exchangeable Al). The high levels of nanocrystalline Al and Fe in the soils at EH sites (humid) help stabilize the high amount of inputted organic matter, and it dominantly contributed to the CEC. Whereas, for the soils at W and EL sites where the conditions are relatively dry, both the variable charge from organic matter and constant charge from minerals contributed almost equally to the total CEC (Fig. 5.7). The constant charge from crystalline minerals was relatively higher and contributed more to the CEC in the A horizon soils than B horizon soils at W and EL, where the crystallization is expected to be promoted (Figs. 6 and 7). The formation of crystalline clay minerals, including smectite, might be promoted when distinct dry and wet cycling occurred in the upper horizon and enlarge the soil CEC (Churchman and Lowe, 2011; Vingiani et al., 2004). Further studies are needed to confirm this. In the particular case of the highest site (EH-1), which was in proximity to the snowline, the vermiculite can also contribute a high constant charge to the CEC (Fig. 5.6a).

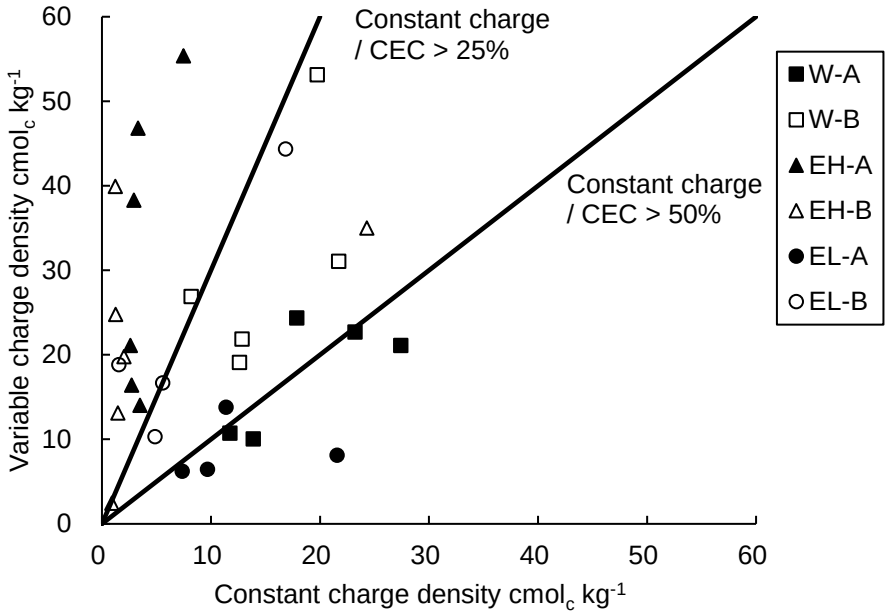

Fig. 5.7 The contribution of constant and variable charges to CEC for soil samples at W, EL, and EH sites. W, EH, and EL mean northwest, high elevations of southeast, and low elevations of southeast slopes of Mt. Kilimanjaro, and A and B mean A and B horizons

5.5 Conclusion

The contribution of organic matter and clay minerals to the soil CEC of Mt. Kilimanjaro differed depending on the climate's spatial pattern. At the humid sites (EH), the contribution of the variable charge to the CEC is relatively high for both A and B horizon soils. At humid and elevated sites with low pH, the content of nanocrystalline Al and Fe is enhanced, and the high organic matter content is preserved by organo-mineral complexes (nanocrystalline Al and Fe associated with organic matter), which significantly enlarge the soil CEC. At the dry sites (W and EL), the variable charge relating to the organo-mineral complexes is lower due to the progressive crystallization of nanocrystalline Al and Fe. In contrast, at the sites of W and EL, the CEC was contributed by the constant charge derived from crystalline clay minerals, which included kaolin minerals, mica, and possibly smectite. This study highlights the importance of moisture and temperature as factors that influence the distributions of organic matter and soil minerals, which control the soil CEC. In addition to the variable charge, the contribution of constant charge from crystalline clay minerals

to the soil CEC should also be considered for the weakly weathered volcanic soils in dry regions.

CHAPTER 6

SUMMARY AND CONCLUSION

6.1 Factors controlling the distribution of soil secondary minerals in volcanic regions of Tanzania

In the volcanic regions of Tanzania, including Mt. Kilimanjaro, Mt. Meru, and Mt. Kieyo, soils are formed on relatively recent tephra deposits. Because of the diversity of climate caused by the volcanic terrain in these regions and different parent material compositions, various soil secondary minerals were expected to form. Hence, here were ideal regions to determine the distribution of secondary minerals in soils formed on tephras in the volcanic regions of Tanzania and to estimate the effects of climate and parent material composition on the distribution of secondary minerals.

The soils in Mt. Kilimanjaro and Mt. Meru were rich in Fe or Mg, whereas soils in Mt. Kieyo were rich in Si, indicating mafic and felsic parent materials, respectively. Soil moisture and temperature are critical factors influencing the distribution of secondary minerals, whereas parent material compositions have less effect on soil minerals in the volcanic regions of Tanzania.

Instead of halloysite, which was expected to be unstable in the soil with significant seasonal drying and the moderate soil pH, kaolinite was rich in low elevation sites. Alternation of moist and dry conditions, especially drying, increased the $H_4SiO_4^0$ activities in soil solution. The high $H_4SiO_4^0$ activities at low elevations found in the kaolinite stability field favor the formation of kaolinite. Besides, the expense of nanocrystalline minerals because of the higher temperatures at low elevations also promotes kaolinite formation. In contrast, gibbsite, which is considered a final product of weathering, was also found in soils from high EP sites (KL-SE and S-KY-R). The relatively high weathering degree and EP decreased $H_4SiO_4^0$ activities and favored the formation of gibbsite.

In the weakly weathered volcanic soils, nanocrystalline Al and Fe are abundant and sensitive

to moisture and temperature changes. In general, low temperature at more elevated sites with sufficient moisture (EP) retards the crystallization and promotes the formation of nanocrystalline minerals in volcanic regions. In dry regions, which experiences at least one clear dry season during a year (EP < 500 mm), insufficient EP would limit the formation of the nanocrystalline minerals. In the regions with a lower weathering degree (MR and S-KY-C), EP still positively influences the distribution of nanocrystalline Al and Fe even at the humid sites (EP > 500 mm). Drying of the soils would accelerate the crystallization of Al and Fe and retard the supply of Fe and Al along with Si to form new nanocrystalline Al and Fe. In humid regions, the temperature is the primary factor: low MAT at high elevations would retard the crystallization. Moreover, the distribution of nanocrystalline Al and Fe, which could preserve organic matter, should not be ignored when studying global C cycle.

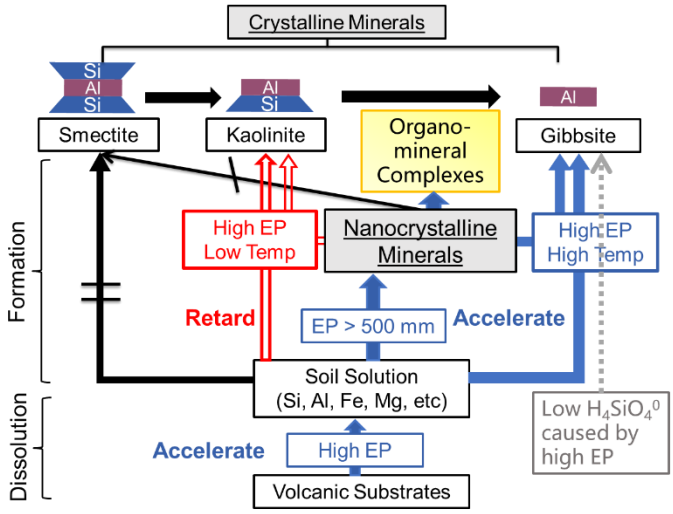

Fig. 6.1 Summary of factors controlling soil secondary mineral formations

6.2 Effects of climatic and geochemical properties on soil organic carbon pools in tropical volcanic regions

Understanding the factors that control the storage of soil organic carbon (SOC) is an urgent priority for mitigating global climate problems. In detail, it is necessary to determine the factors controlling SOC pools with differing stabilities. For this purpose, top (0 to 20 cm) and subsoil (20 to 40 cm) samples were collected along an elevation gradient from four volcanic regions of Tanzania (two regions) and Indonesia (two regions) under largely-undisturbed vegetation. A three-

pool kinetic model was fitted to accumulative CO_2 release curve produced over 343-day incubation to determine the sizes of the labile and intermediate SOC pools (C_L and C_I, respectively) and their mean residence times ($1/K_L$ and $1/K_I$, respectively), where the size of the stable SOC pool (C_S) was measured as non-hydrolyzable carbon. Correlation and path analyses were performed using the results of soil fractionation and model fitting with climatic and geochemical properties.

Fitting the multiple pool first-order kinetic model to the SOC decomposition curves produced over long-term incubation and SOM fractionation is a feasible method for understanding the factors that control SOC pools with different decomposability. The intermediate pool comprised about 50% of total SOC, was responsible for more than half of total accumulative CO_2 release, and controlled total SOC stability for years to decades in both topsoil and subsoil. The content of nanocrystalline minerals was strongly correlated with C_I and C_S, suggesting that organo-mineral complexes are the essential factor that controls C_I and C_S rather than soil texture or pH for both topsoil and subsoil. Temperature also widely affect all SOC pools. The low temperature at the high elevation sites retard the decomposition of the whole SOC. The significant correlations of excess precipitation with $1/K_L$ represent the effect of moisture on the labile SOC pools' potential stabilities by influencing the quantity and quality of C input.

Climatic factors primarily affect relatively labile SOC pools, whereas geochemical factors influence more stable pools and control total SOC. The findings have important implications for understanding the SOC stabilization mechanisms, which is an essential process of the C cycle, in tropical volcanic soils.

6.3 Differences of sizes and stabilities of SOC pools and their controlling factors in topsoil and subsoil

The soil organic carbon in the subsoil may not be so resistant to decomposition, as previously assumed. However, the factors that control the SOC pools in subsoil are still not well-known and should be different from topsoil. By comparing the sizes and stabilities of SOC pools and their controlling factors, the difference of SOC stabilization mechanisms between topsoil and subsoil could be found.

Comparing with topsoil, stabilized organic matters were more in the intermediate rather than stable SOC pool. The predominant contributions of Al_o+1/2Fe_o on both the size and MRT of intermediate SOC pool were found in the subsoil. The organic matters stabilized by minerals were more labile root exudates and microbially processed materials in subsoil, which stability is controlled by the mineral core (nanocrystalline minerals). Also, intermediate SOC pool of subsoil would mainly be contributed by mineral-associated labile C with high carboxyl functions. Consequently, the mineral core (mainly nanocrystalline Al and Fe in volcanic soils) rather than the chemical structure of organic matter, primarily controls the intermediate pool for subsoil. Moreover, the subsoil had a low C saturation, and the mineral phase connected SOC is expected to be barely covered by latterly added organic matters and remain as a long-term decomposable SOC. Moreover, the effect of temperature on stable SOC pool was more substantial in subsoil. Available N for microbes partially controlled the labile and intermediate SOC pools in subsoil (limitated available N for microbes) but not in topsoil. Thus, the subsoil SOC would be more sensitive to climate change than the topsoil SOC. However, the low SOC saturation of nanocrystalline minerals in the subsoil indicates a potential capacity to stabilize more C. For a deeper understanding of C stabilization mechanisms, the chemical composition of SOC and the association between SOC and nanocrystalline minerals should be focused on for further studies.

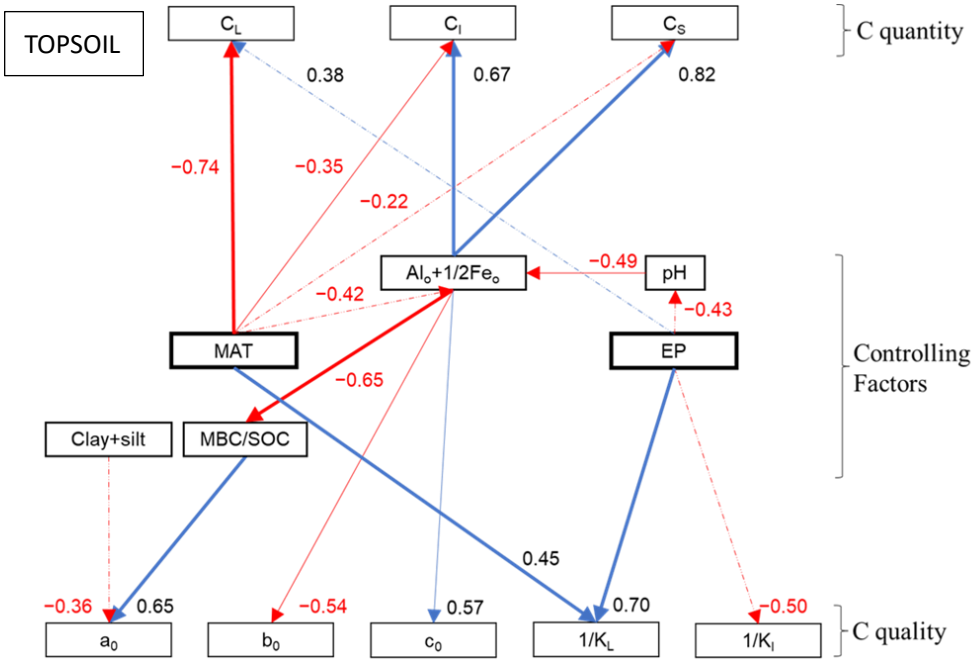

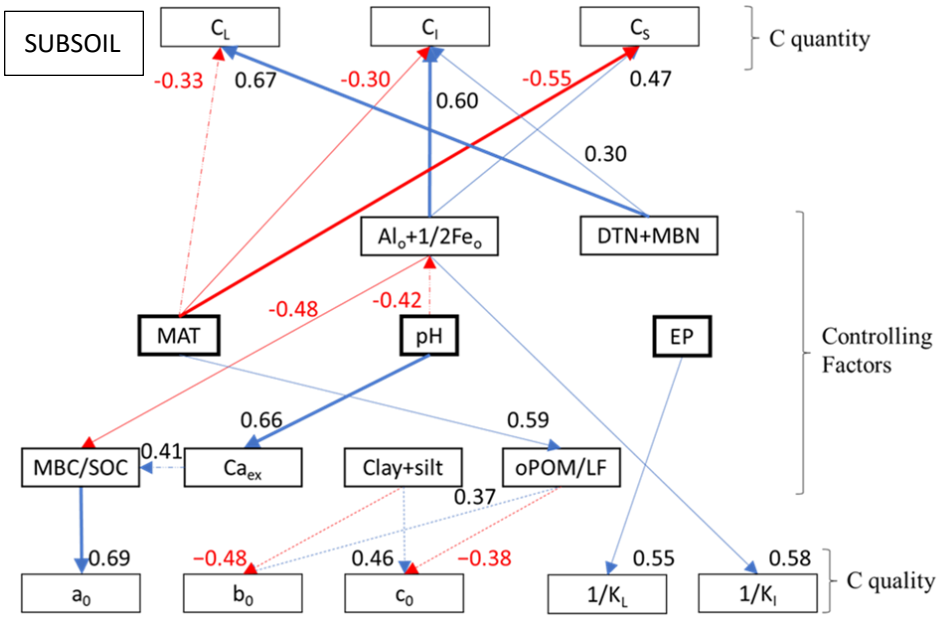

Fig. 6.2 Summary of factors controlling soil organic carbon pools in both topsoil and subsoil

6.4 Control of climate on soil charge characteristics in Kilimanjaro, Tanzania

The soil cation exchange capacity (CEC), which is contributed by constant and variable charges, is a vital indicator of soil fertility and affects elemental cycling. The variable charge of the soil is due to surface functional groups' reactions with ions and depends on the pH, which may mainly be contributed by carboxyl group of organic matter and hydroxy group of nanocrystalline minerals. On the other hand, the permanent isomorphic substitutions of ions in soil clay mineral structures result in a constant charge. The constant charge from crystalline minerals is stable irrespective of the soil pH. Climate is expected to affect soil CEC by controlling secondary minerals and organic matter distributions, which was discussed above, as well as soil pH.

The soils of 15 soil profiles from southeast and northwest slopes of Mt. Kilimanjaro along the elevation gradient (910–2800 m asl.) were collected for determining the factors that control the soil charge characteristics. The results showed that the contribution of the variable charge to CEC was high at the humid sites of the elevated area of the southeast slope. The high content of organic matter at the humid sites, which was stabilized as organo-mineral complexes by nanocrystalline minerals, enlarged the soil CEC, being more evident at cool high elevation sites. On the other hand, at the dry sites on the northwest slope and low elevations of the southeast slope, the constant charge

and variable charge contributed equally to the CEC. The variable charge from organo-mineral complexes was smaller due to the progressive crystallization of nanocrystalline minerals under the dry condition, and the formed crystalline clay minerals would contribute to constant charge density. The moisture and temperature, factors that influence the distributions of nanocrystalline and crystalline secondary minerals and organic matter, control the soil charge characteristics. The enriched organic matter stabilized by nanocrystalline minerals can provide a high variable charge for volcanic soil. However, the constant charge from crystalline clay minerals should also be considered in addition to the variable charge when studying the weakly weathered volcanic soils in the relatively dry regions.

REFERENCES

Angst, G., Messinger, J., Greiner, M., Hausler, W., Hertel, D., Kirfel, K., Kogel-Knabner, I., Leuschner, C., Rethemeyer, J., Mueller, C.W., 2018. Soil organic carbon stocks in topsoil and subsoil controlled by parent material, carbon input in the rhizosphere, and microbial-derived compounds. Soil Biol Biochem 122, 19-30.

Asano, M., Wagai, R., 2014. Evidence of aggregate hierarchy at micro- to submicron scales in an allophanic Andisol. Geoderma 216, 62-74.

Batjes, N.H., 2016. Harmonized soil property values for broad-scale modelling (WISE30sec) with estimates of global soil carbon stocks. Geoderma 269, 61-68.

Best, M.G., 2003. Igneous and metamorphic petrology. John Wiley & Sons.

Blakemore, L.C., 1987. Extractable iron, aluminium and silicon. In methods for chemical analysis of soils. NZ Soil Bureau Scientific Report 80, 71-76.

Breshears, D.D., Barnes, F.J., 1999. Interrelationships between plant functional types and soil moisture heterogeneity for semiarid landscapes within the grassland/forest continuum: a unified conceptual model. Landscape Ecology 14(5), 465-478.

Bruun, T.B., Elberling, B., Christensen, B.T., 2010. Lability of soil organic carbon in tropical soils with different clay minerals. Soil Biol Biochem 42(6), 888-895.

Buol, S.W., Southard, R.J., Graham, R.C., McDaniel, P.A., 2011. Soil genesis and classification. John Wiley & Sons.

Cambardella, C.A., Elliott, E.T., 1992. Particulate Soil Organic-Matter Changes across a Grassland Cultivation Sequence. Soil Science Society of America Journal 56(3), 777-783.

Carmeis Filho, A.C., Penn, C.J., Crusciol, C.A., Calonego, J.C., 2017. Lime and phosphogypsum impacts on soil organic matter pools in a tropical Oxisol under long-term no-till conditions. Agriculture, Ecosystems Environment 241, 11-23.

Chabbi, A., Kogel-Knabner, I., Rumpel, C., 2009. Stabilised carbon in subsoil horizons is located in spatially distinct parts of the soil profile. Soil Biol Biochem 41(2), 256-261.

Chen, R., Senbayram, M., Blagodatsky, S., Myachina, O., Dittert, K., Lin, X., Blagodatskaya, E., Kuzyakov, Y., 2014. Soil C and N availability determine the priming effect: microbial N mining and stoichiometric decomposition theories. Global Change Biology 20(7), 2356-2367.

Chorover, J., Amistadi, M.K., Chadwick, O.A., 2004. Surface charge evolution of mineral-organic complexes during pedogenesis in Hawaiian basalt. Geochimica Et Cosmochimica Acta 68(23), 4859-4876.

Chorover, J., Sposito, G., 1995. Surface-Charge Characteristics of Kaolinitic Tropical Soils. Geochimica Et Cosmochimica Acta 59(5), 875-884.

Churchman, G., Lowe, D., 2011. Alteration, Formation, and Occurrence of Minerals in Soils, Handbook of Soil Sciences. Handbook of Soil Science. CRC Press, pp. 1-72.

Churchman, G., Lowe, D., 2012. Alteration, formation and occurrence of minerals in soils In: Huang PM, Li Y & Sumner ME (Eds.) Handbook of Soil Sciences: Properties and Processes. Boca Raton, CRC Press. p.

Churchman, G.J., Pasbakhsh, P., Lowe, D.J., Theng, B.K.G., 2016. Unique but diverse: some observations on the formation, structure and morphology of halloysite. Clay Minerals 51(3), 395-416.

Churchman, G.J., Pontifex, I.R., McClure, S.G., 2010. Factors Influencing the Formation and Characteristics of Halloysites or Kaolinites in Granitic and Tuffaceous Saprolites in Hong Kong. Clays and Clay Minerals 58(2), 220-237.

Churchman, G.J., Whitton, J.S., Claridge, G.G.C., Theng, B.K.G., 1984. Intercalation Method Using Formamide for Differentiating Halloysite from Kaolinite. Clays and Clay Minerals 32(4), 241-248.

Cleveland, C.C., Townsend, A.R., Taylor, P., Alvarez-Clare, S., Bustamante, M.M., Chuyong, G., Dobrowski, S.Z., Grierson, P., Harms, K.E., Houlton, B.Z., 2011. Relationships among net primary productivity, nutrients and climate in tropical rain forest: a pan-tropical analysis. Ecology letters 14(9), 939-947.

Collins, H.P., Elliott, E.T., Paustian, K., Bundy, L.C., Dick, W.A., Huggins, D.R., Smucker, A.J.M., Paul, E.A., 2000. Soil carbon pools and fluxes in long-term corn belt agroecosystems. Soil Biol Biochem 32(2), 157-168.

Cotrufo, M.F., Ranalli, M.G., Haddix, M.L., Six, J., Lugato, E., 2019. Soil carbon storage informed by particulate and mineral-associated organic matter. Nature Geoscience 12(12), 989-+.

Craine, J.M., Morrow, C., Fierer, N., 2007. Microbial nitrogen limitation increases decomposition. Ecology 88(8), 2105-2113.

Crow, M., Barber, A., 2005. Map: Simplified geological map of Sumatra. Geological Society, London, Memoirs 31(1).

Cunningham, M.J., Lowe, D.J., Wyatt, J.B., Moon, V.G., Churchman, G.J., 2016. Discovery of halloysite books in altered silicic Quaternary tephras, northern New Zealand. Clay Minerals 51(3), 351-372.

Curtin, D., 2002. Possible role of aluminum in stabilizing organic matter in particle size fractions of Chernozemic and Solonetizic soils. Canadian Journal of Soil Science 82(2), 265-268.

Darman, H., Sidi, F.H., Ikatan Ahli Geologi, I., 2000. An outline of the geology of Indonesia. Indonesian Association of Geologists, Jakarta.

Davidson, E.A., Janssens, I.A., 2006. Temperature sensitivity of soil carbon decomposition and feedbacks to climate change. Nature 440(7081), 165-173.

Davidson, E.A., Janssens, I.A., Luo, Y., 2006. On the variability of respiration in terrestrial ecosystems: moving beyond Q10. Global Change Biology 12(2), 154-164.

Del Grosso, S., Parton, W., Stohlgren, T., Zheng, D., Bachelet, D., Prince, S., Hibbard, K., Olson, R., 2008. Global potential net primary production predicted from vegetation class, precipitation, and temperature. Ecology 89(8), 2117-2126.

Diaz, F.J., O'Geen, A.T., Rasmussen, C., Dahlgren, R.A., 2010. Pedogenesis along a thermal gradient in a geothermal region of the southern Cascades, California. Geoderma 154(3-4), 495-507.

Djukic, I., Zehetner, F., Tatzber, M., Gerzabek, M.H., 2010. Soil organic-matter stocks and characteristics along an Alpine elevation gradient. Journal of Plant Nutrition and Soil Science 173(1), 30-38.

Doetterl, S., Stevens, A., Six, J., Merckx, R., Van Oost, K., Pinto, M.C., Casanova-Katny, A., Munoz, C., Boudin, M., Venegas, E.Z., Boeckx, P., 2015. Soil carbon storage controlled by interactions between geochemistry and climate. Nature Geoscience 8(10), 780-+.

Driscoll, C.T., 1984. A Procedure for the Fractionation of Aqueous Aluminum in Dilute Acidic Waters. International Journal of Environmental Analytical Chemistry 16(4), 267-283.

Eusterhues, K., Rumpel, C., Kogel-Knabner, I., 2005. Stabilization of soil organic matter isolated via oxidative degradation. Organic Geochemistry 36(11), 1567-1575.

Fang, C., Smith, P., Moncrieff, J.B., Smith, J.U., 2005. Similar response of labile and resistant soil organic matter pools to changes in temperature. Nature 433(7021), 57-59.

Fick, S.E., Hijmans, R.J., 2017. WorldClim 2: new 1-km spatial resolution climate surfaces for global land areas. International Journal of Climatology 37(12), 4302-4315.

Filimonova, S., Kaufhold, S., Wagner, F.E., Hausler, W., Kogel-Knabner, I., 2016. The role of allophane nano-structure

and Fe oxide speciation for hosting soil organic matter in an allophanic Andosol. Geochimica Et Cosmochimica Acta 180, 284-302.

Fontaine, S., Barot, S., Barre, P., Bdioui, N., Mary, B., Rumpel, C., 2007. Stability of organic carbon in deep soil layers controlled by fresh carbon supply. Nature 450(7167), 277-280.

Fontijn, K., Williamson, D., Mbede, E., Ernst, G.G., 2012. The Rungwe Volcanic Province, Tanzania–A volcanological review. Journal of African Earth Sciences 63, 12-31.

Funakawa, S., Shinjo, H., Kadono, A., Kosaki, T., 2010. Factors controlling in situ decomposition rate of soil organic matter under various bioclimatic conditions of Eurasia. Pedologist 53(3, Special Issue), 50-66.

Garrido, E., Matus, F., 2012. Are organo-mineral complexes and allophane content determinant factors for the carbon level in Chilean volcanic soils? Catena 92, 106-112.

Garten Jr, C.T., 2011. Comparison of forest soil carbon dynamics at five sites along a latitudinal gradient. Geoderma 167, 30-40.

Garten Jr, C.T., Hanson, P.J., 2006. Measured forest soil C stocks and estimated turnover times along an elevation gradient. Geoderma 136(1-2), 342-352.

Gee, G.W., Or, D., 2018. 2.4 Particle-Size Analysis. In: J.H. Dane, G.C. Topp (Eds.), Methods of Soil Analysis. SSSA Book Series, pp. 255-293.

Geological Survey of Tanzania, 1959. Geological Map of Tanganyika. www.gst.go.tz.

Georgoulias, F.A., Moustakas, N.K., 2010. Exploration of soils developing on volcanic materials on the island of Milos, Greece. Catena 81(1), 43-54.

Gong, P., Wang, J., Yu, L., Zhao, Y.C., Zhao, Y.Y., Liang, L., Niu, Z.G., Huang, X.M., Fu, H.H., Liu, S., Li, C.C., Li, X.Y., Fu, W., Liu, C.X., Xu, Y., Wang, X.Y., Cheng, Q., Hu, L.Y., Yao, W.B., Zhang, H., Zhu, P., Zhao, Z.Y., Zhang, H.Y., Zheng, Y.M., Ji, L.Y., Zhang, Y.W., Chen, H., Yan, A., Guo, J.H., Yu, L., Wang, L., Liu, X.J., Shi, T.T., Zhu, M.H., Chen, Y.L., Yang, G.W., Tang, P., Xu, B., Giri, C., Clinton, N., Zhu, Z.L., Chen, J., Chen, J., 2013. Finer resolution observation and monitoring of global land cover: first mapping results with Landsat TM and ETM+ data. International Journal of Remote Sensing 34(7), 2607-2654.

Guicharnaud, R., Paton, G.I., 2006. An evaluation of acid deposition on cation leaching and weathering rates of an Andosol and a Cambisol. Journal of Geochemical Exploration 88(1-3), 279-283.

Gulde, S., Chung, H., Amelung, W., Chang, C., Six, J., 2008. Soil carbon saturation controls labile and stable carbon pool dynamics. Soil Science Society of America Journal 72(3), 605-612.

Haddix, M.L., Gregorich, E.G., Helgason, B.L., Janzen, H., Ellert, B.H., Cotrufo, M.F., 2020. Climate, carbon content, and soil texture control the independent formation and persistence of particulate and mineral-associated organic matter in soil. Geoderma 363, 114160.

Harris, W., Norman White, G., 2015. X-ray Diffraction Techniques for Soil Mineral Identification. In: A.L. Ulery, L. Richard Drees (Eds.), Methods of Soil Analysis Part 5-Mineralogical Methods. SSSA Book Series. Soil Science Society of America, Madison, WI, pp. 81-115.

Harsh, J., 2011. Poorly Crystalline Aluminosilicate Clay Minerals, Handbook of Soil Sciences. Handbook of Soil Science. CRC Press, pp. 1-14.

Hodder, A.P.W., Naish, T.R., Nelson, C.S., 1993. A two-stage model for the formation of smectite from detrital volcanic glass under shallow-marine conditions. Marine geology 109(3-4), 279-285.

Hossner, L., 1996. Dissolution for total elemental analysis. Methods of Soil Analysis Part 3—Chemical Methods (methodsofsoilan3), 49-64.

Huang, P.M., Wang, M.K., Kämpf, N., Schulze, D.G., 2018. Aluminum Hydroxides. In: J.B. Dixon, D.G. Schulze (Eds.), Soil Mineralogy with Environmental Applications. SSSA Book Series. Soil Science Society of America, Madison, WI, pp. 261-289.

Illiger, P., Schmidt, G., Walde, I., Hese, S., Kudrjavzev, A.E., Kurepina, N., Mizgirev, A., Stephan, E., Bondarovich, A., Fruhauf, M., 2019. Estimation of regional soil organic carbon stocks merging classified land-use information with detailed soil data. Sci Total Environ 695, 133755.

Ise, T., Moorcroft, P.R., 2006. The global-scale temperature and moisture dependencies of soil organic carbon decomposition: an analysis using a mechanistic decomposition model. Biogeochemistry 80(3), 217-231.

IUSS Working Group WRB, 2015. World reference base for soil resources 2014. World Soil Resour. Rep. 106. FAO, Rome.

Jobbagy, E.G., Jackson, R.B., 2000. The vertical distribution of soil organic carbon and its relation to climate and vegetation. Ecological Applications 10(2), 423-436.

Joergensen, R.G., 1996. The fumigation-extraction method to estimate soil microbial biomass: calibration of the kEC value. Soil Biol Biochem 28(1), 25-31.

John, B., Yamashita, T., Ludwig, B., Flessa, H., 2005. Storage of organic carbon in aggregate and density fractions of silty soils under different types of land use. Geoderma 128(1-2), 63-79.

Kadono, A., Funakawa, S., Kosaki, T., 2008. Factors controlling mineralization of soil organic matter in the Eurasian steppe. Soil Biol Biochem 40(4), 947-955.

Kaiser, K., Guggenberger, G., 2003. Mineral surfaces and soil organic matter. European Journal of Soil Science 54(2), 219-236.

Karathanasis, A.D., 2018. Mineral Equilibria in Environmental Soil Systems. In: J.B. Dixon, D.G. Schulze (Eds.), Soil Mineralogy with Environmental Applications. SSSA Book Series. Soil Science Society of America, Madison, WI, pp. 109-151.

Klamt, E., Sombroek, W., 1988. Contribution of organic matter to exchange properties of Oxisols.

Kleber, M., Eusterhues, K., Keiluweit, M., Mikutta, C., Mikutta, R., Nico, P.S., 2015. Chapter One – Mineral–Organic Associations: Formation, Properties, and Relevance in Soil Environments. Advances in Agronomy 130, 140.

Kleber, M., Schwendenmann, L., Veldkamp, E., Rossner, J., Jahn, R., 2007a. Halloysite versus gibbsite: Silicon cycling as a pedogenetic process in two lowland neotropical rain forest soils of La Selva, Costa Rica. Geoderma 138(1-2), 1-11.

Kleber, M., Sollins, P., Sutton, R., 2007b. A conceptual model of organo-mineral interactions in soils: self-assembly of organic molecular fragments into zonal structures on mineral surfaces. Biogeochemistry 85(1), 9-24.

Kogel-Knabner, I., Guggenberger, G., Kleber, M., Kandeler, E., Kalbitz, K., Scheu, S., Eusterhues, K., Leinweber, P., 2008. Organo-mineral associations in temperate soils: Integrating biology, mineralogy, and organic matter chemistry. Journal of Plant Nutrition and Soil Science 171(1), 61-82.

Lal, R., 2004a. Soil carbon sequestration impacts on global climate change and food security. Science 304(5677), 1623-1627.

Lal, R., 2004b. Soil carbon sequestration in India. Climatic Change 65(3), 277-296.

Lal, R., 2005. Forest soils and carbon sequestration. Forest Ecology and Management 220(1-3), 242-258.

Lampo, Z., Xueming, Y., Inoue, K., 1993. Morphological, chemical, and humus characteristics of volcanic ash soils in Changbaishan and Wudalianchi, northeast China. Soil Science and Plant Nutrition 39(2), 339-350.

Lavee, H., Sarah, P., Imeson, A.C., 1996. Aggregate stability dynamics as affected by soil temperature and moisture

regimes. Geogr Ann A 78a(1), 73-82.

Le Maitre, R., Streckeisen, A., Zanettin, B., Le Bas, M., Bonin, B., Bateman, P., 2005. Igneous rocks: a classification and glossary of terms: recommendations of the International Union of Geological Sciences Subcommission on the Systematics of Igneous Rocks. Cambridge University Press.

Leuschner, C., Wulf, M., Bauchler, P., Hertel, D., 2014. Forest Continuity as a Key Determinant of Soil Carbon and Nutrient Storage in Beech Forests on Sandy Soils in Northern Germany. Ecosystems 17(3), 497-511.

Li, C.L., Cao, Z.Y., Chang, J.J., Zhang, Y., Zhu, G.L., Zong, N., He, Y.T., Zhang, J.J., He, N.P., 2017. Elevational gradient affect functional fractions of soil organic carbon and aggregates stability in a Tibetan alpine meadow. Catena 156, 139-148.

Lindsay, W.L., 1979. Chemical equilibria in soils. John Wiley and Sons Ltd.

Little, M.G., Lee, C.T.A., 2006. On the formation of an inverted weathering profile on Mount Kilimanjaro, Tanzania: Buried paleosol or groundwater weathering? Chemical Geology 235(3-4), 205-221.

Little, M.G., Lee, C.T.A., 2010. Sequential extraction of labile elements and chemical characterization of a basaltic soil from Mt. Meru, Tanzania. Journal of African Earth Sciences 57(5), 444-454.

Lowe, D.J., 1986. Controls on the rates of weathering and clay mineral genesis in airfall tephras: a review and New Zealand case study. Rates of chemical weathering of rocks and minerals, 265-330.

Lowe, D.J., 2011. Tephrochronology and its application: A review. Quaternary Geochronology 6(2), 107-153.

Lyu, H., Watanabe, T., Kilasara, M., Funakawa, S., 2018. Effects of climate on distribution of soil secondary minerals in volcanic regions of Tanzania. Catena 166, 209-219.

Mack, M.C., D'Antonio, C.M., Ley, R.E., 2001. Alteration of ecosystem nitrogen dynamics by exotic plants: a case study of C4 grasses in Hawaii. Ecological Applications 11(5), 1323-1335.

Matus, F., Rumpel, C., Neculman, R., Panichini, M., Mora, M.L., 2014. Soil carbon storage and stabilisation in andic soils: A review. Catena 120, 102-110.

Mc Bride, M.B., 2018. Surface Chemistry of Soil Minerals, Minerals in Soil Environments. SSSA Book Series, pp. 35-88.

Naidu, R., Bolan, N., Kookana, R.S., Tiller, K., 1994. Ionic-strength and pH effects on the sorption of cadmium and the surface charge of soils. European Journal of Soil Science 45(4), 419-429.

Narendrula-Kotha, R., Nkongolo, K.K., 2017. Microbial Response to Soil Liming of Damaged Ecosystems Revealed by Pyrosequencing and Phospholipid Fatty Acid Analyses. PLoS One 12(1), e0168497.

Neff, J.C., Townsend, A.R., Gleixner, G., Lehman, S.J., Turnbull, J., Bowman, W.D., 2002. Variable effects of nitrogen additions on the stability and turnover of soil carbon. Nature 419(6910), 915-917.

Newmark, W.D., 1991. The Conservation of Mount Kilimanjaro, 16. Iucn.

Nieuwenhuyse, A., vanBreemen, N., 1997. Quantitative aspects of weathering and neoformation in selected Costa Rican volcanic soils. Soil Science Society of America Journal 61(5), 1450-1458.

Nonnotte, P., Benoit, M., Le Gall, B., Hémond, C., Rolet, J., Cotten, J., Brunet, P., Makoba, E., Beccaluva, L., Bianchini, G., Wilson, M., 2011. Petrology and geochemistry of alkaline lava series, Kilimanjaro, Tanzania: New constraints on petrogenetic processes, Volcanism and Evolution of the African Lithosphere. Geological Society of America, pp. 127-158.

Nonnotte, P., Guillou, H., Le Gall, B., Benoit, M., Cotten, J., Scaillet, S., 2008. New K–Ar age determinations of Kilimanjaro volcano in the North Tanzanian diverging rift, East Africa. Journal of Volcanology and Geothermal Research 173(1), 99-112.

Parfitt, R., Yuan, G., Theng, B., 1999. A 13C-NMR study of the interactions of soil organic matter with aluminium and allophane in podzols. European Journal of Soil Science 50(4), 695-700.

Parfitt, R.L., 2009. Allophane and imogolite: role in soil biogeochemical processes. Clay Minerals 44(1), 135-155.

Parfitt, R.L., Giltrap, D.J., Whitton, J.S., 1995. Contribution of Organic-Matter and Clay-Minerals to the Cation-Exchange Capacity of Soils. Communications in Soil Science and Plant Analysis 26(9-10), 1343-1355.

Parton, W., Schimel, D.S., Cole, C., Ojima, D., 1987. Analysis of factors controlling soil organic matter levels in Great Plains Grasslands 1. Soil Science Society of America Journal 51(5), 1173-1179.

Paul, E., Collins, H., Leavitt, S., 2001a. Dynamics of resistant soil carbon of Midwestern agricultural soils measured by naturally occurring 14C abundance. Geoderma 104(3-4), 239-256.

Paul, E., Morris, S., Bohm, S., 2001b. The determination of soil C pool sizes and turnover rates: biophysical fractionation and tracers, Assessment methods for soil carbon, pp. 193-206.

Peel, M.C., Finlayson, B.L., McMahon, T.A., 2007. Updated world map of the Koppen-Geiger climate classification. Hydrology and Earth System Sciences 11(5), 1633-1644.

Pennock, D., Yates, T., Braidek, J., 2007. Soil sampling designs, Soil Sampling and Methods of Analysis, pp. 1-14.

Qi, R.M., Li, J., Lin, Z.A., Li, Z.J., Li, Y.T., Yang, X.D., Zhang, J.J., Zhao, B.Q., 2016. Temperature effects on soil organic carbon, soil labile organic carbon fractions, and soil enzyme activities under long-term fertilization regimes. Applied Soil Ecology 102, 36-45.

Rasmussen, C., Dahlgren, R.A., Southard, R.J., 2010. Basalt weathering and pedogenesis across an environmental gradient in the southern Cascade Range, California, USA. Geoderma 154(3-4), 473-485.

Rasmussen, C., Heckman, K., Wieder, W.R., Keiluweit, M., Lawrence, C.R., Berhe, A.A., Blankinship, J.C., Crow, S.E., Druhan, J.L., Pries, C.E.H., Marin-Spiotta, E., Plante, A.F., Schadel, C., Schimel, J.P., Sierra, C.A., Thompson, A., Wagai, R., 2018. Beyond clay: towards an improved set of variables for predicting soil organic matter content. Biogeochemistry 137(3), 297-306.

Rasmussen, C., Matsuyama, N., Dahlgren, R.A., Southard, R.J., Brauer, N., 2007. Soil genesis and mineral transformation across an environmental gradient on andesitic lahar. Soil Science Society of America Journal 71(1), 225-237.

Rasse, D.P., Rumpel, C., Dignac, M.-F., 2005. Is soil carbon mostly root carbon? Mechanisms for a specific stabilisation. Plant and Soil 269(1-2), 341-356.

Rey, A., Jarvis, P., 2006. Modelling the effect of temperature on carbon mineralization rates across a network of European forest sites (FORCAST). Global Change Biology 12(10), 1894-1908.

Reynolds, R.C., 1971. Clay Mineral Formation in an Alpine Environment. Clays and Clay Minerals 19(6), 361-&.

Righi, D., Terribile, F., Petit, S., 1999. Pedogenic formation of kaolinite-smectite mixed layers in a soil toposequence developed from basaltic parent material in Sardinia (Italy). Clays and Clay Minerals 47(4), 505-514.

Rizinjirabake, F., Pilesjo, P., Tenenbaum, D.E., 2019. Dissolved organic carbon leaching flux in a mixed agriculture and forest watershed in Rwanda. Journal of Hydrology-Regional Studies 26, 100633.

Rowley, M.C., Grand, S., Verrecchia, E.P., 2018. Calcium-mediated stabilisation of soil organic carbon. Biogeochemistry 137(1-2), 27-49.

Rumpel, C., Rodriguez-Rodriguez, A., Gonzalez-Perez, J.A., Arbelo, C., Chabbi, A., Nunan, N., Gonzalez-Vila, F.J., 2012. Contrasting composition of free and mineral-bound organic matter in top- and subsoil horizons of Andosols. Biology and Fertility of Soils 48(4), 401-411.

Running, S.W., Thornton, P.E., Nemani, R., Glassy, J.M., 2000. Global terrestrial gross and net primary productivity

from the earth observing system, Methods in ecosystem science. Springer, pp. 44-57.

Salome, C., Nunan, N., Pouteau, V., Lerch, T.Z., Chenu, C., 2010. Carbon dynamics in topsoil and in subsoil may be controlled by different regulatory mechanisms. Global Change Biology 16(1), 416-426.

Sanchez-Gonzalez, A., Chapela-Lara, M., German-Venegas, E., Fuentes-Garcia, R., del Rio-Portilla, F., Siebe, C., 2017. Changes in quality and quantity of soil organic matter stocks resulting from wastewater irrigation in formerly forested land. Geoderma 306, 99-107.

Schimel, J.P., Weintraub, M.N., 2003. The implications of exoenzyme activity on microbial carbon and nitrogen limitation in soil: a theoretical model. Soil Biol Biochem 35(4), 549-563.

Schlesinger, W.H., 1995. An overview of the carbon cycle. Soils and Global Change 25, 9-25.

Schulze, D.G., 2018. An Introduction to Soil Mineralogy. In: J.B. Dixon, S.B. Weed (Eds.), Minerals in Soil Environments. SSSA Book Series. Soil Science Society of America, Madison, WI, pp. 1-34.

Semenov, V.M., Pautova, N.B., Lebedeva, T.N., Khromychkina, D.P., Semenova, N.A., de Gerenyu, V.O.L., 2019. Plant Residues Decomposition and Formation of Active Organic Matter in the Soil of the Incubation Experiments. Eurasian Soil Science 52(10), 1183-1194.

Sharma, A., Weindorf, D.C., Wang, D.D., Chakraborty, S., 2015. Characterizing soils via portable X-ray fluorescence spectrometer: 4. Cation exchange capacity (CEC). Geoderma 239, 130-134.

Simkin, T., Siebert, L., 1994. Volcanoes of the World. Geoscience Press. Inc. Tusson.

Six, J., Jastrow, J., 2002. Organic matter turnover. Encyclopedia of Soil Science, 936-942.

Soil Survey Laboratory Staff, 1996. Soil survey laboratory methods manual. US Gov. Print. Office, Washington, DC.

Soil Survey Staff, 2014. Keys to Soil Taxonomy, 12th ed. USDA-Natural Resources Conservation Service, Washington, DC.

Sokol, N.W., Bradford, M.A., 2019. Microbial formation of stable soil carbon is more efficient from belowground than aboveground input. Nature Geoscience 12(1), 46-+.

Sollins, P., Kramer, M.G., Swanston, C., Lajtha, K., Filley, T., Aufdenkampe, A.K., Wagai, R., Bowden, R.D., 2009. Sequential density fractionation across soils of contrasting mineralogy: evidence for both microbial- and mineral-controlled soil organic matter stabilization. Biogeochemistry 96(1-3), 209-231.

Steinmann, T., Welp, G., Wolf, A., Holbeck, B., Große-Rüschkamp, T., Amelung, W., 2016. Repeated monitoring of organic carbon stocks after eight years reveals carbon losses from intensively managed agricultural soils in Western Germany. Journal of Plant Nutrition and Soil Science 179(3), 355-366.

Stergiadi, M., van der Perk, M., de Nijs, T.C.M., Bierkens, M.F.P., 2016. Effects of climate change and land management on soil organic carbon dynamics and carbon leaching in northwestern Europe. Biogeosciences 13(5), 1519-1536.

Takahashi, T., Dahlgren, R.A., 2016. Nature, properties and function of aluminum–humus complexes in volcanic soils. Geoderma 263, 110-121.

Takeda, A., Kimura, K., Yamasaki, S., 2004. Analysis of 57 elements in Japanese soils, with special reference to soil group and agricultural use. Geoderma 119(3-4), 291-307.

The Vegetationmap4africa team, 2017. Potential natural vegetation of eastern Africa, http://vegetationmap4africa.org

Thompson, M.L., Ukrainczyk, L., 2002. Micas. In: J.B. Dixon, D.G. Schulze (Eds.), Soil mineralogy with environmental applications, pp. 431-466.

Thornthwaite, C.W., 1948. An Approach toward a Rational Classification of Climate. Geographical Review 38(1), 55-94.

Tian, Q., He, H., Cheng, W., Bai, Z., Wang, Y., Zhang, X., 2016. Factors controlling soil organic carbon stability along a temperate forest altitudinal gradient. Scientific reports 6, 18783.

Torn, M.S., Trumbore, S.E., Chadwick, O.A., Vitousek, P.M., Hendricks, D.M., 1997. Mineral control of soil organic carbon storage and turnover. Nature 389(6647), 170-173.

Trumbore, S.E., Zheng, S.H., 1996. Comparison of fractionation methods for soil organic matter C-14 analysis. Radiocarbon 38(2), 219-229.

Tsai, C.C., Chen, Z.S., Kao, C.I., Ottner, F., Kao, S.J., Zehetner, F., 2010. Pedogenic development of volcanic ash soils along a climosequence in Northern Taiwan. Geoderma 156(1-2), 48-59.

Van Breemen, N., Brinkman, R., 1976. Chemical equilibria and soil formation. Developments in Soil Science 5, 141-170.

van der Gaast, S.J., Mizota, C., Jansen, J., 1986. Curved smectite in soils from volcanic ash in Kenya and Tanzania: a low-angle X-ray powder diffraction study. Clays and Clay Minerals 34(6), 665-671.

Van Ranst, E., Utami, S., Verdoodt, A., Qafoku, N., 2008. Mineralogy of a perudic Andosol in central Java, Indonesia. Geoderma 144(1-2), 379-386.

Vancampenhout, K., De Vos, B., Wouters, K., Swennen, R., Buurman, P., Deckers, J., 2012. Organic matter of subsoil horizons under broadleaved forest: Highly processed or labile and plant-derived? Soil Biol Biochem 50, 40-46.

Vingiani, S., Righi, D., Petit, S., Terribile, F., 2004. Mixed-layer kaolinite-smectite minerals in a red-black soil sequence from basalt in Sardinia (Italy). Clays and Clay Minerals 52(4), 473-483.

von Lützow, M., Kögel-Knabner, I., 2009. Temperature sensitivity of soil organic matter decomposition—what do we know? Biology and Fertility of Soils 46(1), 1-15.

von Lützow, M., Kögel-Knabner, I., Ekschmitt, K., Flessa, H., Guggenberger, G., Matzner, E., Marschner, B., 2007. SOM fractionation methods: relevance to functional pools and to stabilization mechanisms. Soil Biol Biochem 39(9), 2183-2207.

Wagai, R., Kajiura, M., Asano, M., 2020. Iron and aluminum association with microbially processed organic matter via meso-density aggregate formation across soils: organo-metallic glue hypothesis. SOIL Discuss. 2020, 1-42.

Wagai, R., Kajiura, M., Asano, M., Hiradate, S., 2015. Nature of soil organo-mineral assemblage examined by sequential density fractionation with and without sonication: Is allophanic soil different? Geoderma 241, 295-305.

Wang, X.Y., Yu, D.S., Xu, Z.C., Pan, Y., Pan, J.J., Shi, X.Z., 2017. Regional patterns and controls of soil organic carbon pools of croplands in China. Plant and Soil 421(1-2), 525-539.

Waring, B.G., Weintraub, S.R., Sinsabaugh, R.L., 2014. Ecoenzymatic stoichiometry of microbial nutrient acquisition in tropical soils. Biogeochemistry 117(1), 101-113.

Watanabe, T., Funakawa, S., Kosaki, T., 2006. Clay mineralogy and its relationship to soil solution composition in soils from different weathering environments of humid Asia: Japan, Thailand and Indonesia. Geoderma 136(1-2), 51-63.

Watanabe, T., Hasenaka, Y., Hartono, A., Sabiham, S., Nakao, A., Funakawa, S., 2017. Parent Materials and Climate Control Secondary Mineral Distributions in Soils of Kalimantan, Indonesia. Soil Science Society of America Journal 81(1), 124-137.

Wattel- Koekkoek, E.J.W., Buurman, P., Van Der Plicht, J., Wattel, E., Van Breemen, N., 2003. Mean residence time

of soil organic matter associated with kaolinite and smectite. European Journal of Soil Science 54(2), 269-278.

White, G.N., Dixon, J.B., 2002. Kaolin–serpentine minerals. In: J.B. Dixon, D.G. Schulze (Eds.), Soil mineralogy with environmental applications, pp. 389-414.

Wiedemeier, D.B., Bloesch, U., Hagedorn, F., 2012. Stable forest-savanna mosaic in north-western Tanzania: local-scale evidence from δ13C signatures and 14C ages of soil fractions. Journal of Biogeography 39(2), 247-257.

Wilkinson, P., Mitchell, J., Cattermole, P., Downie, C., 1986. Volcanic chronology of the Men–Kilimanjaro region, Northern Tanzania. Journal of the Geological Society 143(4), 601-605.

Wisawapipat, W., Kheoruenromne, I., Suddhiprakarn, A., Gilkes, R.J., 2010. Surface charge characteristics of variable charge soils in Thailand. Aust. J. Soil Res. 48(4), 337-354.

Wiseman, C.L.S., Puttmann, W., 2006. Interactions between mineral phases in the preservation of soil organic matter. Geoderma 134(1-2), 109-118.

Wordell-Dietrich, P., Don, A., Helfrich, M., 2017. Controlling factors for the stability of subsoil carbon in a Dystric Cambisol. Geoderma 304, 40-48.

Yan, D., Li, J., Pei, J., Cui, J., Nie, M., Fang, C., 2017. The temperature sensitivity of soil organic carbon decomposition is greater in subsoil than in topsoil during laboratory incubation. Scientific reports 7(1), 5181.

Yang, L., Lyu, M., Li, X., Xiong, X., Lin, W., Yang, Y., Xie, J., 2020. Decline in the contribution of microbial residues to soil organic carbon along a subtropical elevation gradient. Science of the Total Environment 749, 141583.

Yigini, Y., Panagos, P., 2016. Assessment of soil organic carbon stocks under future climate and land cover changes in Europe. Sci Total Environ 557-558, 838-850.

Yu, G., Xiao, J., Hu, S., Polizzotto, M.L., Zhao, F., McGrath, S.P., Li, H., Ran, W., Shen, Q., 2017. Mineral Availability as a Key Regulator of Soil Carbon Storage. Environmental Science & Technology 51(9), 4960-4969.

Zehetner, F., Miller, W.P., West, L.T., 2003. Pedogenesis of volcanic ash soils in Andean Ecuador. Soil Science Society of America Journal 67(6), 1797-1809.

Zelazny, L.W., He, L., Vanwormhoudt, A., 2018. Charge Analysis of Soils and Anion Exchange, Methods of Soil Analysis. SSSA Book Series, pp. 1231-1253.

Zhang, X.M., Guo, J.H., Vogt, R.D., Mulder, J., Wang, Y.J., Qian, C., Wang, J.G., Zhang, X.S., 2020. Soil acidification as an additional driver to organic carbon accumulation in major Chinese croplands. Geoderma 366, 114234.

Zhao, Q., Callister, S.J., Thompson, A.M., Kukkadapu, R.K., Tfaily, M.M., Bramer, L.M., Qafoku, N.P., Bell, S.L., Hobbie, S.E., Seabloom, E.W., Borer, E.T., Hofmockel, K.S., 2020. Strong mineralogic control of soil organic matter composition in response to nutrient addition across diverse grassland sites. Science of the Total Environment 736, 137839.

APPENDIX

SUPPLEMENTARY DATA

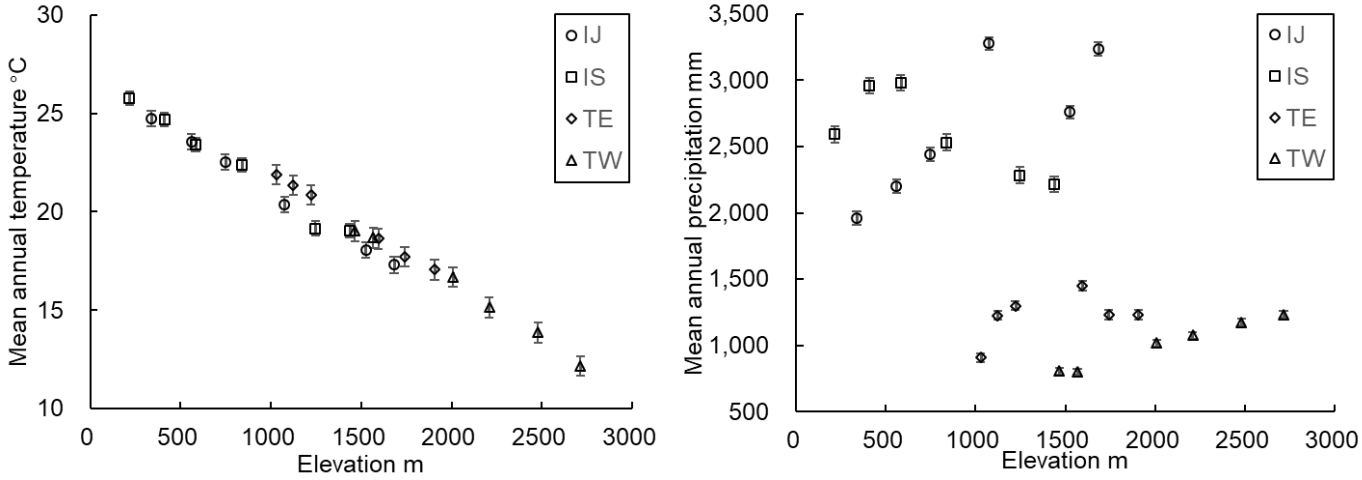

Fig. S3.1 The distribution of mean annual temperature and precipitation along the elevation gradient for each site.

IJ, Java (Indonesia); IS, Sumatra (Indonesia); TE, southeast slope of Kilimanjaro (Tanzania), TW, northwest slope of Kilimanjaro (Tanzania). The error bars represent the spatially aggregated root-mean-squared error (RMSE) values for each site.

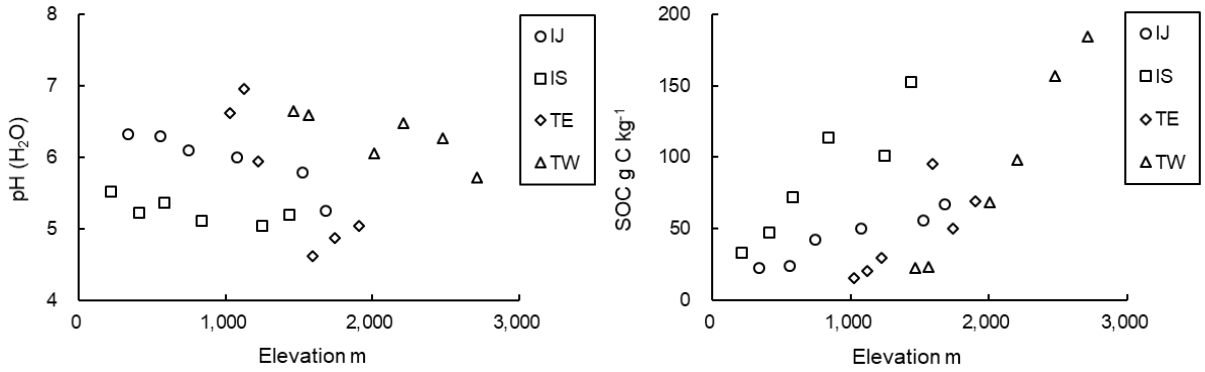

Fig. S3.2 The distribution of soil pH and soil organic carbon along the elevation gradient for each site.

IJ, Java (Indonesia); IS, Sumatra (Indonesia); TE, southeast slope of Kilimanjaro (Tanzania), TW, northwest slope of Kilimanjaro (Tanzania).

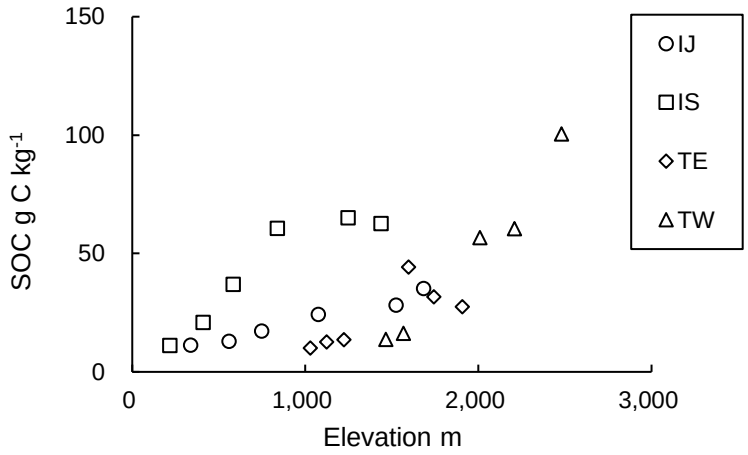

Fig. S4.1 Soil organic carbon content of the subsoil (20–40 cm) at each site along the elevation gradient

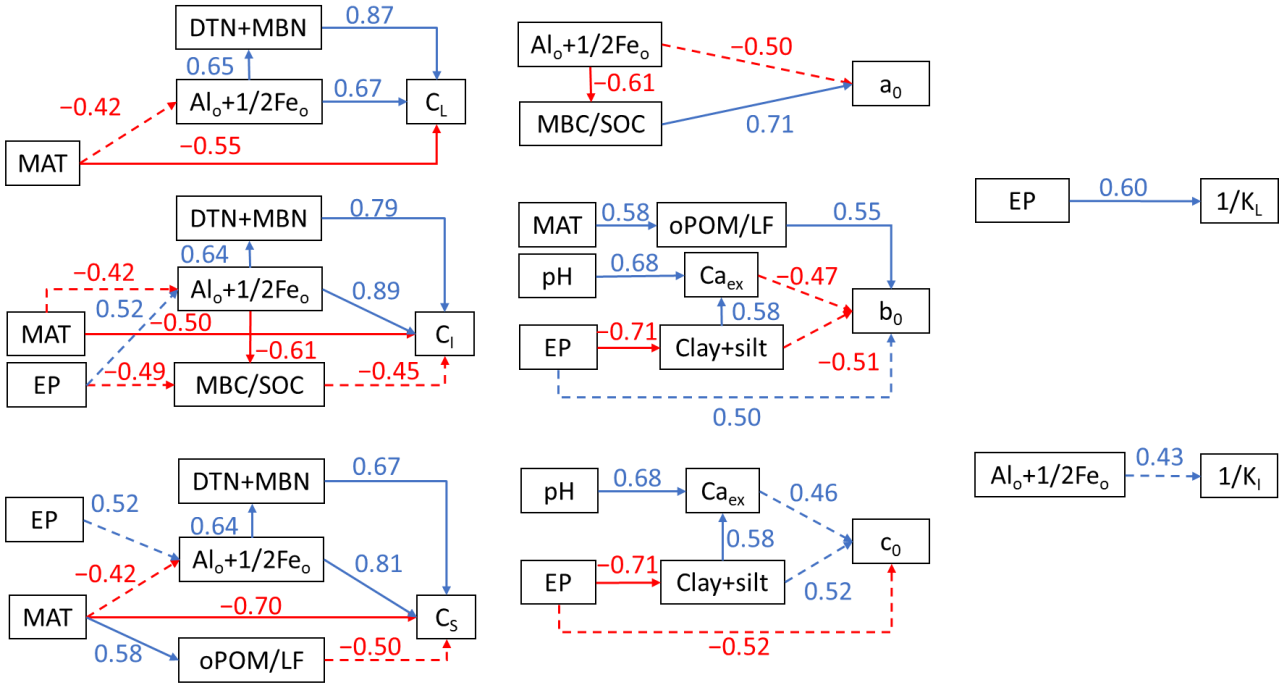

Fig. S4.2 Schematic diagram of single correlations of the subsoils (20–40 cm) for sizes (labile: C_L, intermediate: C_I, and stable: C_S), proportions (labile: a_0, intermediate: b_0, and stable: c_0), and mean residence times (labile: $1/K_L$ and intermediate: $1/K_I$) of three SOC pools, and related properties including the climate (MAT: mean annual temperature and EP: excess precipitation), geochemical properties, dissolved total nitrogen and microbial biomass nitrogen (DTN + MBN), a proportion of microbial biomass carbon in SOC (MBC/SOC) and aggregation index (oPOM/LF). Type of arrow line represents the significance of correlation, i.e., solid line: $P < 0.01$, and dotted line: $P < 0.05$. The number above an arrow is the correlation coefficient.

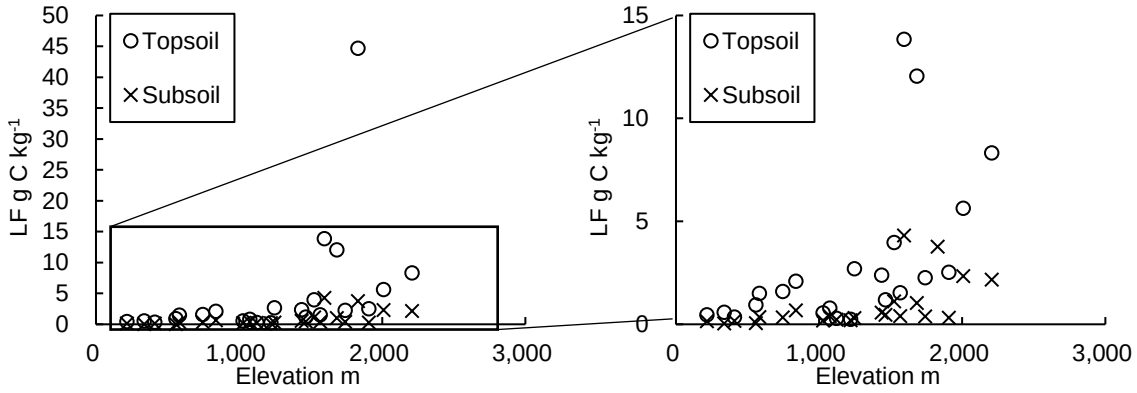

Fig. S4.3 The contents of light fraction (LF) for the topsoil (0–20 cm) and subsoil (20–40 cm) at each site.

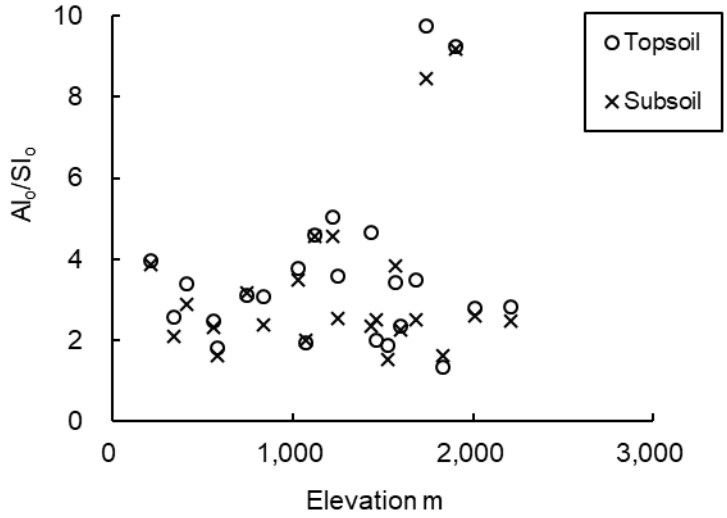

Fig. S4.4 The ratio of oxalate extractable Al to Si for the topsoil (0–20 cm) and subsoil (20–40 cm) at each site.

Table S3.1 Physicochemical properties of soil from each site

Site	Elevation	pH (H_2O)	CEC	Total SOC	Total N	Clay	Silt	Sand	Ca_{ex} [b]	Al_o +1/2Fe_o [c]	oPOM C [d]
	m		$cmol_c\ kg^{-1}$	$g\ kg^{-1}$	$g\ kg^{-1}$	%	%	%	$cmol_c\ kg^{-1}$	$g\ kg^{-1}$	$g\ kg^{-1}$
IJ-1 [a]	340	6.3	21.6	22.6	1.8	51	38	12	10.3	10.1	0.6
IJ-2	560	6.3	22.3	23.6	1.6	40	40	20	11.6	11.5	0.3
IJ-3	750	6.1	23.6	42.5	2.5	29	49	22	17.4	13.5	0.8
IJ-4	1080	6.0	34.8	49.7	3.1	27	45	29	18.4	19.3	1.2
IJ-5	1530	5.8	27.3	55.9	4.1	26	40	34	13.6	23.7	1.0
IJ-6	1680	5.3	18.6	67.1	4.7	8	45	48	4.3	20.1	1.2
IS-1	220	5.5	16.8	33.4	2.4	51	28	23	4.7	6.2	1.2
IS-2	410	5.2	18.2	46.9	3.2	23	35	42	4.6	12.6	1.8
IS-3	580	5.4	24.0	71.8	4.6	19	36	45	4.1	42.8	3.4
IS-4	840	5.1	35.1	113.5	5.9	17	56	29	0.5	52.5	4.4
IS-5	1250	5.0	40.1	100.8	5.7	25	64	15	0.7	42.3	6.7
IS-6	1440	5.2	43.0	152.4	7.2	25	58	20	0.2	58.7	8.8
TE-1	1030	6.6	17.8	15.6	0.9	26	64	11	10.3	9.6	0.3
TE-2	1120	7.0	18.6	20.2	2.2	35	54	11	10.6	10.6	0.4
TE-3	1220	5.9	17.8	29.3	1.0	38	51	11	5.2	12.2	1.5
TE-4	1600	4.6	27.9	95.0	5.2	5	67	28	0.4	39.5	1.7
TE-5	1740	4.9	17.2	49.7	3.5	33	49	18	0.1	16.3	2.3
TE-6	1900	5.0	24.1	68.8	1.8	32	54	14	2.9	25.6	2.1
TW-1	1470	6.6	26.9	22.6	1.3	25	67	8	15.9	6.5	0.6
TW-2	1570	6.6	18.9	23.3	1.9	23	71	6	8.3	7.8	0.4
TW-3	2010	6.1	40.4	68.3	5.6	13	81	6	29.3	26.5	0.6
TW-4	2210	6.5	42.3	98.4	8.4	15	80	6	47.4	37.7	0.9
TW-5	2480	6.3	60.1	156.7	15.8	23	73	4	48.1	35.7	0.8
TW-6	2710	5.7	50.0	184.2	15.7	30	54	16	20.5	51.1	2.8

[a] IJ, Java (Indonesia); IS, Sumatra (Indonesia); TE, southeast slope of Kilimanjaro (Tanzania); TW, northwest slope of Kilimanjaro (Tanzania). The numbers following site ID represent the elevation of the sampling site, being higher from 1 to 6.

[b] Ca_{ex}, exchangeable Ca.

[c] Al_o+1/2Fe_o, the content of nanocrystalline minerals.

[d] oPOM, occluded particulate organic matter in aggregates.

Table S3.2 Correlations between climate and soil properties

	MAT [a]	EP	pH(H_2O)	CEC	Ca_{ex} [b]	Clay + silt	Al_o + 1/2Fe_o [c]	MBC/SOC [d]
Elevation	−0.99**			0.52**		0.41*	0.42*	
MAT				−0.55**			−0.44*	
EP			−0.49*			−0.84**		
pH(H_2O)					0.74**	0.52**	−0.58**	0.53**
CEC							0.75**	−0.42*
Ca_{ex}								
Clay + silt								
Al_o + 1/2Fe_o								−0.77**
MBC/SOC								

[a] MAT, mean annual temperature; EP, excess precipitation.

[b] Ca_{ex}, exchangeable Ca.

[c] Al_o+1/2Fe_o, the content of nanocrystalline minerals.

[d] MBC/SOC, a proportion of microbial biomass carbon in SOC.

Table S4.1 Physicochemical properties of the soil from each site

Site	Elevation	pH (H_2O)	CEC	Total SOC	Total N	Al_o +1/2Fe_o [a]	Clay +silt	Ca_{ex}	Aggregation Index	MBC/SOC	DON+MBN
	m		$cmol_c$ kg^{-1}	g kg^{-1}	g kg^{-1}	g kg^{-1}	%	$cmol_c$ kg^{-1}		%	g kg^{-1}
IJ-1 [b]	340	6.3	23.4	11.2	0.9	9.5	91	9.0	1.1	0.96	0.04
IJ-2	560	6.4	22.9	13.0	0.9	11.8	87	10.3	1.7	0.98	0.04
IJ-3	750	6.0	18.9	17.2	1.0	14.2	92	6.6	0.4	1.14	0.06
IJ-4	1080	6.0	23.3	24.2	1.6	23.0	70	8.8	0.7	0.12	0.04
IJ-5	1530	5.7	30.6	28.2	1.4	46.7	84	8.8	0.1	0.85	0.07
IJ-6	1680	6.0	10.8	35.1	2.2	27.4	39	2.4	0.6	0.32	0.04
IS-1	220	5.3	21.2	11.1	0.9	5.5	79	1.3	2.4	1.19	0.09
IS-2	410	5.3	14.3	20.8	1.4	16.4	48	1.2	2.3	0.66	0.11
IS-3	580	5.3	19.2	37.0	2.5	55.7	60	0.5	1.4	0.64	0.16
IS-4	840	5.4	27.4	60.7	2.9	85.8	57	0.1	1.2	0.17	0.12
IS-5	1250	5.2	26.1	65.1	3.1	90.3	80	0.2	1.0	0.18	0.14
IS-6	1440	5.6	23.7	62.6	2.7	110.2	73	0.3	1.1	0.15	0.10
TE-1	1030	6.2	15.3	10.1	0.6	9.4	90	6.7	0.6	0.67	0.03
TE-2	1120	6.5	16.2	12.7	0.8	11.0	89	7.6	0.8	0.79	0.04
TE-3	1220	5.6	19.8	13.5	1.8	11.9	90	13.6	2.5	0.74	0.04
TE-4	1600	5.1	21.2	44.2	2.6	51.0	72	0.4	0.3	0.93	0.13
TE-5	1740	5.3	12.7	31.7	1.8	16.2	78	0.0	1.4	0.41	0.10
TE-6	1900	5.1	33.6	27.5	5.6	25.6	92	7.1	1.8	1.10	0.14
TW-1	1470	6.3	24.2	13.8	0.9	7.1	93	13.0	0.3	1.74	0.05
TW-2	1570	6.5	17.1	16.3	1.5	8.6	94	7.1	0.6	1.32	0.05
TW-3	2010	6.4	38.8	56.7	4.9	25.2	94	31.8	0.3	1.60	0.17
TW-4	2210	6.8	40.4	60.5	5.4	43.4	88	34.6	0.1	1.06	0.15
TW-5	2480	5.2	44.6	100.4	9.4	55.6	95	5.8	0.3	0.15	0.13

[a] Al_o + 1/2Fe_o, the content of nanocrystalline minerals; Ca_{ex}, exchangeable Ca; Aggregation Index, an index showing the degree of aggregation obtained dividing oPOM C by light fraction C; MBC/SOC, the content of microbial biomass carbon in soil organic carbon; DTN + MBN, dissolved total nitrogen plus microbial biomass nitrogen.

[b] IJ, Java (Indonesia); IS, Sumatra (Indonesia); TE, southeast slope of Kilimanjaro (Tanzania); TW, northwest slope of Kilimanjaro (Tanzania). The following numbers represent the elevation gradient of the site, getting higher from 1 to 6.

Table S4.2 Correlations between climate, geochemical and biotic properties of the subsoil (20–40 cm)

	MAT	EP	pH (H_2O)	Al_o + 1/2Fe_o	Clay+silt	Ca_{ex}	MBC /SOC	DON+ MBN	Aggregation Index
MAT [a]									.58**
EP				.52*	-.70**		-.52*		
pH (H_2O)				-.48*		.68**	.45*	-.43*	
Clay+silt		-.70**		-.43*		.58**	.60**		
Al_o +1/2Fe_o		.52*	-.48*		-.43*	-.46*	-.61**	.64**	
Ca_{ex}			.68**	-.46*	.58**		.55**		
MBC/SOC		-.52*	.45*	-.61**	.60**	.55**			
DON+MBN			-.43*	.64**					
Aggregation Index	.58**								

[a] MAT, Mean annual temperature; EP, excess precipitation; NPP, net primary production (potential); Al_o + 1/2Fe_o, contents of nanocrystalline minerals; Ca_{ex}, exchangeable Ca; MBC, microbial biomass carbon; MBC/SOC, the content of microbial biomass carbon in soil organic carbon, DTN + MBN, dissolved total nitrogen and microbial biomass nitrogen; POM C/SOC, the content of occluded particle organic matter carbon in soil organic carbon; Aggregation Index, an index obtained dividing oPOM C by light fraction C.

The contribution of the labile, intermediate and stable SOC pools to the cumulative C-CO_2 release until day t of incubation was calculated by the Equation:

$$P_x = \frac{C_x - C_x \times e^{-K_x \times t}}{C_{cum}} \quad \text{(S1)}$$

where Px is the contribution of the one of SOC pools (x is labile, intermediate or stabile pool) to the cumulative C-CO_2 release; C_x is the pool size of the pool x; Kx is the mineralization rate constant of the pool x; t is the time of incubation, and C_{cum} is the amount of cumulative C-CO_2 release until day t of incubation.

PUBLICATIONS

Chapter 2

Lyu, H., Watanabe, T., Kilasara, M., Funakawa, S., 2018. Effects of climate on distribution of soil secondary minerals in volcanic regions of Tanzania. *Catena* 166, 209-219. https://doi.org/10.1016/j.catena.2018.04.005

Chapter 3

Lyu, H., Watanabe, T., Kilasara, M., Hartono, A., Funakawa, S., 2020. Soil organic carbon pools controlled by climate and geochemistry in tropical volcanic regions. *Science of The Total Environment*, 143277. https://doi.org/10.1016/j.scitotenv.2020.143277

Chapter 4

Lyu, H., Watanabe, T., Zhong R., Kilasara, M., Hartono, A., Funakawa, S., 2020. Factors controlling sizes and stabilities of soil organic carbon pools in subsoil of tropical volcanic regions. *Science of The Total Environment*, 144842. https://doi.org/10.1016/j.scitotenv.2020.144842

Chapter 5

Lyu, H., Watanabe, T., Sugimoto, S., Kilasara, M., Funakawa, S., 2020. Control of climate on soil charge characteristics through organic matter and clay mineral distributions in Kilimanjaro, Tanzania. *Soil Science and Plant Nutrition*, http://dx.doi.org/10.1080/00380768.2021.1883998.